IN VIVO ANALYSIS OF THE ROLE OF FTSZ1 AND FTSZ2 PROTEINS IN CHLOROPLAST DIVISION IN *ARABIDOPSIS THALIANA*

A Dissertation

by

CAROL BEATRICE JOHNSON

Submitted to the Office of Graduate Studies of
Texas A&M University
in partial fulfillment of the requirements for the degree of

DOCTOR OF PHILOSOPHY

May 2012

Major Subject: Biology

In Vivo Analysis of the Role of FtsZ1 and FtsZ2 Proteins in Chloroplast Division in *Arabidopsis thaliana*

IN VIVO ANALYSIS OF THE ROLE OF FTSZ1 AND FTSZ2 PROTEINS IN CHLOROPLAST DIVISON IN *ARABIDOPSIS THALIANA*

A Dissertation

by

CAROL BEATRICE JOHNSON

Submitted to the Office of Graduate Studies of
Texas A&M University
in partial fulfillment of the requirements for the degree of

DOCTOR OF PHILOSOPHY

Approved by:

Chair of Committee,	Andreas Holzenburg
Committee Members,	Karl Aufderheide
	David Stelly
	Alan Pepper
Head of Department,	U. Jack McMahan

May 2012

Major Subject: Biology

ABSTRACT

In Vivo Analysis of the Role of FtsZ1 and FtsZ2 Proteins in Chloroplast Division in *Arabidopsis thaliana*. (May 2012)

Carol Beatrice Johnson, B.S., Texas Southern University; M.A., Sam Houston State University

Chair of Advisory Committee: Dr. Andreas Holzenburg

Chloroplasts divide by a constrictive fission process that is regulated by FtsZ proteins. Given the importance of photosynthesis and chloroplasts in general, it is important to understand the mechanisms and molecular biology of chloroplast division. An FtsZ gene is known to be of prokaryotic origin and to have been transferred from a symbiont's genome to host genome via lateral transfer. Subsequent duplication of the initial FtsZ gene gave rise to the FtsZ1 and FtsZ2 genes and protein families in eukaryotes. These proteins co-localize mid-chloroplast to form the Z-ring. Z-ring assembly initiates chloroplast division, and it serves as a scaffold for other chloroplast division proteins. Little is known, however, about the FtsZ protein subunit turnover within the Z-ring, the effects of accessory proteins on Z-ring turnover assemblies, as well as the *in vivo* ultrastructure of the Z-ring in plants. To investigate the *Arabidopsis thaliana* FtsZ subunit turnover rate within the Z-ring, a section of the Z-ring in the chloroplasts of living plants expressing fluorescently tagged FtsZ1 or FtsZ2 proteins was photobleached and the recovery rate was monitored. The results show that the

fluorescence recovery half times for the FtsZ1 and FtsZ2 proteins are 117s and 325s, respectively. This is significant as these data mirror their differences in GTP hydrolysis rates.

To elucidate *in vivo* structure and ultrastructure of the Z-ring, a protocol was established that maintained fluorescence during high pressure freezing, freeze substitution and low temperature embedding. Afterwards, a correlative microscopy approach was employed to visualize and identify fluorescently labeled puncta, circular structures, at the light microscopy level. These puncta were further resolved as mini-rings using optical microscopy eXperimental (OMX) superresolution microscopy. Electron microscopy (EM) analysis imaged mini-rings and filament assemblies comprised of dense subunits. Electron tomography (ET) showed mini-rings composed of protofilaments.

DEDICATION

To my parents, Uriah and Jessie, for their guidance, support, and encouragement. To my grandmother, Willie B., for her wisdom and for the joy that she has brought to my life. To my Uncle T.L. for encouragement, support and mentoring. To my siblings, nieces, and nephews for their support throughout this journey.

To my best friends, Stephanie Maeweather and Lilly Nguyen, who I thank for being there and for listening.

To Ashton and Auston Johnson, thank you for making me a better person.

To those family members who paved the way for me.

ACKNOWLEDGEMENTS

I would like to thank my advisor, Dr. Andreas Holzenburg for the opportunity to work in his lab and to contribute to the research; for his advice, support, encouragement, and guidance throughout my studies.

I also thank Dr. Stanislav Vitha for teaching and advising me throughout my studies and for his patience.

Special thanks to my committee members, Dr. Alan Pepper, Dr. Karl Aufderheide, and Dr. David Stelly for their insight, time, and encouragement.

I thank Dr. Jack McMahan for his recommendations, support and guidance and for the use of his laboratory equipment and other lab resources, he was instrumental in the completion of this project.

I thank Robert Marshall for his time, guidance, and patience.

I thank the staff of Microscopy and Imaging Center for all of their help.

Thank you to my past and current lab members: Dr. Christos Savva, Dr. Aaron Smith and Alvin Tang.

In addition, I thank Ginger Stuessy for her help with the plants and their maintenance and all of the laboratories and persons who supported me throughout this research with their resources.

NOMENCLATURE

ARC3	Accumulation and replication of chloroplast 3
ARC5	Accumulation and replication of chloroplast 5
ARC6	Accumulation and replication of chloroplast 6
arc	Accumulation and replication of chloroplast mutants
At	*Arabidopsis thaliana*
C-terminus	carboxyl terminus of a protein
Col-0	Columbia
ECL	Chemiluminescent detection
EM	Electron microscopy
ET	Electron tomography
FEG	Field emission gun
FRAP	Fluorescence recovery after photobleaching
FRET	Fluorescence resonance energy transfer
FP	Fluorescent protein
FS	Freeze Substitution
FtsZ	Filamentation temperature sensitive Z protein
FtsZ1	Filamentation temperature sensitive Z1 protein
FtsZ2	Filamentation temperature sensitive Z2 protein
ftsZ2-1	FtsZ 2-1 null mutant
ftsZ2-2	FtsZ 2-2 null mutant

GFP	Green fluorescent protein
GTP	Guanosine triphosphate
HAADF	High angle annular dark field
HPF	High pressure freezing
KO	Knockout
KD	Knockdown
Ler-0	Landsberg *erecta*
LM	Confocal laser scanning microscope
mCFP	Monomeric cyan fluorescent protein
MEMK6.5	Protein assembly buffer
Min	minute
MOLSCRIPT	A program for displaying 3D molecular structure
μm	micrometer
mYFP	Monomeric yellow fluorescent protein
nm	namometer
N-terminus	amino terminus of a protein
OMX	Optical microscope eXperimental
PAGE	polyacrylamide gel electrophoresis
PARC6	paralog of ARC6
Pb	Lead
PBS	Phosphate buffered saline
PDV1	PLASTID DIVISION 1

PDV2	PLASTID DIVISION 2
PPD	paraphenylenediamine
QFS	Quick freeze substitution
SDS	Sodium dodecyl sulfate
STEM	scanning transmission electron microscope
T_1	Transgenic line one
$t_{1/2}$	Half time to fluorescence recovery
TBST	Tris buffered saline plus tween 20
TEM	Transmission electron microscope
UA	Uranyl acetate
vol	Volume
wt	Weight
WS-0	Wassilewskija
WT	Wild-type

TABLE OF CONTENTS

Page

ABSTRACT iii

DEDICATION v

ACKNOWLEDGEMENTS vi

NOMENCLATURE vii

TABLE OF CONTENTS x

LIST OF FIGURES xii

LIST OF TABLES xiv

CHAPTER

I INTRODUCTION 1

- Chloroplasts 1
- Chloroplast Division 2
- FtsZ 3
- Chloroplast Division Proteins 7
- *Arabidopsis thaliana* 14
- Fluorescence 16

II DIFFERENTIAL TURNOVER DYNAMICS OF CHLOROPLAST DIVISION PROTEINS FTSZ1-1 AND FTSZ2-1 IN *ARABIDOPSIS THALIANA* 19

- Introduction 19
- Results 22
- Discussion 37
- Material and Methods 43

CHAPTER Page

III MAINTAINING SPECIFIC FLUORESCENCE IN *ARABIDOPSIS THALIANA* AFTER HIGH PRESSURE FREEZING, FREEZE SUBSTITUTION AND EMBEDDING 49

Introduction 49
Results 54
Discussion 60
Materials and Methods 65

IV USING CORRELATIVE MICROSCOPY TO EXPLORE FTSZ ASSEMBLY STRUCTURE 73

Introduction 73
Results 75
Discussion 80
Materials and Methods 81

V CONCLUSIONS AND FUTURE DIRECTIONS 87

Conclusions 87
Future Directions 88

REFERENCES 94

APPENDIX A 108

APPENDIX B 109

APPENDIX C 118

APPENDIX D 126

APPENDIX E 138

APPENDIX F 144

APPENDIX G 145

APPENDIX H 148

VITA 150

LIST OF FIGURES

FIGURE		Page
1	The four types of polymers formed by FtsZ in MEMK6.5, a protein assembly buffer	4
2	Schematic representation of the origin and evolution of the plastid FtsZ families	6
3	Co-localization of *At*FtsZ1-1 and *At*FtsZ2-1 rings revealed by immunofluorescence	8
4	Min proteins in *Escherichia coli* oscillate to assist in FtsZ-ring positioning	9
5	Model of the chloroplast division proteins	13
6	Scanning electron micrographs of starch granule containing amyloplasts from wild-type potato and transgenic lines GBSS-S04, GBSS-S12 and GBSS-S25.	15
7	Schematic drawing of the backbone of GFP produced by the program MOLSCRIPT. Schematic drawing of the overall fold of GFP	17
8	A timeline of major achievements in the improvement of fluorescent proteins	18
9	Complementation tests of FtsZ mutants	24
10	Immunoblot analysis of FtsZ1 and FtsZ2 protein in leaf extracts	28
11	Localization of FtsZ in leaf mesophyll chloroplasts by fluorescent tag expression	29
12	Localization of fluorescently tagged FtsZ1 and FtsZ2 in leaf mesophyll chloroplasts	30
13	FRAP analysis of FtsZ1-mYFP and FtsZ2-mYFP filament assembly dynamics in leaf epidermal chloroplasts	36
14	Stability FtsZ assemblies in chloroplasts	55

15 The chemical structure of 1-hexadecene 58

16 Fluorescence localization of mYFP-tagged FtsZ protein in leaf chloroplasts in whole-mount tissue and in resin sections after high pressure freezing and freeze substitution 61

17 QFS warming curve of high pressure frozen tissue 62

18 Cryovial set up QFS and SQFS 72

19 Correlative microscopy for FtsZ2-1-mYFP assemblies in *Arabidopsis* chloroplasts 77

20 Ultrastructure of FtsZ2-1-mYFP assemblies 78

21 0° tilt projection of an electron tomographic data set using scanning transmission microscopy 79

LIST OF TABLES

TABLE		Page
1	Components of the cytosolic and stromal plastid division machineries	12
2	Phenotypes of chloroplasts from the leaf mesophyll of FtsZ mutant T1 plants transformed with an FtsZ -GFP transgene.....	26
3	FtsZ subunit turnover dynamics in plants and bacteria	43
4	The effect of fixatives, dehydration solvents and lyses procedures on fluorescent signals in chloroplasts.....	56
5	Conventional, QFS-rapid, and QFS-gradual fixation procedures	70

CHAPTER I

INTRODUCTION

Chloroplasts

Plastids are proplastid-derived cellular organelles that originated in meristematic and other cells. These plastids divide and differentiate into specialized organelle types during differentiation and development to facilitate molecule storage or for specific activities within different cell types (Pyke, 1997; Pyke, 2007). In some cases, the names of these plastids are indicative of either the types of compound they store or their functions. For example, (i) amyloplasts store starch, (ii) chromoplast store pigments (iii) elaioplastids store oil and (iv) chloroplasts are the site of photosynthesis (Pyke, 2009) . In addition to their role in photosynthesis in plants and algae, chloroplasts are also involved in the synthesis of some amino acids, membrane lipids and enzyme cofactors (Osteryoung, 2011). These small (several microns in diameter) organelles are composed of a double membrane (inner and outer) envelope that isolates the stroma from the cellular cytosol. Chloroplasts evolved over 1.5 billion years ago during an apparent endosymbiotic event between a free-living photosynthetic cyanobacterium and a non-photosynthetic eukaryote (Douglas, 1998; Martin and Herrmann, 1998; McFadden, 1999a). Chloroplast evolution is consistent with Mereschkowsky's hypothesis that cyanobacteria are symbionts (Mereschkowsky, 1905).

This dissertation follows the style of Molecular Plant.

Chloroplasts are abundant in plant mesophyll cells (Pyke, 1998). They divide via binary fission to maintain adequate cellular levels during cell proliferation, and to produce smaller chloroplasts that are capable of phototaxis (Jeong et al., 2002; Leech et al., 1981; Osteryoung and Nunnari, 2003; Possingham and Lawrence, 1983).

Chloroplast Division

Chloroplast division is initiated and regulated by two nuclear encoded and plastid targeted prokaryotic homologs of the Filamentation temperature sensitive Z (FtsZ) protein (Miyagishima et al., 2004; Osteryoung and McAndrew, 2001; Osteryoung and Nunnari, 2003; Osteryoung et al., 1998b; Stokes and Osteryoung, 2003). Electron microscope (EM) observations provided the first glimpse into the ultrastructural events that occur during plastid division, which include the formation of a centrally located constriction site within dividing chloroplasts, as well as morphological changes within the plastid (Leech et al., 1981). Although the role of FtsZ in the formation of this constriction site has been established and will be discussed in detailed in the next section, its role in the generation of the force necessary for division is unknown.

Although little is known about the mechanism of constriction, an *in vitro* bacterial study demonstrated that the self-assembly of FtsZ into rings within liposomes provided the constriction force for division (Erickson et al., 2010; Osawa et al., 2008) which suggests that FtsZ is a force generator during division. During bacterial division, the energy from GTP hydrolysis of FtsZ protofilaments in conjunction with induced FtsZ conformational changes may be the generating force during division (Li et al., 2007; Lu

et al., 2000). However, the absence of a significant GTP-hydrolysis induced conformational change in the FtsZ-ring of chloroplasts suggests the existence of another constriction force generating mechanism has yet to be discovered (Olson et al., 2010; Smith et al., 2010). Dynamin, a GTPase, has been implicated as the generating force in the physical separation of daughter organelles at the conclusion of chloroplast division and is known to mediate vesicle fission in the cells of eukaryotes (Gao et al., 2003; Yoshida et al., 2006). Thus, the role of FtsZ in force generation during chloroplast division has yet to be determined. In view of the facts that bacterial FtsZ has been studied extensively and that chloroplast FtsZ originated evolutionary from bacteria, a comprehensive review of bacterial FtsZ will facilitate an improved understanding of chloroplast division.

FtsZ

FtsZ is a filament forming, self-assembling GTPase (Jaiswal et al., 2007; Lu et al., 2001; Margalit et al., 2004; Oliva et al., 2003; RayChaudhuri and Park, 1994). It is a bacterial homolog of tubulin. It is ubiquitous in bacteria, where it assembles into a Z-ring along the major axis of the cell during the early stages of cell division (Bi and Lutkenhaus, 1991). *In vitro* evidence has also shown that the bacterial FtsZ protein polymerizes into tubes and sheets (Figure 1) (Löwe, 1998). Addinall et al., (Addinall et al., 1996) found that FtsZ mutations in *Escherichia coli* inhibit cell division, which confirms that FtsZ is required for normal cell division.

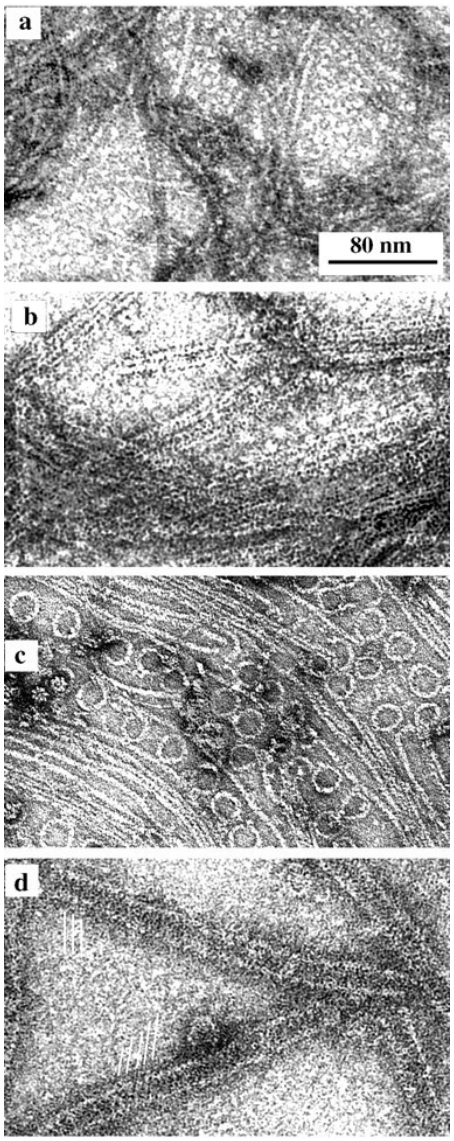

Figure 1. The four types of polymers formed by FtsZ in MEMK6.5, a protein assembly buffer. (a) Straight protofilaments formed with GTP but without DEAE-dextran; (b) sheets of straight protofilaments assembled from FtsZ plus DEAE-dextran; (c) minirings assembled with GDP and adsorbed onto a cationic lipid monolayer; (d) FtsZ tubes assembled with GDP and DEAE-dextran. The parallel white lines indicate the helical protofilaments in these tubes. Reprinted with permission from American Society for Microbiology (Lu et al., 2000).

The conserved N-terminal domain of FtsZ, where the Rossman fold, a protein structural motif for nucleotide binding, is formed, contains a tubulin signature motif, GGGTG (T/S) G where S represents either a G or C,
that is important for GTP binding (de Boer et al., 1992).The N-terminal domain also houses the T7 loop which is a part of the GTP hydrolysis active site (Scheffers et al., 2002). Even though the C-terminal core domain is conserved, it does contain a variable region. This region facilitates interactions between the FtsZ-ring and the membrane anchoring proteins during division (Ma et al., 2003).

The discovery of FtsZ in plants during a search to find prokaryotic cell division genes in the genomes of higher plants (Osteryoung and Vierling, 1995) provided powerful evidence in support of the endosymbiotic theory. Bacteria contain a single FtsZ gene and chloroplasts contain two phylogenetically distinct FtsZ gene families, FtsZ1 and FtsZ2. These two families evolved when a single FtsZ gene from the cyanobacterial endosymbiont was apparently transferred to the nucleus of the host cell and duplicated (Figure 2) (Miyagishima et al., 2004; Osteryoung et al., 1998b; Stokes and Osteryoung, 2003). The FtsZ1 family has one FtsZ gene product, FtsZ1-1 and the FtsZ2 family has two FtsZ gene products, FtsZ2-1 and FtsZ2-2 (Osteryoung et al., 1998a) all of which are chloroplast targeted (McAndrew et al., 2001; McAndrew et al., 2008). The FtsZ2 family of proteins is more similar to the bacterial FtsZ protein because they contain the conserved C-terminal motif (Osteryoung and McAndrew, 2001; Vaughan et al., 2004) while the FtsZ1family member does not have the C-terminal conserved motif (Figure 2). In *A. thaliana,* the members of the FtsZ2 family members are functionally redundant, as

illustrated by the findings that *At*ftsZ2-1 restored chloroplast division in *ftsz2-2* and likewise *At*ftsZ2-2 restored chloroplast division in *ftsz2*-1, as long as the total FtsZ2

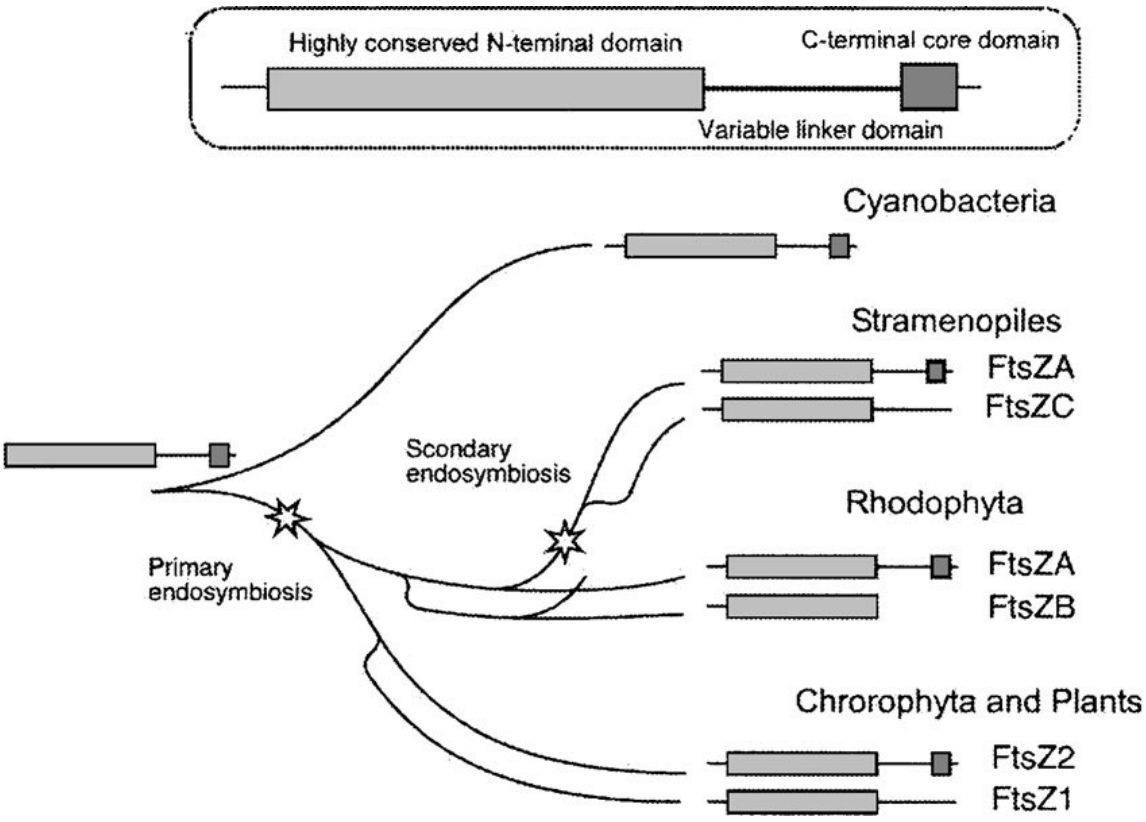

Figure 2. Schematic representation of the origin and evolution of the plastid FtsZ families. Reprinted with permission from Springer. (Miyagishima et al., 2004)

levels were near the typical FtsZ2 levels in WT (Schmitz et al., 2009). Hence the research focuses on FtsZ1-1 and FtsZ2-1. FtsZ1 and FtsZ2 have been shown to have

distinct non-redundant roles in chloroplast division (Osteryoung et al., 1998a; Schmitz et al., 2009).

The co-localization of FtsZ1 and FtsZ2 in the middle of the chloroplasts, at the division site on the stromal side of the plasma membrane to form a Z-ring (Vitha et al., 2001), was confirmed by double immunofluorescent labeling of the *At*FtsZ1-1 and *At*FtsZ2-1(Figure 3). *In vivo* bacterial studies have demonstrated that the Z-ring is dynamic (Anderson et al., 2004; Stricker et al., 2002) and Chapter II of this dissertation demonstrates the dynamic nature of the Z-ring in plants. The FtsZ1: FtsZ2 molar ratio in the stroma of *A.thaliana* chloroplast is 1: 2 (McAndrew et al., 2008). Z-ring morphology is affected by alterations in *At*FtsZ1-1 and *At*FtsZ2-1 levels (Osteryoung et al., 1998a; Stokes et al., 2000; Vitha et al., 2001). The Z-ring serves as a scaffold for the division machinery in bacteria (Goehring and Beckwith, 2005) and is thought to act as a recruitment and interaction site for chloroplast division proteins in plants.

Chloroplast Division Proteins

Several components of the division apparatus have been identified, and their discovery has contributed to a better understanding of the mechanisms involved in chloroplast division. This section will review some of those components. The spatial regulation and positioning of the Z-ring assembly is determined by the Min system proteins, and mutations in these proteins give rise to “minicells” (de Boer et al., 1989). This inhibitory system ensures that chloroplasts divide centrally along their long axis so

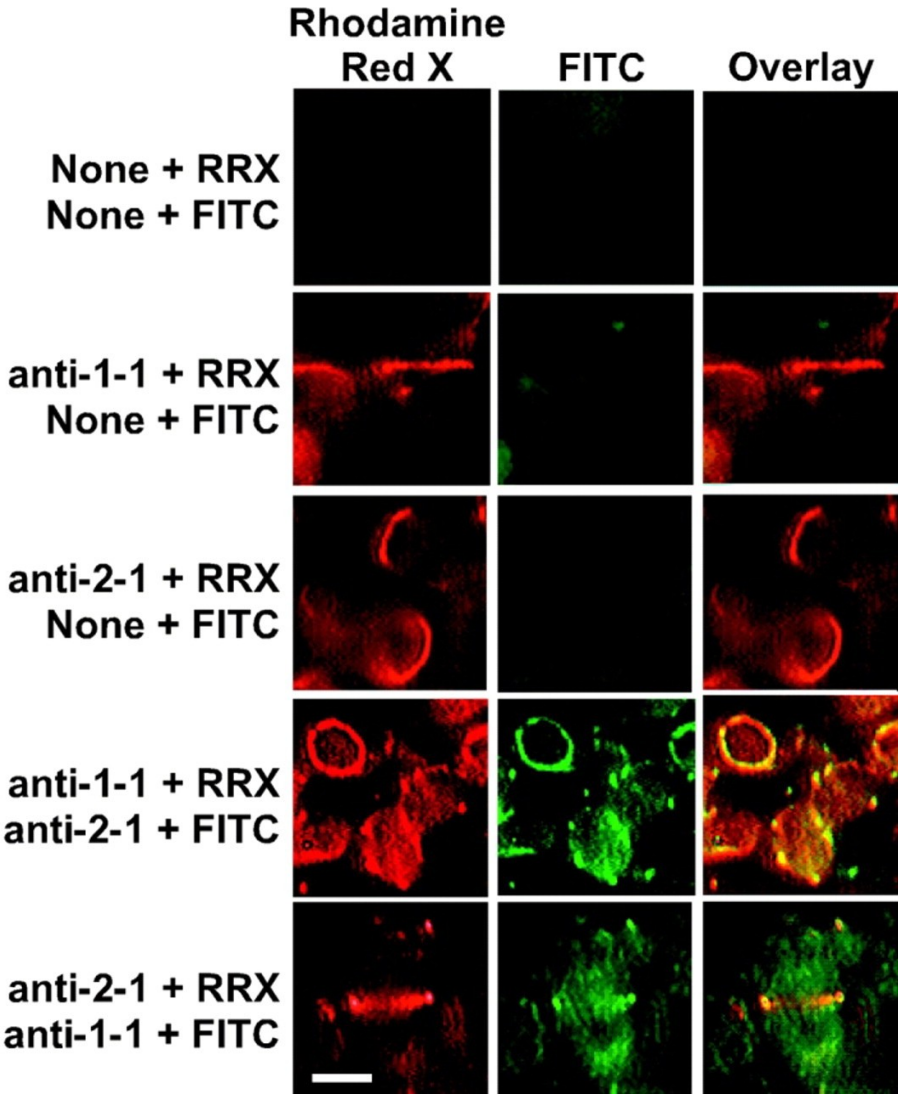

Figure 3. Co-localization of *At*FtsZ1-1 and *At*FtsZ2-1 rings revealed by immunofluorescence. Leaf sections from wild-type Arabidopsis plants were subjected to sequential, double immunofluorescence labeling of *At*FtsZ1-1 and *At*FtsZ2-1. The order of antibody application is indicated on the left. Tissue sections were incubated first with no antibodies (None), anti–*At*FtsZ1-1 antibodies (anti–1-1), or anti–*At*FtsZ2-1 antibodies (anti–2-1), followed by monovalent anti–rabbit antibody conjugated to Rhodamine red–X (RRX). Sections were then treated with no, anti–*At*FtsZ1-1, or anti–*At*FtsZ2-1 antibody, followed by anti–rabbit FITC conjugate. The labeled sections were viewed using FITC (green) and Texas red (red) filter sets. The yellow color in the overlay of the red and green signals indicates colocalization of *At*FtsZ1-1 and *At*FtsZ2-1. Bar, 2 μm. Reprinted with permission from (Vitha et al., 2001).

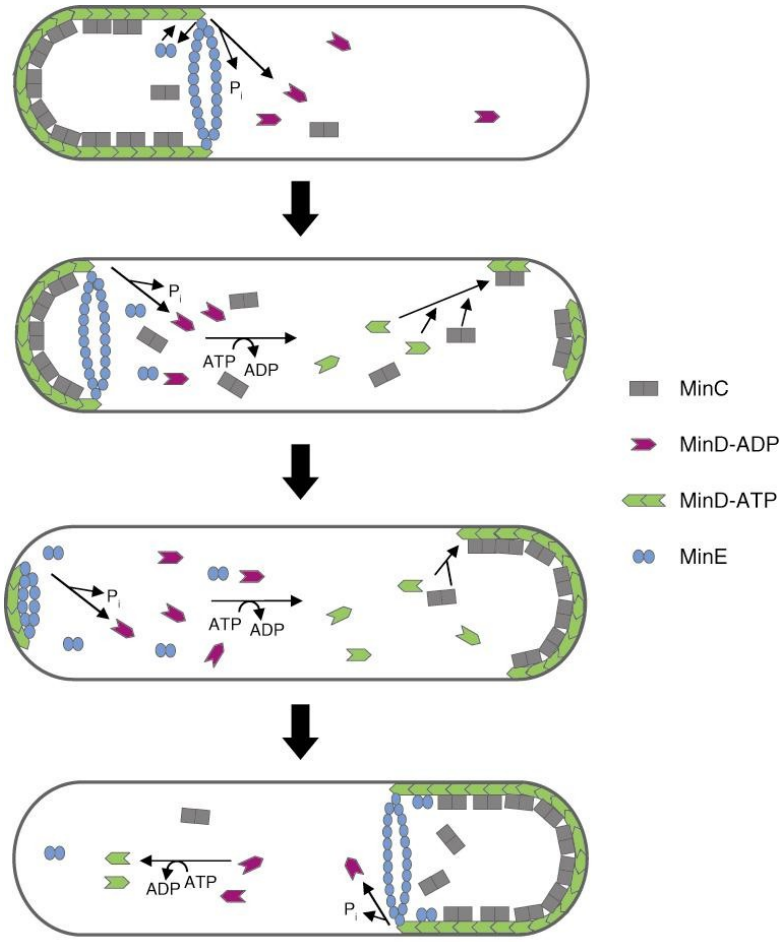

Lutkenhaus J. 2007.
Annu. Rev. Biochem. 76:539–62

Figure 4. Min proteins in *Escherichia coli* oscillate to assist in FtsZ-ring positioning. MinD-ATP binds to the membrane and recruits MinC. MinE displaces MinC and stimulates MinD ATPase, causing release of the proteins from the membrane. Whereas released MinE can immediately rebind to MinD on the membrane, the released MinD must undergo nucleotide exchange to regenerate MinD-ATP. In the model by Huang et al., the concentration of MinD-ATP in the vicinity of the old pole is lowered because it binds cooperatively to the membrane already containing bound MinD. In contrast, the MinD-ATP concentration increases at the other pole, which lacks bound MinD. As the concentration rises, it eventually binds, forming a new polar zone. As MinE is released from the old pole, it binds to the ends of the MinD polar zone. Reprinted with permission from American Chemical Society (Lutkenhaus, 2007).

that the end product is two equal daughter cells. The bacterial components of this system include MinCDE (Figure 4). Even though the Min CD complex is positioned at the poles (Shapiro and Losick, 2000) its swift oscillation from pole to pole (Raskin and de Boer, 1999a; Raskin and de Boer, 1999b) inhibits the mislocalization of the Z-ring. MinC interacts directly with FtsZ to thwart Z-ring localization at the poles (Hu et al., 1999). MinD is a GTPase that is required for MinC concentration (Hu et al., 1999; Marston and Errington, 1999). In *E. coli* MinE cycles rapidly between the poles where it undergoes rapid assembly and disassembly (Raskin and de Boer, 1999b). This dynamic process inhibits Min CD formation midcell by restricting MinCD activity (Fu et al., 2001; Hu and Lutkenhaus, 1999; Raskin and de Boer, 1999b; Rowland et al., 2000).

The Z-ring positioning system within the chloroplasts of plants contains many conserved homologs of the bacterial Min system. For example, the *A. thaliana* MinD and MinE genes are bacterial homologs (Glynn et al., 2007; Maple and Moller, 2007; Yang et al., 2008) that have been functionally characterized (Colletti et al., 2000; Fujiwara et al., 2004; Itoh et al., 2001). To date, no bacterial homolog of MinC has been identified in plants. The direct interactions between the *E. coli* FtsZ and MinC system and *At*FtsZ1 and ARC3 suggests that ARC3 may be a functional analog of MinC.

ARC3 is a plant-specific protein with similarity to prokayotic FtsZ (Shimada et al., 2004). It was first isolated when Pyke and others performed a mutant screen to identify plants containing a few large chloroplasts. ARC3 has been implicated in the regulation and positioning of the Z-ring and studies have shown that *arc3* mutants contain multiple Z-rings (Glynn et al., 2007). The mid-plastid localization (Shimada et al., 2004) and

FtsZ1 exclusive interactions (Maple et al., 2007) of ARC3 indicates that it may function in FtsZ1 positioning.

ARC6 is a homolog of the bacterial Ftn2 (Koksharova and Wolk, 2002). It is a transmembrane protein that interacts with the FtsZ2 Z-ring to stabilize the Z-ring during chloroplast division (Vitha et al., 2003). Homozygous *arc*6 mutants contain one large chloroplast and exhibit severe chloroplast division defects (Pyke and Leech, 1994).

PARC6 is an inner envelope protein that it unique to chloroplasts which appears to inhibit FtsZ assembly (Glynn et al., 2009). It has been shown to function in the positioning of PDV1to the cytosolic side of the chloroplast (Glynn et al., 2009).

ARC5 is a dynamin-like chloroplast division protein of eukaryotic origin (Gao et al., 2003) that is located mid-chloroplast on the cytosolic face of the chloroplast. ARC5 appears to be recruited to the division site late in division by PVD1 or PDV2 (Miyagishima et al., 2006). Homozygous *arc5* mutants (Pyke and Leech, 1994) have a characteristic dumbbell morphology because they become arrested in the final stages of chloroplast division and are unable to separate into two daughter cells. The algal homolog of ARC5, CmDnm2 may function in the force generation during chloroplast division (Yoshida et al., 2006).

PDV1 and PDV2 function in the recruitment of ARC5 (Miyagishima et al., 2006) to the chloroplast late in division. The PDV2-ARC6 interaction determines the positioning of PDV2 (Glynn et al., 2009). To date, no other role for either in chloroplast division had been identified.

Table 1. Components of the cytosolic and stromal plastid division machineries. Reprinted with permission from Elsevier (Maple and Moller, 2007).

Machinery	**Protein**	**Suborganellar localization**	**Evolutionary origin**	**Eukaryotic homologues**
Stromal	AtFtsZ1-1, AtFtsZ2-1	Ring associated with inner membrane	Cyanobacteria	Plants, green algae
	ARC6	Discontinuous ring; spans inner membrane	Cyanobacteria	Plants
	ARC3	Ring and polar loci	Cyanobacteria	Plants
	AtMinE1	Polar loci	Cyanobacteria	Plants, green algae
	AtMinD1	Polar loci	Cyanobacteria	Plants, green algae
	GC1 (AtSulA)	Associated with inner membrane	Cyanobacteria	Plants, green algae
	Inner plastid division ring	Ring localized to inner envelope	Components unknown	Components unknown
Cytosolic	ARC5	Cytosolic patches; ring associate with outer envelope	Eukaryotic	Plants
	PDV1	Transmembrane protein; ring associate with outer envelope	Eukaryotic	Plants
	PDV2	Predicted transmembrane protein; ring associate with outer envelope	Eukaryotic	Plants
	Outer plastid division ring	Ring localized to outer envelope	Components unknown	Components unknown

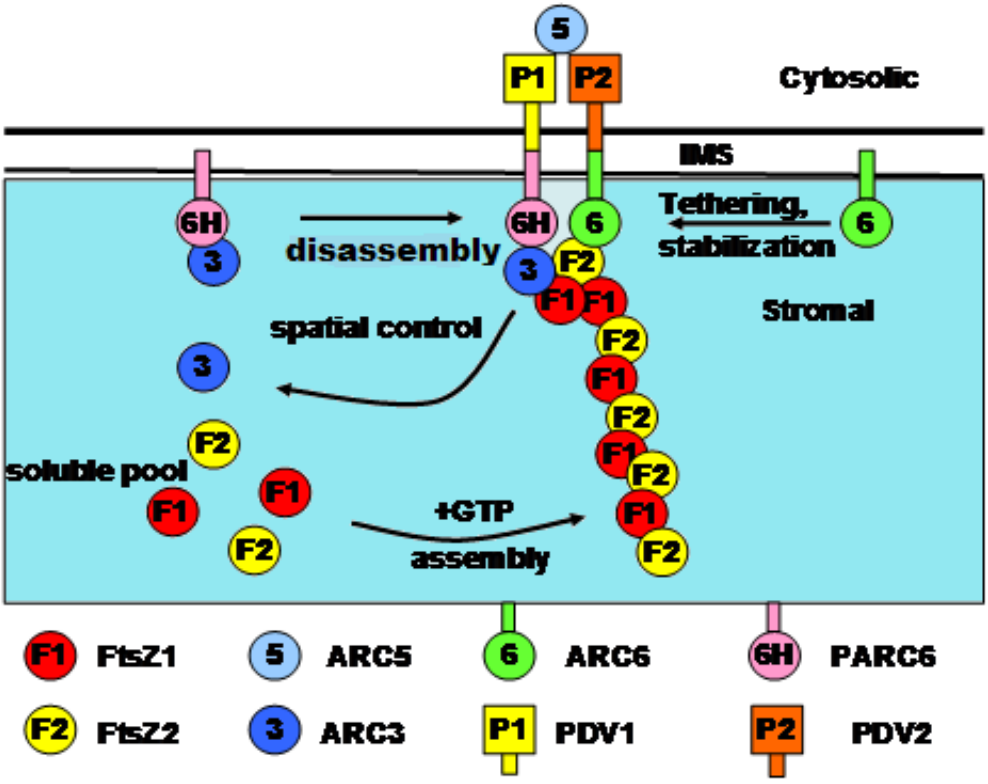

Figure 5. Model of the chloroplast division proteins. FtsZ1(red) and FtsZ2 (yellow) assemblies mid-chloroplast. The localization of the FtsZ proteins initiates the interaction of other division proteins.

The chloroplast division machinery has to orchestrate the complex assembly of stromal and cytosolic proteins across a double membrane envelope (Table 1). From an evolutionary standpoint, the prokaryotic and eukaryotic origins of the division machinery proteins indicates its complexity. Current models indicate that the assembly of the FtsZ1 and FtsZ2 into a Z-ring (McAndrew et al., 2001; Vitha et al., 2006; Vitha et al., 2001) initiates a cascade of localization and assembly events between other

essential chloroplast division proteins such as ARC3, ARC5, ARC6, PARC6 and PDV1 as well as PDV2 (Figure 5).

Analysis and understanding of plastid division proteins and their mechanism of action bears agricultural impact as it is thought that the ability to manipulate plastid size will result in control over starch granules dimensions. For example, FtsZ proteins have been shown to play a role in determining amyloplast size and in turn, starch granule size in potatoes (Figure 6) (de Pater et al., 2006). This is of commercial importance because control of starch granule size can translate into increases in wet-milling efficiency and starch yield improvements in the order of $280 million per year (Gutierrez et al., 2002).

Arabidopsis thaliana

Arabidopsis, a small weed, is a member of the Brassicaceae and was discovered in the sixteenth century by Johannes Thal. In 1943 while describing his research findings, Laibach noted that *Arabidopsis* (i) has a short generation time, (ii) is easily crossed and (iii) is amenable to mutagenesis. Based on those findings, he recommended that it be categorized as a model organism (Meyerowitz, 2001). This plant has only five chromosomes - they have all been mapped. The life cycle of the *At* WT Col-O ecotype is approximately eight weeks from seed germination to flowering (Boyes, 2001). It is geographically distributed throughout the Northern Hemisphere, but its native range includes Northwest Africa, Europe and Asia. The three most common ecotypes used for experimentation are Landsberg *erecta*, Columbia, and Wassilewskija.

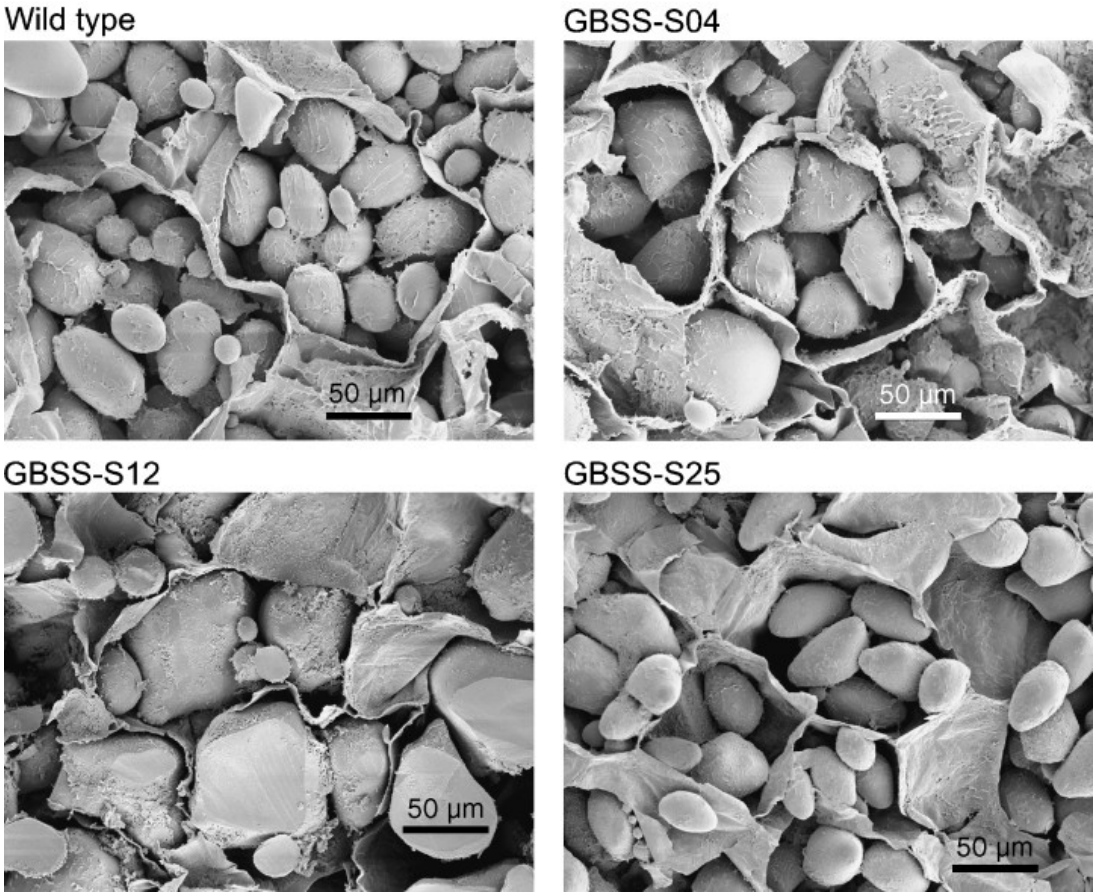

Figure 6. Scanning electron micrographs of starch granule containing amyloplasts from wild-type potato and transgenic lines GBSS-S04, GBSS-S12 and GBSS-S25. The scale bars are 50 µm. GBSS, granule-bound starch synthase. Reprinted with permission from John Wiley and Sons (de Pater et al., 2006).

Arabidopsis has been useful in isolating *arc* mutants and these mutants have aided the design of a working model of chloroplast division (Pyke and Leech, 1994). These *arc* mutants are useful when testing models and understanding the mechanism of chloroplast division. Genes can be introduced and expressed in the *Arabidopsis* genome via *Agrobacterium*-mediated transformation (Clough and Bent, 1998).

Fluorescence

Fluorescent proteins such as green fluorescent protein (GFP) have been used to label proteins in living cells and organisms. GFP was first isolated from the jellyfish, *Aequorea victoria* (Shimomura et al., 1962). This 238 amino acid protein is encoded by a single gene and contains a chromophore that is composed of modified amino acid residues (Ser 65-Tyr 66-Gly 67) (Prasher et al., 1992). The chemical structure of the fluorescence emitting chromophore was first characterized in 1979 (Shimomura, 1979). The fluorescent protein is composed of eleven β strands that form a barrel around the chromophore (Figure 7) (Ormo et al., 1996). Fluorescence detection is dependent on protein folding and chromophore maturation (Chudakov et al., 2010). GFP is a stable protein that has been introduced into cells of various species for *in vivo* labeling. For example, the protein product from complementary DNA of the *Aequorea victoria* GFP was shown to fluoresce in *E. coli* and *Caenorhabditis elegans* cells when excited with blue light (Chalfie et al., 1994). Two absorption maxima at 395 nm and 475 nm and a single emission maxima at 509 nm was observed in both of the expressed cell types and in the purified native protein (Chalfie et al., 1994; Ormo et al., 1996). Based on this information it was proposed that GFP would be a useful tool for gene expression and protein localization (Chalfie et al., 1994; Luby-Phelps et al., 2003; Vitha et al., 2006; Vitha et al., 2001). GFP variants with altered absorption and emission spectra and enhanced brightness have been shown to improve fluorescence (Heim et al., 1995; Kirk et al., 2011). The determination of the crystal structure of GFP (Ormo et al., 1996), the discovery of additional GFP-like proteins in other organisms, and the identification of

variants and homologs all contributed to the expansion of the fluorescent protein color palette (Figure 8) (Heim et al., 1995; Shaner et al., 2004; Shaner et al., 2007).

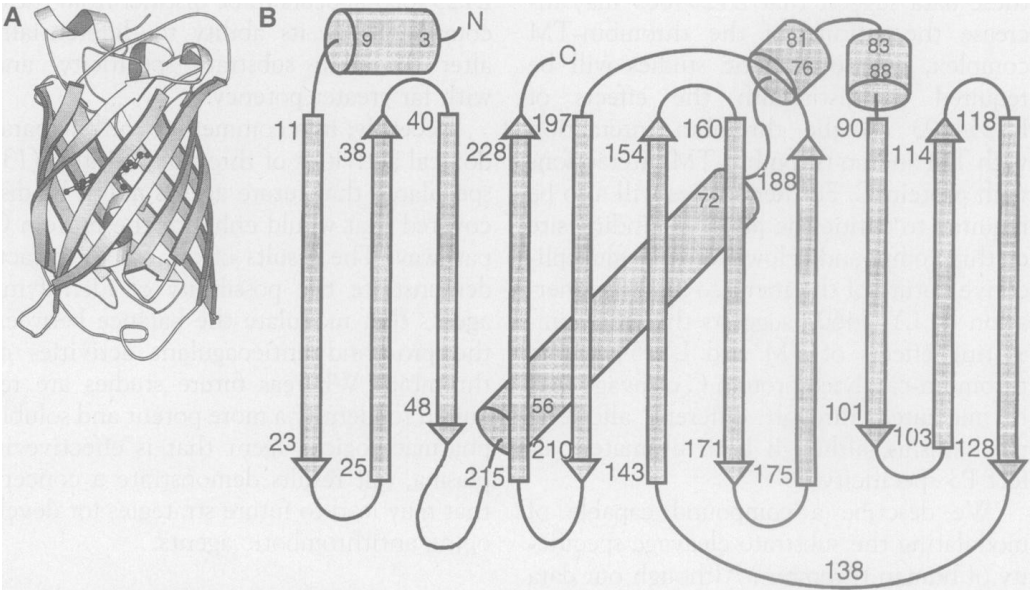

Figure 7. (A) Schematic drawing of the backbone of GFP produced by the program MOLSCRIPT (32). The chromophore is shown as a ball and stick model. (B) Schematic drawing of the overall fold of GFP. Approximate residue numbers mark the beginning and ending of the secondary structure elements. N, NH2-terminus; C, COOH-terminus. Reprinted with permission from The American Association for the Advancement of Science (Ormo et al., 1996).

Fluorescent proteins can be used for a wide array of applications that include protein tagging, as was first demonstrated by Chalfie in 1994 (Chalfie et al., 1994). Protein

mobility studies using FRAP techniques (Lippincott-Schwartz et al., 2003), super-resolution microscopy (Hell et al., 2004), bimolecular fluorescence complementation (Kerppola, 2008), and monitoring protein conformations and interactions using FRET (Miyawaki and Tsien, 2000) are all possible applications of GFP technology.

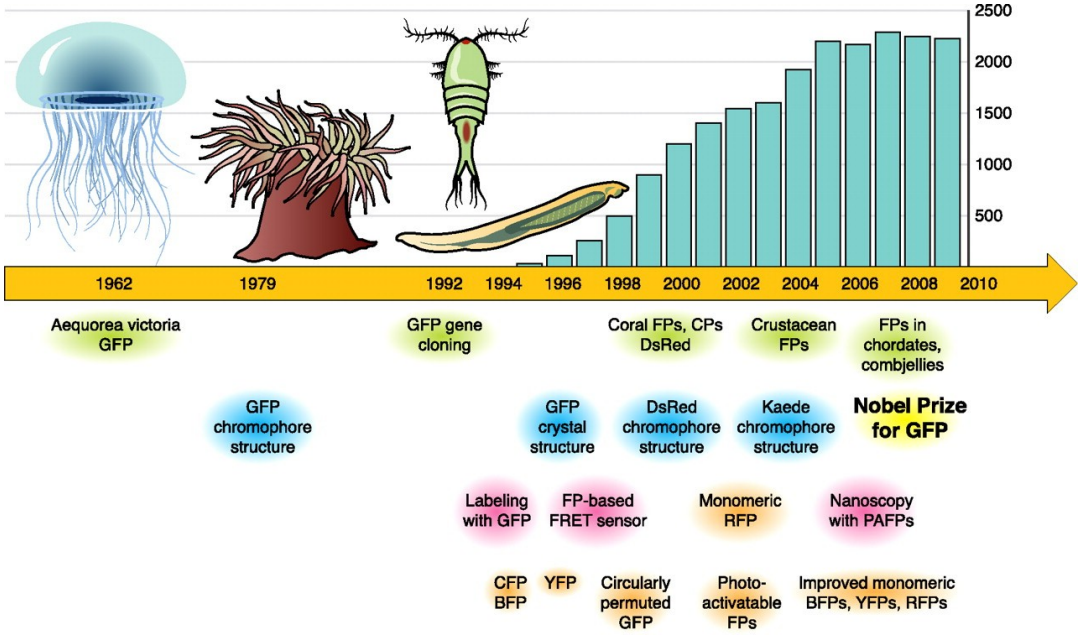

Figure 8. A timeline of major achievements in the improvement of fluorescent proteins. Green color below the text highlights basic studies of natural diversity of green fluorescent protein (GFP)-like proteins; blue, structural insights; orange, development of novel fluorescent protein (FP) variants; magenta, appearance of FP-based technologies. Drawings of representative animals having FPs are shown above the timeline (from left to right: jellyfish, sea anemone, copepod, and lancelet). Columns above the timeline show the number of scientific articles per corresponding year that can be found searching PubMed with the term green fluorescent protein (this search is not comprehensive but reflects the general dynamics of publications on fluorescent proteins). Reprinted with permission from Physiological Reviews (Chudakov et al., 2010).

CHAPTER II

DIFFERENTIAL TURNOVER DYNAMICS OF CHLOROPLAST DIVISION PROTEINS FTSZ1-1 AND FTSZ2-1 IN *ARABIDOPSIS THALIANA*

Introduction

Plastids such as chloroplasts arose over 1.5 billion years ago as a result of an endosymbiotic event between a cyanobacterium and a non-photosynthetic eukaryote (Douglas, 1998; Martin and Herrmann, 1998; McFadden, 1999b). Chloroplasts are the site of photosynthesis in plants and are composed of an outer and an inner membrane which surrounds a large space known as the stroma. Chloroplasts divide via binary fission to maintain adequate organellar numbers during cell division and to produce smaller chloroplasts that are capable of phototaxis (Leech et al., 1981; Osteryoung and Nunnari, 2003; Possingham and Lawrence, 1983; Spriet et al., 2008). This division process is initiated and regulated by the nuclear-encoded and plastid-targeted Filamentation temperature sensitive Z (FtsZ) proteins (Glynn et al., 2007; Maple and Moller, 2007; Miyagishima, 2011; Miyagishima and Kabeya, 2010; Miyagishima et al., 2004; Osteryoung, 2001; Osteryoung and Nunnari, 2003; Osteryoung and Pyke, 1998; Stokes and Osteryoung, 2003). The FtsZ protein was first discovered in bacteria where it is essential for cell division (Bi et al., 1991). The prokaryotic FtsZ is a tubulin homolog GTPase (Jaiswal et al., 2007; Lu et al., 2001; Margalit et al., 2004; Oliva et al., 2003; RayChaudhuri and Park, 1994) that assembles into a ring (Z-ring) and acts as a

scaffold for the division machinery in bacteria (2002; Larsen et al., 2007). FtsZ in the Z-ring assembly may also provide the contractile force during cell division in bacteria (Erickson et al., 2010; Ghosh and Sain, 2008; Ghosh and Sain, 2011; Osawa et al., 2008).

The discovery of nuclear-encoded chloroplast targeted FtsZ in plants (Osteryoung and Vierling, 1995) provided powerful evidence in support of the endosymbiotic theory. The single FtsZ gene from the cyanobacterial endosymbiont was transferred to the nucleus of the host cell, apparently underwent gene duplication, and evolved into two gene families, FtsZ1 and FtsZ2 in plants (Miyagishima et al., 2004; Osteryoung et al., 1998b; Stokes and Osteryoung, 2003).FtsZ1 has one family member (*At*FtsZ1-1) and FtsZ2 has two family members *(At*FtsZ2-1, 2-2) that share 83% amino acid sequence identity and have redundant functions (Osteryoung et al., 1998b; Schmitz et al., 2009). Henceforth the terms FtsZ1 and FtsZ2 will refer to *At*FtsZ1-1 and *At*FtsZ2-1, respectively. FtsZ1 and FtsZ2 have been shown to have distinct non-redundant roles in chloroplast division (Osteryoung et al., 1998b; Schmitz et al., 2009). FtsZ proteins play a role in determining amyloplast size and in turn, starch granule size in crop plants (de Pater et al., 2006).

Prior to chloroplast division, the FtsZ proteins co-localize mid-chloroplast on the stromal side of the chloroplast membrane to form the Z-ring (Vitha et al., 2001). Alterations in FtsZ1 and FtsZ2 levels within the chloroplast lead to defects in both Z-ring formation and chloroplast division (Kiessling et al., 2000; McAndrew et al., 2001; Osteryoung et al., 1998b; Stokes et al., 2000; Yoder et al., 2007). The Z-ring serves as a

site for the interactions between Z-ring localized FtsZ proteins and accessory proteins during chloroplast division. These are important because specific interactions are vital for the maintenance of chloroplast division (Glynn et al., 2009; Maple and Moller, 2007). The Z-ring is a dynamic structure and undergoes subunit exchange from the continued polymerization and depolymeration of the component FtsZ subunits. *In vivo* and *in vitro* studies showed Z-ring subunit exchange rates in *E. coli* to be 8s (Anderson et al., 2004) and 10s (Srinivasan et al., 2008), respectively. In addition, the *in vivo* subunit turnover rate within the Z-ring of *Bacilus subtilis* was determined to be 9s (Anderson et al., 2004). Although the dynamic nature of the Z-ring has been shown in bacteria, there is little information about the Z-ring protein dynamics within the chloroplasts of higher plants and the effect that the accessory proteins may have on the Z-ring subunit exchange rate. In plants, FtsZ turnover rates can be coupled with GTPase activity assays (Olson et al., 2010; Smith et al., 2010) in order to determine if there is a correlation between FtsZ subunit turnover and FtsZ GTPase activity. To date, the lack of functional fluorescently tagged FtsZ proteins expressed inside the chloroplasts of plant tissue at levels that do not greatly alter the FtsZ1 and FtsZ2 chloroplast stoichiometric ratios and the absence of transgenic plant lines containing FtsZ tagged monomeric fluorescent proteins that have a minimum likelihood of protein dimerization which could interfere with the FtsZ protein function (Zacharias et al., 2002) have likely hindered the research. In this study we [1] determine the *in vivo* FtsZ1 and FtsZ2 subunit turnover rates within the Z-ring of *A. thaliana* chloroplasts, [2] demonstrate that FtsZ1 fluorescently tagged proteins complement null mutants and [3] show that fluorescently

labeled FtsZ1 and FtsZ2 proteins form Z-ring assemblies when the fluorescent protein fusion is expressed at levels comparable or lower than those of WT. We hypothesize that high FtsZ expression in transgenics will cause artifactual assembly characteristics.

Results

AtFtsZ1 Null Mutants Were Complemented by AtFtsZ1-FP Constructs but AtFtsZ2 Null Mutants Were Not Complemented AtFtsZ2-FP

Establishing the functionality of fluorescently tagged FtsZ proteins was necessary before future experiments could be conducted because the presence of a fluorescent protein (FP) tag could either inhibit the function of the protein or cause its performance to differ from that of the intrinsic protein.

Initial complementation assays we performed using *At*FtsZ1-GFP and *At*FtsZ2-GFP (Vitha et al., 2001) plants that were on hand. The FtsZ1-GFP constructs were able to complement the *Arabidopsis ftsZ1* knockout (KO), SALK073878 (Alonso et al., 2003), plants but the *At*FtsZ2-GFP constructs were not able to complement FtsZ2-1 knockdown (KD), SALK134970 (Alonso et al., 2003), mutants. To ensure that the fluorescent protein was not dimerizing and interfering with the function of the FtsZ protein (Zacharias et al., 2002), we designed *At*FtsZ1 and *At*FtsZ2 monomeric yellow protein, mYFP, and monomeric cyan fluorescent protein, mCFP, constructs under the control of their native promoters. The *At*FtsZ1-mFP constructs were transformed via *Agrobacterium*-mediated transformation (Clough and Bent, 1998) into SALK_073878

plants and the *At*FtsZ2-mFP constructs were transformed using the same method into SALK_134970 and *ftsZ2-1/ftsZ2-2* double KO plants.

Light microscopy analysis of FtsZ1 T1 leaf mesophyll chloroplasts revealed that both the mFP and GFP version of FtsZ1 constructs were able to rescue the null mutant phenotype (Figure 9A). Phenotypes were categorized as "mutant-like" when the chloroplast contained 1 to 5 large chloroplasts per cell, "intermediate" for 6 to 20 oversized chloroplasts per cell, and "wild-type-like" for 30 to 60 chloroplasts per cell. The distribution for the FtsZ1-GFP T1 expressed in FtsZ1-1 null mutant background plants expressing mutant-like, intermediate, and wild-type-like phenotypes were 59%, 38%, and 3%, respectively (Table 2). The FtsZ1- mFP phenotype distributions in T1 plants were 16%, 62%, and 22% for mutant-like, intermediate, and wild-type like phenotypes, respectively (Table 2). Approximately, 41% of FtsZ1-GFP and 84% of FtsZ1-mFP proteins had phenotypes more similar to intermediate or wild-type-like. This indicates that the fluorescent protein does not inhibit the function of FtsZ1.

Additionally, phenotypic analysis of FtsZ2-GFP and FtsZ2-mFP constructs in the FtsZ2-1 KD and FtsZ2 double- KO backgrounds revealed that 100% of the T1 plant chloroplasts for both constructs have mutant-like phenotypes (Table 2). Neither the GFP tagged nor the mFP tagged FtsZ2 proteins were able to restore chloroplast division in the FtsZ2-1 KD background (Figure 9A) or in the FtsZ2 double -KO background (Figure 9A) as indicated by the absence of intermediate and wild-type like chloroplast phenotypes (Table 2). This signifies that the tagged FtsZ2 protein is not fully functional.

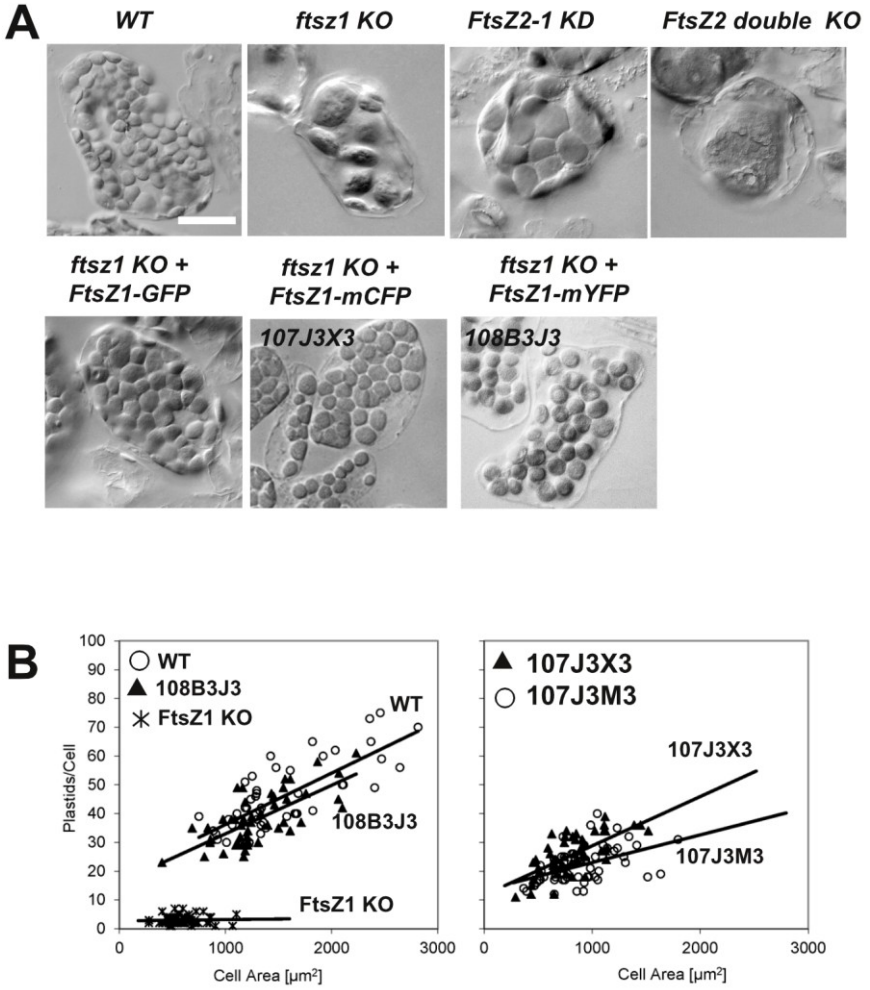

Figure 9. Complementation tests of FtsZ mutants. A) Chloroplast phenotypes in a leaf mesophyll cell in wild-type (WT), FtsZ1 knock-out (FtsZ1 KO), FtsZ2-1 knock-down (FtsZ2-1-KD), FtsZ2-1/FtsZ2-2 double knock-out (FtsZ2 double KO) and transgenic FtsZ1 KO plants expressing at low- to moderate levels FtsZ1 tagged with either GFP, mCFP or mYFP. Bar = 20 µm. B) Quantitative analysis of chloroplast numbers in leaf mesophyll cells. Numbers of chloroplasts/cell are plotted relative to the cell area. Shown are three different transgenic lines, expressing either FtsZ1-mCFP (107J3M3, 107J3X3) or FtsZ1-mYFP (108B3J3). R-squared values for the linear regression lines, and the probability value *P* of the F-test in ANOVA are as follows: WT (R^2=0.58; Significance F = 4.68 x10^{-8}), FtsZ1 KO (0.002; 0.73), 108B3J3 (0.49; 5.28 x10^{-8}), 107J3M3 (0.23; 2.08 x10^{-4}), 107J3X3 (0.45; 4.69 x10^{-8}). *P*-values below 0.01 indicate that the linear regression is highly significant.

Quantitative analysis showed that there was a strong correlation between chloroplasts and mesophyll cell area for the wild-type (R^2=0.58) and for the FtsZ1-mYFP (108B3J3) (R^2=0.49) transgenic plant line. A best-fit line of the plotted data showed that this particular FtsZ1-mYFP transgenic line restored chloroplast division to a level that closely paralleled that of WT and that the null mutant was fully complemented (Figure 9B). A best-fit line of the FtsZ1-mCFP lines (107J3M3 and 107J3X3) showed that although there was a positive correlation between the number of chloroplasts and the mesophyll cell area expansion for both, their slopes (R^2= 0.23 and 0.45, respectively) were less than that of WT (Figure 9B). These values indicate that partial complementation occurred in these two lines. The F-test in ANOVA *P*-values for the three transgenic lines (107J3M3, 107J3X3,108B3J3) and the WT are highly significant as indicated by their values of 2.08 $x10^{-4}$, 4.69 $x10^{-8}$, 5.28 $x10^{-8}$, 4.68 $x10^{-8}$, respectively. The F-test in ANOVA *P*-value of 0.73 for the FtsZ1 KO was not significant.

FtsZ Expression Levels Vary in Transgenic Plant Lines

FtsZ fluorescent protein fusion constructs expressed under the control of their native promoters in order to minimize chloroplast division defects caused by overexpression (Stokes et al., 2000) designed in our laboratory and those previously constructed (Vitha et al., 2001) were used in this study. The transgenic plant lines were produced in WT, FtsZ1 KO and FtsZ2 double-KO backgrounds and their FtsZ expression levels were determined by immunoblotting leaf extracts from these lines and comparing their expression to immunoblots from wild-type leaf extracts.

Table 2. Phenotypes of chloroplasts from the leaf mesophyll of FtsZ mutant T1 plants transformed with an FtsZ -GFP transgene.

Genetic Background	Transgene	Plastid #/phenotype		
		1-5	6-15	30+
FtsZ1-1 null mutant	FtsZ1-1GFP	37	24	2
	FtsZ1-1mCFP	4	10	4
	FtsZ1-1mYFP	2	13	4
FtsZ2-1 knockdown	FtsZ2-1GFP	20	0	0
FtsZ2 double knockout	FtsZ2-1mCFP	38	0	0
	FtsZ2-1mYFP	34	0	0

Endogenous *At*FtsZ1 expression levels were used as the control for these experiments (Figure 10A, lane 1). No FtsZ1 was detected in the *ftsZ*1 knockout mutants. Although the immunoblot showed undetectable FtsZ1-mYFP expression levels (Figure 10A, lane 4), the fusion protein complemented the null mutant (Figure 9A) and localized into a ring mid-chloroplast (Figure 11B). The 1-1 antibody recognized moderate FtsZ1-mCFP expression at ~75 kDa in the FtsZ1 null mutant complemented line (Figure 10A, lane 5) and chloroplast numbers (20-25) for this transgenic protein were slightly below wild-type (30 plus) in the mesophyll cells of these transgenic plants during phenotype analysis (Figure 9B). The intrinsic FtsZ1 protein of ~42 kDA and the transgenic FtsZ1 protein of ~73kDa in FtsZ1-GFP (Figure 10A, lane 3) and –mYFP (Figure 10A, lane 11) expressed in wild-type backgrounds were detected on the immunoblot and the transgenics had expression levels were close to WT (Figure 9A). Rings were observed in the epidermal

cells and centralized localization patterns were observed in the mesophyll cells of these mYFP fusion proteins (Figure 11D and Figure 12B). Endogenous FtsZ1 protein levels in the FtsZ2-1KD (Figure 10A, lane 6), the FtsZ2 double KO (Figure 10A, lane 8) and the FtsZ2 double KO + FtsZ2-mYFP (Figure 10A, lane 9 and lane 10), and the FtsZ2-mYFP + WT (Figure 10A, lane 12) were all considerably higher than in the WT FtsZ1, which indicated that alterations in the FtsZ2 levels affected the FtsZ1 levels in these plants. In the FtsZ2-KD and FtsZ2-mYFP + WT plants, elevated FtsZ1 levels did not seem to affect Z-ring localization of chloroplast morphology (Figure 11C and Figure 12C). Grossly enlarged mesophyll chloroplasts containing an abundance of puncta and filaments of the FtsZ2-mYFP construct (Figure 12D, inset) were observed in some of the FtsZ2 double KO + FtsZ2-mYFP. Another observation within a different region of the same plant showed larger mesophyll chloroplasts containing a few filaments and dumbbell-shaped filament containing epidermal chloroplasts (Figure 12E).

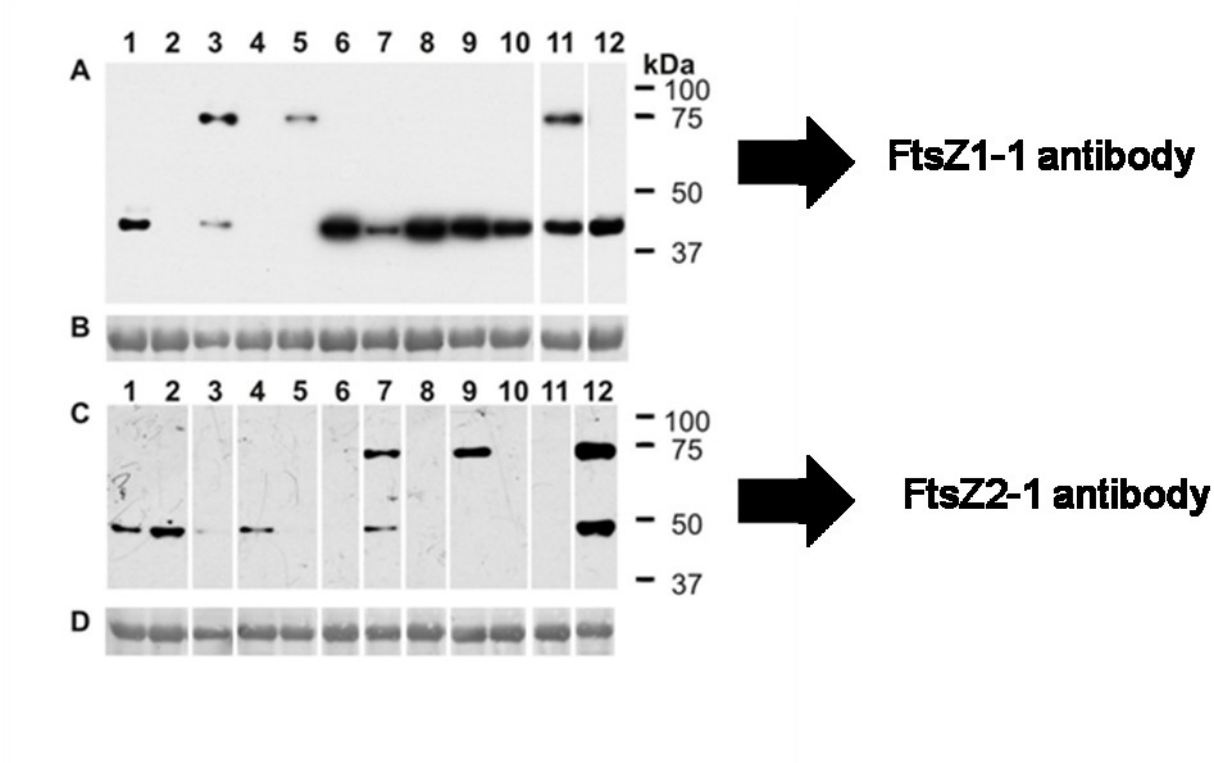

Figure 10. Immunoblot analysis of FtsZ1 and FtsZ2 protein in leaf extracts. Immunoblot (A) was probed with FtsZ1-1 antibody and immunoblot (C) was probed with FtsZ2-1 antibody. Gel loading was normalized to equal amount of total protein, based on the Coomassie-stained gel. Extracts from approximately 1 mg fresh-weight of tissue were loaded per lane. A, C) Lanes 1) WT, 2) FtsZ1 KO, 3) WT+FtsZ1-GFP overexpressor, 4) FtsZ1 KO + FtsZ1-mYFP expressed at very low levels, 5) FtsZ1 KO + FtsZ1-mCFP, with WT-like chloroplast division, 6) FtsZ2-1 KD, 7) WT + FtsZ2-1-GFP, 8) FtsZ2 double KO, 9, 10) FtsZ2 double KO + FtsZ2-mYFP, 11) WT + FtsZ1-mYFP, 12) WT + FtsZ2-mYFP. B, D) Equal loading was confirmed by Ponceau-S staining of the membrane after transfer. The ~50 kDa RuBisCo band is shown in the bottom panel. All lanes are from the same immunoblot, irrelevant lanes were deleted as indicated by the white gaps between lanes. The approximate molecular mass is indicated on the right.

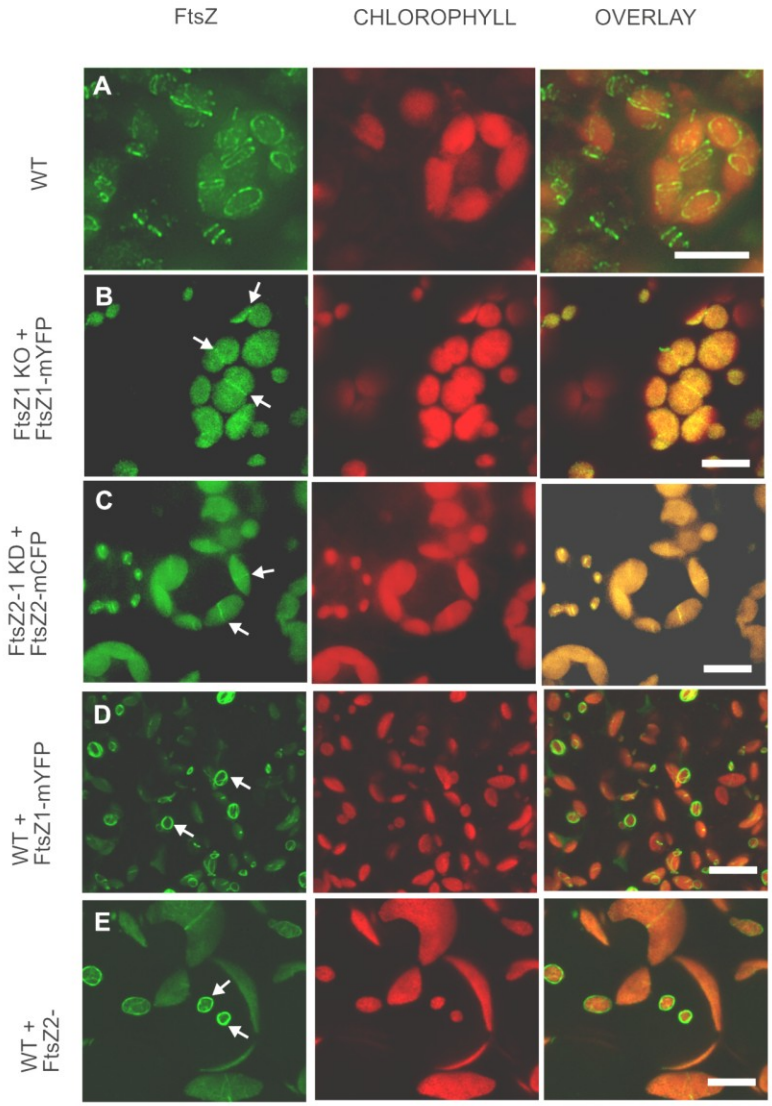

Figure 11. Localization of FtsZ in leaf mesophyll chloroplasts by fluorescent tag expression. Fluorescence of mYFP or mCFP –tagged FtsZ is shown in the green channel, chlorophyll autofluorescence in the red channel. FtsZ localization in the wild-type chloroplasts was achieved by immunofluorescence labeling with anti-FtsZ1 antibodies. A) Wild type; B) FtsZ1-null mutant complemented by FtsZ1-mYFP shows relatively weak fluorescence signal, localized to the division site (arrows). C) FtsZ2-mYFP expressed at low levels in the FtsZ2-1- knock-down background is localized to Z-rings at mid-chloroplast (arrows). D) FtsZ1-mYFP in WT background expressed at low levels forms Z-rings in the small epidermal chloroplasts (arrows), while the fluorescence signal in mesophyll chloroplasts is not discernible. E) FtsZ2-mYFP in WT background at low levels shows similar localization as in D). Scale bar = 10 µm.

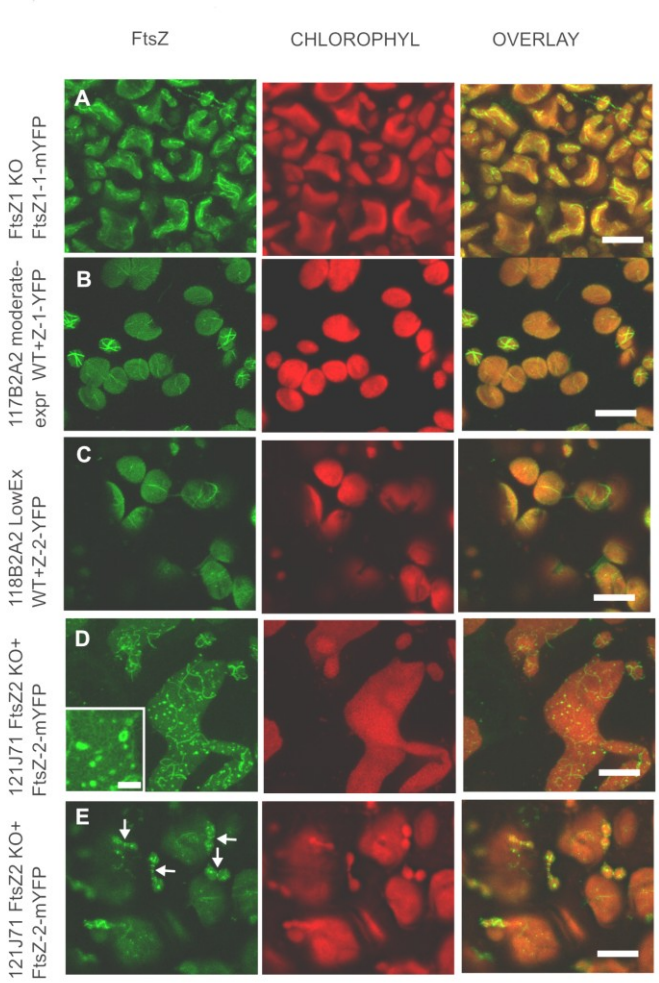

Figure 12. Localization of fluorescently tagged FtsZ1 and FtsZ2 in leaf mesophyll chloroplasts. Fluorescence of FtsZ-mYFP (green channel), chlorophyll autofluorescence (red channel) and a color overlay of the fluorescent channels are shown. A) Aberrant FtsZ localization in FtsZ1-null mutant with high expression of FtsZ1-mYFP; B) A plant with with moderate expression of FtsZ1-mYFP in WT background. Mid-plastid localization of FtsZ1-mYFP in mesophyll cells, aberrant localization in epidermal chloroplasts. C) A plant with low- to moderate expression of FtsZ2-mYFP in WT background. Mid-plastid localization of FtsZ2-mYFP in mesophyll chloroplasts. D) FtsZ2 double KO mutant with high expression of FtsZ2-mYFP. Both linear and circular assemblies are present. E) FtsZ2 double KO mutant with moderate to expression of FtsZ2-mYFP. Small dumbbell-shaped epidermal chloroplast show FtsZ2-mYFP signal at the constriction site (arrows), in addition to FtsZ assemblies elsewhere. Scale bar = 10 µm, except for the inset in D), where it represents 2 µm.

The FtsZ2 protein expression levels in *ftsZ*1 knockout mutants (Figure 10C, lane 2) were approximately twice that of the WT (Figure 9C, lane 1). The barely detectable FtsZ2 level in FtsZ1-GFP expressed in wild-type plants (Figure 10C, lane 3) indicates that the transgenic expression altered the native FtsZ2 protein expression. The identification of an FtsZ2 level that was slightly lower than WT in FtsZ1 KO+ FtsZ1-mYFP complemented plants (Figure 10C, lane 4) is in contrast to the lack of detectable FtsZ2 protein signal on the immunoblot for the FtsZ1 KO+ FtsZ1-mCFP complemented plants (Figure 10C, lane 5). Neither the FtsZ2-1 KD (Figure 10C, lane 6) nor the FtsZ2 double KO (Figure 10C, lane 8) expressed FtsZ2 protein. The transgenic FtsZ2 protein level for the FtsZ2-GFP + WT (Figure 10C, lane7) was near the WT level but the endogenous FtsZ2 level for this leaf extract was slightly lower than WT. FtsZ2-mYFP + WT (Figure 10C, lane 12) transgenic and native FtsZ2 levels were considerably higher than WT. There was a lack of transgenic and native FtsZ2 protein expression in one of the FtsZ2-mYFP +FtsZ2 double KO leaf extracts (Figure 10C, lane 10) and in the FtsZ1-mYFP + WT (Figure 10C, lane 11). The other FtsZ2-mYFP +FtsZ2 double KO leaf extracts (Figure 10C, lane 9) had a transgenic expression level that was slightly higher than WT.

Fluorescently Tagged FtsZ1 and FtsZ2 Proteins Form Z-ring Assemblies at the Division Site when Expressed at Low Levels

Previous work has indicated that the fluorescently tagged FtsZ1 and FtsZ2 were capable of assembly and were probably co-assembling with the endogenous FtsZ in chloroplasts (Fujiwara et al., 2009; Vitha et al., 2001). In transgenic plants, FtsZ1-mYFP as well as the –mCFP and –GFP tagged versions were localized to mid-plastid when expressed at low levels in either the FtsZ1 null mutant background, where it restored chloroplast division, or the wild-type background, as described above (Figure 11B and 11D). These chloroplasts were not enlarged and their morphology was similar to that of the WT chloroplasts (Figure 11A). At higher expression levels of the transgene (as judged visually by fluorescence microscopy from the strength of the FP signal, as well as by immunoblotting analysis), we observed enlarged, irregularly shaped chloroplasts containing networks of filaments throughout the organelle (Figure 12A). Moderate expression of the FtsZ1-mYFP protein in the WT background resulted in the formation of multiple filamentous networks in some mesophyll chloroplasts and in the formation of a Z-ring mid-chloroplast in other chloroplasts (Figure 12B).

When low-expressing FtsZ2-mYFP constructs were transformed and expressed in a wild-type background, FtsZ assemblies localized to the periphery of the epidermal chloroplasts and mid-chloroplast in several of the mesophyll chloroplasts (Figure 11E and Figure 12C). In the FtsZ2 double-KO transformed with FtsZ2-mYFP expression is high, chloroplast division is almost completely blocked, the mesophyll chloroplasts are extremely large and of irregular shape, and it is no longer possible to locate the mid-

plastid (Figure 12D). In leaf epidermal cells of FtsZ2-KO transformed with FtsZ2-mYFP transgenic plants, the chloroplasts were much smaller and quite often were elongated or dumbbell-shaped. The FtsZ2-mYFP inside the chloroplasts formed Z-ring assemblies mid-plastid and formed mini-rings and filaments away from the constriction site (Figure 12E). These observations confirmed that low level expression of the fluorescently tagged FtsZ protein does not significantly disturb chloroplast division in the wild-type background, and they show that localization patterns and chloroplasts sizes in complemented mutants are similar to wild-type. These plants with protein expression levels and FtsZ localization patterns similar to those of WT were used for analysis of FtsZ turnover in the Z-ring by fluorescence recovery after photobleaching (FRAP).

AtFtsZ1 and AtFtsZ2 Exhibit Dynamic Subunit Turnover in the Z-ring of the Chloroplast

FtsZ1 and FtsZ2 co-localize in the mid-chloroplast area (Vitha et al., 2001),and bacterial studies show that they form a Z-ring that is dynamic (Anderson et al., 2004; Stricker et al., 2002). This Z-ring serves as a scaffold for accessory proteins and the ring constricts during chloroplast division. The *in vivo* substructure of the Z-ring has not been elucidated, but experiments aimed at providing additional information about the ring behavior could contribute to the current model of the Z-ring structure. For example, information about the FtsZ1 and FtsZ2 turnover rates in the ring can be used to make connections between known GTPase activities and FtsZ protein dynamics. These experiments could also ascertain how accessory protein interactions affect subunit turnover. FRAP data of FtsZ1 and FtsZ2 Z-ring protein dynamics in various mutant

backgrounds could be compared to their turnover rates in native-like environments to draw conclusions about the effect of accessory protein interactions on Z-ring proteins.

The results of pilot experiments conducted in our laboratory indicated that both FtsZ1-GFP and FtsZ2-GFP exhibit dynamic turnover in and out of the Z-ring and that their half- time-to-recovery ($t_{1/2}$) values range from tens to hundreds of seconds for FtsZ1-GFP and FtsZ2-GFP, respectively. For these preliminary experiments, we used transgenic plants expressing FtsZ fusions with GFP (Vitha et al., 2001) at relatively high levels. These elevated expression levels were of concern because the overexpression of FtsZ causes artifactual localization (Kiessling et al., 2000; McAndrew et al., 2001; Stokes et al., 2000; Vitha et al., 2001). We were also concerned that the stoichiometry between FtsZ1 and FtsZ2 is significantly altered in such plants, which may affect the observed turnover rates. Furthermore, many of the fluorescent proteins derived from GFP are weakly dimeric (Zacharias et al., 2002), which may affect their dynamic behavior. Therefore, plants expressing FtsZ1 or FtsZ2 tagged with monomeric forms of CFP and YFP (Zacharias et al., 2002) at low levels in wild-type background were chosen for this experiment. FtsZ-mFP fluorescence is detectable in epidermal plastids, but generally is barely detectable in mesophyll chloroplasts in these plants. The mYFP fluorescence was brighter and more photostable than that from mCFP and therefore FtsZ1-mYFP and FtsZ2-mYFP were investigated in FRAP experiments. These experiments were hindered by the high scattering of the leaf tissue, even after vacuum infiltration with water or infiltration with fluorocarbon oil (Littlejohn et al., 2010) and imaging with a water immersion objective. Another difficulty with imaging fluorescent

proteins in leaf mesophyll chloroplasts is the high autofluorescence of chloroplast pigments which prevents imaging of weakly fluorescing structures at a sufficient signal-to-noise ratio during extended time-lapse sequences. In order to minimize these hindrances, we chose to investigate FtsZ turnover in the leaf epidermal chloroplasts, which tend to provide brighter signal and lower background and are optically more conducive to live imaging.

We used fluorescence recovery after photobleaching (FRAP) to measure the FtsZ subunit turnover rate within the Z-ring of leaf epidermal chloroplasts. A time series of these FRAP experiments show that fluorescence recovery in the bleached region of interest is apparent over time (Figure 13A and 13B). The ($t_{½}$) was 117 ± 62 s and 325 ± 117 s for FtsZ1-mYFP and FtsZ2-mYFP, respectively (Figure 13C and 13D). The FtsZ1-mYFP turnover was slower than was measured in the pilot experiments in plants expressing either FtsZ1-GFP (data not shown) or FtsZ1-mYFP at very high levels ($t_{½}$= 57 ± 41 s, and 59 ± 31 s, respectively).

Controls with either fixed tissue (Figure 13E) or whole-chloroplast photobleaching (Figure 13F) did not show any recovery of fluorescence, indicating that reversible photobleaching of the fluorescent protein is not significant under these experimental conditions and that recovery of fluorescence in the Z-ring is due to subunit exchange in the Z-ring.

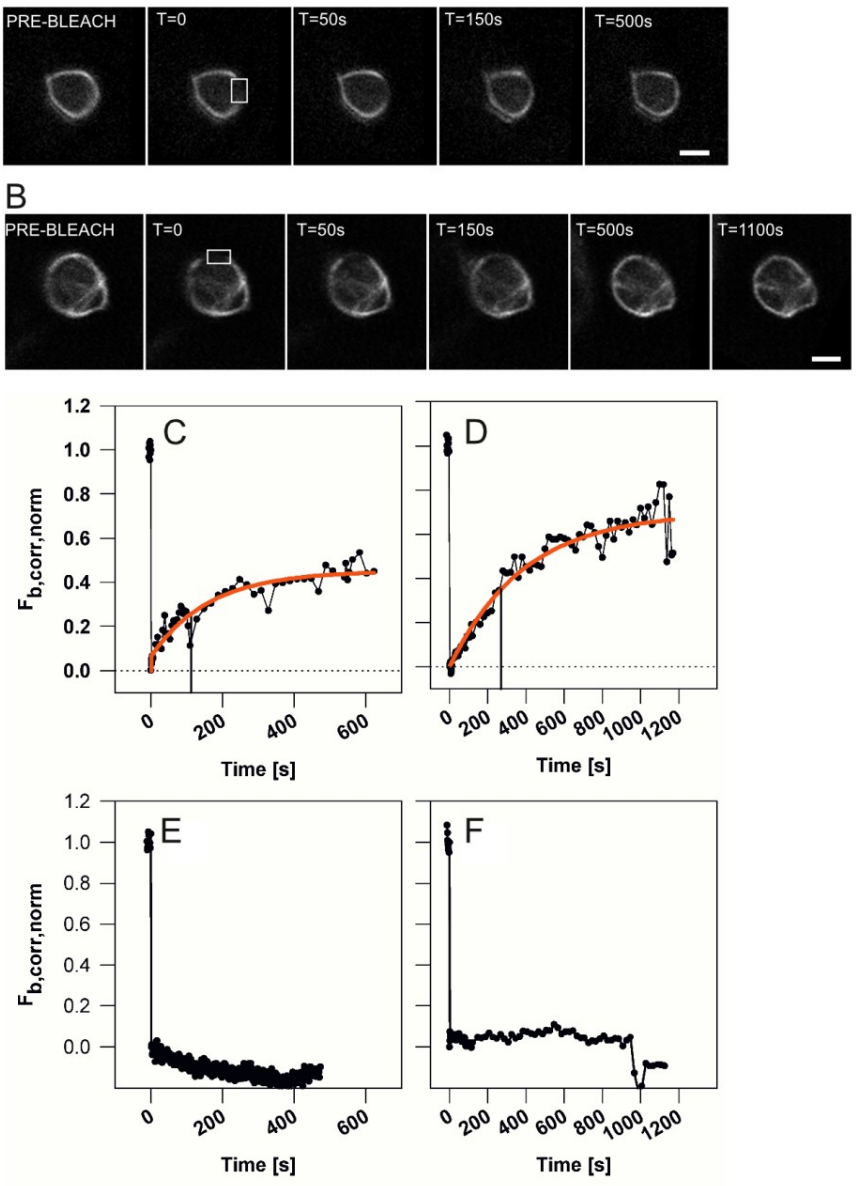

Figure 13. FRAP analysis of FtsZ1-mYFP and FtsZ2-mYFP filament assembly dynamics in leaf epidermal chloroplasts. A) Montage of selected frames from the time-lapse sequence for FtsZ1-mYFP and FtsZ2-mYFP-expressing plants. Because of the substantially longer recovery of FtsZ2-mYFP fluorescence, the data collection was extended to ~20 min (1200 s). The boxed area at T=0 indicates the bleached region. Bar = 5 µm. B, C) an example of a FRAP curve for FtsZ1-mYFP and FtsZ2-mYFP, respectively. The drop line indicates the time of 50% recovery ($t_{1/2}$). E) Control, fixed tissue. F) Control, live tissue, photobleaching of the entire chloroplast. The dip in the signal at T=1000s is due to a focus shift.

Discussion

Complementation Is Affected by FtsZ Expression Levels

FtsZ expression levels affect chloroplast division (Colletti et al., 2000; Osteryoung et al., 1998b; Reddy and Day, 2001; Stokes et al., 2000; Vitha et al., 2001). For this reason, FtsZ expression levels during complementation of mutants are indicative of the functionality of the fluorescently labeled FtsZ protein. For example, high transgene expression levels alter the 1: 2 stoichiometric ratio of FtsZ1 to FtsZ2 that is necessary for normal chloroplast division. An altered ratio results in chloroplast division defects. Differences in FtsZ-FP expression levels are also responsible for the wild-type like, intermediate and severe phenotypes that were observed within the complementation lines.

Since it is difficult to discern small changes in chloroplasts size, quantitative analysis of chloroplast phenotypes were used to determine similarities and differences in the transformants. The FtsZ1-mYFP complement (Figure 10A, lane 4) with undetectable immunoblot transgenic protein levels had chloroplasts per cell area numbers that were more similar to WT than the FtsZ1-mYFP complement with transgenic expression levels similar to WT (Figure 10A, lane 5). Low transgenic expression levels may be more representative of WT levels.

The FtsZ1-GFP transgene is functional and able to restore chloroplast division as indicated by the intermediate and wild type-like phenotypes observed in the T1 chloroplasts.

The lack of intermediate and wild type-like T1 chloroplast phenotypes in the FtsZ2-GFP complementation test results shows that this fusion protein was unable to restore chloroplast division in the mutants (Table 2). The FP tag attached to the C-terminus of the FtsZ2 protein could adversely affect the Z-ring formation as this is the site of the FtsZ2-ARC6 interaction (Schmitz et al., 2009; Vitha et al., 2003). This interaction plays a major role in Z-ring anchoring because ARC6 tethers the Z-ring to the inner chloroplast membrane (Vitha et al., 2003).

Construction of an FtsZ2-FP construct that will be inserted in the variable region of the C-terminus is underway in our laboratory. This new construct will be used to complement the FtsZ2 double-KO mutants and to confirm if the current constructs interfere with the tethering of the Z-ring to ARC6. Since this block in chloroplast division was observed in both the GFP and the mFP forms of the tag, it is unlikely that the tag itself is hindering complementation and more feasible that the placement of the tag is the issue.

FtsZ Expression Levels Affect Chloroplast Division

FtsZ protein expression levels measured by Western Blot correlate to the FtsZ localization patterns observed with light microscopy and it appears that slight overexpression does not affect chloroplast division. For example, low to moderate expressors have Z-rings that assemble mid-chloroplast (Figure 11B, 11C, 12B and 12C). Light microscopy images of low expressing FtsZ1 null mutant plants transformed with FtsZ1-mYFP show Z-ring localization mid-chloroplast and contain chloroplasts that are similar in size to wild-type (Figure 11B). However, when the same transformant was

expressed at high levels deformed mesophyll chloroplasts containing lots of filaments were noticed (Figure 12A). Based on these findings, it appears that FtsZ expression levels have a direct effect on chloroplast division and that they are instrumental in determining FtsZ localization patterns. When the FtsZ1-mYFP construct was expressed in a WT background in moderate amounts as determined immunoblotting data, mid-chloroplast localization of the Z-ring was not as prevalent and filamentous networks within the chloroplast seemed to dominate Figure 12B). This wild-type like Z-ring localization and size trend was also seen in low-expressing FtsZ2-mYFP constructs expressed in a wild-type background (Figure 12C). Overexpression of FtsZ2-mYFP in a WT background blocked chloroplast division as indicated by grossly enlarged mesophyll chloroplasts and the appearance of filamentous networks in epidermal chloroplasts (Figure 11E). Although high FtsZ2 transgenic expression levels occurred in the FtsZ2-mYFP-WT constructs they were unable to restore chloroplast division as evidenced by low numbers of mesophyll chloroplasts per cell, the abundance of ring-like assemblies (Figure 12D, inset) and filaments in the dumbbell-shaped epidermal chloroplasts (Figure12E, white arrows).

For the 2-1 antibody immunoblots, although no transgenic FtsZ2-1 was detected in one of the FtsZ1 KO complemented lines (Figure 10C, lane 5), the chloroplast numbers for these this leaf extract (Figure 9B) were near WT, which indicates that FtsZ2-2 levels probably compensated for the low FtsZ2-1 level as these two proteins have been shown to be functionally redundant (Schmitz et al., 2009). Our analysis did not specifically determine FtsZ2-1 levels, so the lack of a detectable transgenic protein in one of the two

FtsZ2 double KO + FtsZ2-mYFP leaf extracts (Figure 10C, lanes 9 and 10) may have been caused by the low expression of FtsZ2-mYFP in the latter. The lack of endogenous protein in the FtsZ1-mYFP + WT leaf extract (Figure 10C, lane 11) was also caused by low construct expression levels. Taken together, these conclusions point to the idea that low expression levels of tagged proteins do not alter chloroplast division and they show that these proteins can be helpful in understanding the chloroplast division machinery.

Fluorescently Labeled FtsZ Localization Patterns

Regardless of the background, low expression levels of fluorescently tagged FtsZ1 or FtsZ2 protein do not completely inhibit the formation and localization of the Z-ring. It seems that the small increases in overall FtsZ protein concentrations do not alter the stoichiometry in a way that blocks chloroplast division. Mesophyll cells of WT plants transformed with FtsZ1-mYFP or FtsZ2-mYFP constructs resulted in altered FtsZ localization. This could be due to a partial block of chloroplast division as a result of changes in the FtsZ ratio within the chloroplast. Mild FtsZ stoichiometry changes do not seem to affect mid-mesophyll cell localization as observed in the case of FtsZ1-mYFP expressed in the FtsZ1 KO (Figure 11B). This localization pattern was missing in moderately expressed FtsZ1-mYFP in a wild-type background (Figure 9B). Since wild-type FtsZ-mFP has low expression patterns, it seems that the FtsZ expression levels in these lines are close to native levels. Based on these findings it could be concluded that there is a direct correlation between low FtsZ-mFP construct expression levels in wild-type backgrounds and FtsZ functionality. Low FtsZ expression may minimize chloroplast division disruptions associated with FtsZ overexpression.

Z-ring Dynamics

Interactions between the Z-ring proteins and accessory chloroplast division proteins (ARC3, ARC6, PARC6, PDV1, PDV2, and ARC5) may affect Z-ring dynamics and the subsequent rate of Z-ring turnover. The slower rate of *At*FtsZ-mYFP recovery when compared to that of bacteria could be due to interactions that are occurring between the Z-ring proteins (FtsZ1 and FtsZ2) and one or several of the accessory proteins. FRAP studies on the microtubule dynamics in *Arabidopsis* showed a similar phenomenon (Shaw et al., 2003), although the analysis occurred over a shorter time period. FRAP studies on more stable structures like interphase microtubule arrays (Saxton et al., 1984) and actin stress fibers (Wang, 1987) have ($t_{½}$) values of 200 s and 500s seconds, respectively. The slower turnover rate within the Z- ring could be advantageous for its role as a scaffold for other accessory proteins as well as for it role in force generation during chloroplast division.

The FtsZ2-mYFP ($t_{½}$) value was more than two times that of FtsZ1-mYFP. Binding interactions with assembly proteins like ARC6 could have affected the movement and thus the recovery rate of the FtsZ2 protein. Another possibility could be that the tagged FtsZ2 protein is being outcompeted for assembly by the intrinsic, non-tagged FtsZ2, which would decrease the number of tagged FtsZ2 subunits that are incorporated into the Z-ring. Slow diffusion rates, as reported previously (Sprague and McNally, 2005), could also contribute to a delay in the recovery time. The shorter recovery times observed in FtsZ1-GFP than in FtsZ2-mYFP pilot samples may be attributed to the possibility that the abundance of fluorescently tagged protein outcompeted the native FtsZ protein

during Z-ring incorporation. Those samples had high FtsZ expression levels. The longer recovery rate observed in the FtsZ2-mYFP overexpressing line (325 s) when compared to FtZ1-mYFP overexpressing line (117 s) could be the result of FtsZ2 accessory protein interactions (Figure 13C and 13D). It is thought that the Z-ring dynamics observed in low FtsZ-mFP expressing lines reflect those of the native FtsZ expression levels since the localization patterns of these fluorescently labeled FtsZ proteins was similar to those seen in wild-type tissue.

The FtsZ subunit turnover rates in the Z-ring for both FtsZ1-1 and FtsZ2-1 were slow than those of bacteria (Table 3). It is possible that the interaction between FtsZ2 and ARC6 could slow the subunit turnover. The difference in the turnover rates may have been influenced by the presence of the two FtsZ proteins in plants. There is a correlation between GTPase activity and subunit turnover with FtsZ1 having a faster GTP hydrolysis rate than FtsZ2 (Olson et al., 2010; Smith et al., 2010).

Table 3. FtsZ subunit turnover dynamics in plants and bacteria.

System	$t_{1/2}$ (sec)
A.thaliana-FtsZ1	117 ± 62
A.thaliana-FtsZ2	325 ± 117
E. coli	9 ± 3
B.subtilius	8 ± 3
M. smegmatics	34

Materials and Methods

Plant Material and Growth

All *Arabidopsis thaliana* plants used in the experiments are in the ecotype Columbia (Col-O) background. All seeds were sown on Redi-Earth (SunGro Horticulture, Bellevue, WA). The pots were covered with a humidity lid and stratified at 6 ºC for 72 hours. Afterwards the pots were transferred to a rooftop greenhouse and grown at a temperature of 22 ºC and a relative humidity of 62%. The lids were removed after 5 days and the plants were grown for 4 weeks and watered as needed.

Plasmid Constructs

The complementation constructs mCFP and mYFP obtained from Dr. Roger Tsien's Lab (University of California, San Diego) were amplified by PCR using primer 5'-GATGACTAGTAAGGGCGAGGAGCTGTTC (forward) containing a 5' SpeI site and 5'-AAATGTTTACTTGTACAGCTCGTCCATGC (reverse) containing a 3' STOP codon, cloned into pBluescript plasmid and sequenced to confirm that no PCR errors

were introduced into the coding sequence. The mYFP were excised using a SpeI-PstI double digest and cloned into SpeI-PmlI digested site in pCAMBIA_BAR 1302 (GenBank accession no. AF234298) (Shaner et al., 2004)which carries glufosinate ammonium resistance. This produced vectors for C-terminal tagging with mYFP. The construct design for mCFP was identical to that of mYFP.

Construction of AtFtsZ-mCFP and AtFtsZ-mYFP Transgenes

The FtsZ1 genomic sequence was amplified using primers 5'-TAGAATTCGCATGCGCAAAGTCAGT (forward) and 5'-TATGGATCCTGGAAGAAAAGTCTACGGGGA (reverse) to create an EcoRI forward restriction site (underlined) and a BamHI reverse restriction site (underlined). The *At*FtsZ2cDNA sequence was also amplified by PCR using primers 5'-GCATGAATTCTCAGCACCGTAAATGTAGC (forward) and 5'-ATAGGATCCTGGACTCGGGGATAACGAG (reverse) to create an EcoRI forward restriction site (underlined) and a BamHI reverse restriction site (underlined). The ~2.2-kb *At*FtsZ1 amplicon and the ~2.8-kb *At*FtsZ2 amplicon were inserted in front of either a mCFP or mYFP in the tagging vectors. The transgenics were sequenced to confirm that no PCR errors were introduced into the coding sequence and to confirm that the insert was in frame with the mFP coding sequence. The FtsZ-mFP construct was excised and inserted into the plant transformation vector pMLBART_BAR 1302 in front of the mFP.

Plant Transformation

The FtsZ-FP constructs were introduced into plants via *Agrobacterium*-mediated transformation as described (Clough and Bent, 1998) followed by germination of T_1

seedlings on soil. T1 seedlings were sprayed three times (7, 10, 16 days) with glufosinate herbicide herbicide containing 120 mg/liter glufosinate ammonium as the active compound. Leaves from the surviving plants were visualized using fluorescence microscopy.

Microscopy

Immunofluorescence localization of FtsZ1 using specific anti-FtsZ1 antibody was performed as described previously (Vitha et al., 2001). Laser scanning confocal microscopy of fluorescently tagged FtsZ proteins in *Arabidopsis* leaf tissue was performed using an Olympus FV1000 confocal microscope equipped with a 60x/1.2 water immersion objective and lasers appropriate for the fluorescent proteins (405 nm for mCFP, 488 nm for GFP and mYFP). Leaves were infiltrated with water to remove air pockets and improve image quality. In FRAP experiments, 10 pre-bleach images were collected at 2-sec intervals. A small region of interest, of approximately 1.5 x 1.5 μm was then bleached at 100% laser intensity.

In order to achieve good temporal resolution of the post-bleach recovery and to minimize the overall light dose and phototoxicity by the imaging beam, the post-bleach images were acquired with a variable progressively longer time interval. The post-bleach imaging sequence consisted of three segments (10 x 2s, 20 x 5s, up to 50x 20s). The individual imaging segments were joined (appended) in the confocal software (FV10-ASW, ver. 1.7c) and the image stacks and the corresponding time stamps for each frame were exported for analysis. Since chloroplasts exhibit significant phototropic movements when irradiated with the blue imaging laser, the images were processed

using stack alignment with ImageJ software (http://rsb.info.nih.gov/ij) and the "stackreg" stack registration plugin.

Analysis of the FRAP image sequence was performed as described (Anderson et al., 2004) and involved background subtraction, correction for photobleaching by the imaging laser, and normalization relative to pre-bleach levels. A single exponential fit of the post-bleach fluorescence intensity was performed using the Solver module in MS Excel.

Control leaf tissue for the FRAP experiments was vacuum-infiltrated with 3% formaldehyde in phosphate-buffered saline (PBS, 0.14 M NaCl, 2.7 mM KCl, 6.5 mM Na_2HPO_4, 5 mM KH_2PO_4, 3.0 mM NaN_3; pH = 7.3) and incubated at room temperature for 30 min. Prior to microwave processing, the sample was subjected to a vacuum cycle for 30s. It was then fixed in a Pelco Biowave laboratory microwave processor equipped with a ColdSpot temperature control system, with power set to 250W and a 6-minute cycle (2 min on, 2 min off, 2 min on). The temperature cut-off was set to 37° C. Tissue was then rinsed in PBS three times, with microwave irradiation 1 min at 250W power in each rinse and then used for imaging.

Plastid counting was accomplished using a Zeiss Axiophot equipped with a 40x/0.75 objective and a Coolsnap cf (Photometrics, Tucson, AZ) digital camera**.**

Separating Cells for Plastid Counting

A central segment of an almost fully expanded leaf was excised and fixed in 3% (v/v) glutaraldehyde using a microwave processor as described above. The fixative was

then replaced with 0.1M EDTA (pH 9) and the samples received another 6 minute microwave treatment before being incubated at 55º C for 60 minutes.

Immunoblotting

Light microscopy analysis was employed to confirm the presence of a fluorescent signal in transgenic plant lines. Extracts from expanding leaves from approximately 5-week old plants were prepared as described previously (Stokes et al., 2000). The homogenates were heated at 70º C for 15 minutes, filtered through Miracloth (Calbiochem) and stored at -20º C. Prior to the start of electrophoresis the samples were heated at 70º C for 1 minute and vortexed briefly.

Proteins were separated by SDS-PAGE on a 1.5 mm polyacrylamide gel (10% (w/v) separating polyacrylamide gels and 4% (w/v) stacking polyacrylamide gels) using the Mini-PROTEAN 3 system (Bio-Rad) (Laemmli, 1970) and transferred via electroblot to 0.2 μm nitrocellulose membranes (Bio-Rad). Equal gel loading was ensured by measuring the relative amount of total protein by densitometry of a Coomassie-stained gel.

One membrane was blocked for 1 hour in TBST (Tris-HCl, pH 7.4, 200mM NaCl, and 0.2% (v/v) Tween 20) that included 2% (v/v) cold water fish gelatin (Sigma-Aldrich, Saint Louis, MO). Next the blot was incubated overnight in TBST containing 2% (v/v) cold water fish gelatin and FtsZ1-1 (1:10,000) affinity-purified antibody (McAndrew et al., 2008; Stokes et al., 2000; Vitha et al., 2001) at 4º C on a vigorously agitating orbital shaker. After four ten-minute washes in TBST, the blot was incubated in a (1:10,000) dilution of FtsZ1 horseradish peroxidase-conjugated affinipure goat anti-

rabbit IgG secondary antibody (Jackson ImmunoResearch, West Grove, PA) diluted in TBST plus 2% (v/v) cold water fish gelatin for two hours at 21º C on a vigorously agitating orbital shaker. The membrane was washed in TBST two times for 10 minutes each and in TBS two minutes for 10 minutes each. Membranes were developed using the SuperSignal West Pico Chemiluminescent Substrate Kit (Thermo Scientific, Portsmouth, NH) and the signal was recorded on 5" by 7" Blue X-Ray Film (Phenix Research Products, Candler, NC). The second membrane was blocked for 30 minutes in TBST (Tris-HCl, pH 7.4, 200mM NaCl, and 0.05% (v/v) Tween 20) that included 0.25% (v/v) cold water fish gelatin. Afterwards the second blot was incubated for 4 hours in TBS containing 0.05% (v/v) Tween 20 and 0.25% (v/v) cold water fish gelatin and FtsZ2-1 (1:25) affinity-purified antibody at 23º C on a vigorously agitating orbital shaker. After two 20-minute washes in TBS plus 0.2% (v/v) Tween 20, the blot was incubated (1:10,000) dilution of rabbit anti-goat IgG, horseradish peroxidase-conjugate seconday antibody (Millipore, Billerica, MA) diluted in TBS plus 0.05% (v/v) Tween 20 and 0.25% (v/v) cold water fish gelatin for one hour at 21 ºC on a vigorously agitating orbital shaker. The membrane was washed in TBS plus 0.05% (v/v) Tween 20 two times for 5 minutes. The membrane was developed as described above.

Blot Quantification

Relative densities of the bands were determined for the immunoblots using Image J.

CHAPTER III

MAINTAINING SPECIFIC FLUORESCENCE IN *ARABIDOPSIS THALIANA* AFTER HIGH PRESSURE FREEZING, FREEZE SUBSTITUTION AND EMBEDDING

Introduction

To glean the maximum amount of information from ultrastructural studies of biological samples, it is important to preserve samples as close to their natural state as possible (Gilkey and Staehelin, 1986; Nicolas, 1991; Robards and Sleytr, 1985). This involves instantaneous immobilization via rapid freezing (milliseconds) and fixation of structures using a suitable cryogenic protocol. The most common methods used for this type of cryofixation include propane jet freezing, slam freezing, plunge freezing and high pressure freezing (HPF) (Gilkey and Staehelin, 1986; Plattner and Bachmann, 1982) . Of the methods mentioned, only HPF allows samples up to 0.6 mm to be frozen by subjecting them to pressures above 2000 bar and freezing in liquid nitrogen (LN_2) without distorting ice crystal damage because this pressure maximally suppresses ice crystal nucleation and growth (Dahl and Staehelin, 1989; Gilkey and Staehelin, 1986; McDonald, 1999). The higher cooling rates associated with HPF accommodate the formation of smaller ice crystals which have been shown to minimize the formation of hexagonal ice which could damage tissues and lead to artifacts (Dahl and Staehelin, 1989; Hoppert and Holzenburg, 2003; McDonald, 1999; Studer, 1992). Another advantage of using this procedure is that it minimizes the extraction of intracellular

components such as proteins and lipids (Plattner and Bachmann, 1982) and it is suitable for immobilizing animal and plant tissue and microorganisms (Studer et al., 1989a). In essence, HPF works by reducing the critical freezing rate of water to -22° C thereby keeping it liquid and lowering the ice crystal nucleation rate and growth rate (Dahl and Staehelin, 1989). The latter is also supported by the fact that freezing at high pressure produces amorphous ice of a higher density than water (Franks, 1982). Among the different cryoimmobilization procedures in use, HPF has been determined to be suitable for preparing a number of model organisms, such as *A. thaliana, C. elegans, N. tabacum*, *Sacchromyces cerevisiae*, *Schizosaccharomyces pombe* and *E. coli* for electron microscopic imaging (Austin and Staehelin, 2011; Kang, 2010; Kiss, 1995; Kukulski et al., 2011; McDonald et al., 2007; McDonald and Webb, 2011).

Cryoprotectants aid in ultrastructure preservation by keeping tissue water in a liquid state at low temperatures and by increasing the number of small ice crystals or nucleation centers which in turn minimizes ice crystal growth (Gilkey and Staehelin, 1986; Skaer, 1982). Cryoprotectants fill empty spaces within the volume of the planchette in order to prevent air pockets from becoming barriers to HPF and to prevent these pockets from collapsing during pressurization and deforming the sample prior to freezing (Dahl and Staehelin, 1989). In addition, some of these protective agents increase the success rate in obtaining well frozen samples by reducing extracellular ice crystal formation and by suppressing heat release during crystallization (Dahl and Staehelin, 1989). Since the overall goal of HPF is to stabilize tissue without disrupting its natural processes, cryoprotectants must be chosen based on their cellular interactions.

If these interactions are intracellular, the agents are classified as penetrating, but if these interactions are extracellular, they are classified as non-penetrating (McDonald et al., 2007; Meryman, 1971). Intracellular cryoprotective compounds penetrate the cells and decrease large ice crystal formation by increasing intracellular viscosity (Gilkey and Staehelin, 1986; McDonald et al., 2007; Meryman, 1971); special considerations should taken when using these agents as they have the ability to alter cellular permeability properties (McDonald et al., 2007; Skaer, 1982) . Non-penetrating cryoprotective agents are hydrophobic substances with low osmotic activity that protect samples by increasing the viscosity of extracellular water, which increases the heat capacity of water and thereby the cooling rate (Skaer, 1982). To avoid internal cell disruption, the non-penetrating agent 1-hexadecene (Sigma-Aldrich, Saint Louis, MO), was chosen. 1-hexadecene is an inert, hydrophobic agent, with a low viscosity and surface tension that may facilitate replacement of intracellular air through interactions with the specimen surface (Studer et al., 1989b). In the same study Studer et al. (1989) showed that with 1-hexadecene as the cryoptotectant, there was a 90-100% yield of cryoimmobilized samples. This study also reported successful cryofixation of other biological samples when1-hexadecene was substituted for water. Furthermore, 1-hexadecene has been reported to have no physiological effect on thick-walled plant and fungal specimens during several minutes of exposure (Hess, 2007; Studer et al., 1989b) and it has also been shown to permeate the intercellular air spaces in plant tissue (Kang, 2010).

Fluorescence microscopy is a useful tool in the localization of cellular structures and fluorescent protein expressing cells (Heim et al., 1995; Hernandez-Boussard et al., 2011;

Kirk et al., 2011; Luby-Phelps et al., 2003) and in protein dynamic studies (Lee et al., 2011; McDonald et al., 2011; Wong et al., 2012) as it permits identification and visualization of subcellular structures. For instance, fluorescence recovery after photobleaching (FRAP) experiments have been employed to observe fluorescently labeled FtsZ protein dynamics in living *A. thaliana*, *E. coli*, *B. subtilis*, and *Schizosaccharomyces pombe* (Johnson et al., in preparation) (Anderson et al., 2004; Ryder et al., 2011; Srinivasan et al., 2008; Stricker et al., 2002).

This research focuses on the assembly of FtsZ a tubulin-like cytoskeletal protein localized in the chloroplast stroma (McAndrew et al., 2001). The assembly of the FtsZ filaments into the so-called FtsZ ring is essential for chloroplast division (Osteryoung et al., 1998a; Osteryoung and Vierling, 1995; Stokes and Osteryoung, 2003). There are many studies of FtsZ assembly *in vitro*, but the detailed structure of FtsZ filaments *in vivo* is not known. Our approach is to use correlative imaging to identify FP-tagged FtsZ assemblies by fluorescence microscopy and then investigate the same assemblies by electron microscopy. FtsZ-ring structure was investigated by cryo-EM tomography in a small bacterium (*C. crescentus)* (Li et al., 2007), but this approach is not directly applicable to plant tissues. Even intact isolated chloroplasts are too thick (2-3 μm)to permit cryo-EM tomography at 200 kv acceleration voltage (results not shown).

Two routes were explored, chloroplast isolation and fractionation. A report by Yoshida (2006) showed that it is possible to isolate functional FtsZ rings from chloroplasts of synchronized cultures of unicellular algae *C. merolae* (Yoshida et al., 2006). For plant leaf tissue, the procedure entails isolation of intact chloroplasts, lysis

and density gradient centrifugation to separate the fraction containing FP-tagged FtsZ assemblies. The fraction containing FtsZ assemblies is then plunge-frozen on an EM grid and FP-labeled FtsZ assemblies are localized by cryo-fluorescence followed by cryo-EM tomography. In the second approach, the leaf tissue is stabilized by chemical or physical means, dehydrated, embedded in resin and sectioned. FtsZ assemblies are then correlatively studied in thin sections on an EM grid using fluorescence and electron microscopy. In both approaches, it is essential to preserve the FtsZ assemblies. These are highly dynamic structures undergoing rapid turnover of FtsZ molecules (Johnson et al., in preparation) and unfavorable preservation or isolation conditions lead to complete disassembly. The preparation protocol must also preserve the fluorescent protein signal and minimize the autofluorescence background.

In the experiments described here, the chloroplast isolation and fractionation approach was hampered by high autofluorescence background, low FP signal and low yield of isolated FtsZ assemblies. Therefore, the second approach was pursued motivated by reports that a FP expressed in zebrafish embryos, *S. cerevisiae, S. pombe,* and MDCK cells continued to fluoresce after high pressure freezing, freeze substitution, and low-temperature embedding (Kukulski et al., 2011; Nixon et al., 2009). Literature that employed these methods to retain fluorescence in *Arabidopsis thaliana* was not encountered. Plant tissue poses a challenge due to its dense cell wall, large vacuole, and abundant air spaces explaining perhaps the overall paucity of literature on fluorescence visualization in freeze-substituted *Arabidopsis thaliana* tissue. This study presents a

cryo-fixation and embedding protocol that permits retention of specific attenuation of background autofluorescence and reservation of GFP antigencity.

Results

Whole-Mount Versus Chloroplast Isolation Approaches

When whole-mount tissue was subjected to cold microwave-assisted (CMA) fixation in the presence of 3% formaldehyde (w/v)/0.1% glutaraldehyde (v/v) and macerated on a microscope slide an abundance of FtsZ mini-ring assemblies were detected in the tissue (Figure 14A and 14B) but less than 1% of the FtsZ assemblies were released after this procedure. Attempts to reproducibly and effectively lyse the chloroplasts causing a quantitative release of the remaining assemblies using chemical (Nonidet NP-40, Sigma-Aldrich, Saint Louis, MO) and mechanical (sonication, razor blade, syringe) methods would have been desirable but were unsuccessful. Autofluorescence did not pose a problem in tissue dehydrated in ethanol unless the ethanol concentration during dehydration exceeded 90%. In contrast, dehydration resulted in high autofluorescence and the lack of a detectable signal when 1% (w/v) paraphenylenediamine (PPD) which was used as a contrasting agent was added to ethanol during dehydration. Dehydration in methanol (up to 90%), whether in the absence or presence of 1% PPD produced high autofluorescence in whole-mount samples. Fixatives containing acrolein had high autofluorescence. Since maceration was not effective in releasing Z-ring assemblies from chloroplasts, a different strategy was pursued which entailed the extraction and isolation of intact chloroplasts from homogenized leaf tissue. In these isolates,

chlorophyll autofluorescence reduced the signal-to-noise ratio of the fluorescently tagged proteins beyond detection. Additionally, since no protease inhibitors were incorporated into the isolation buffer, disassembly could account for the absence of detectable FtsZ filaments. The different treatments and there outcomes vis-à-vis fluorescent signal generation for the fixed whole-mount samples and the isolated chloroplasts suspensions and are summarized in Table 4.

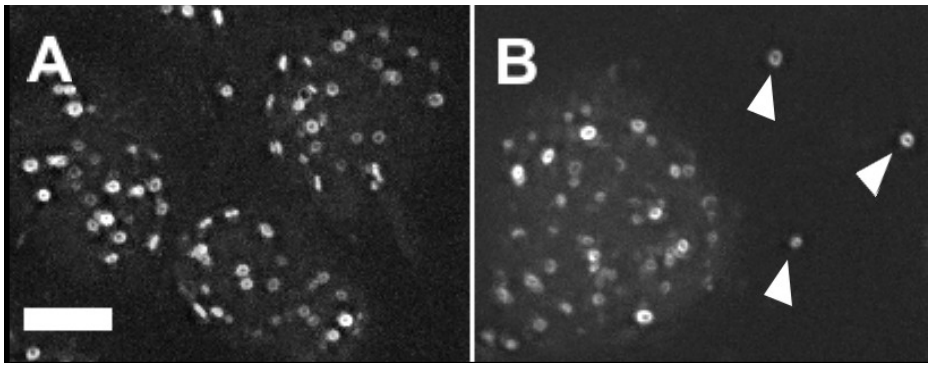

Figure 14. Stability of FtsZ assemblies in chloroplasts. *Arabidopsis* plants overexpressing AtFtsZ2-1-GFP show giant chloroplast phenotype and an easily noticeable FtsZ mini-ring localization pattern. A) Intact leaf tissue. B) Free-floating FtsZ assemblies (arrowheads) from chloroplast lysates in the vicinity of an isolated, intact chloroplast 15 min after maceration of the leaf. Scale bar = 10 μm.

Table 4. The effect of fixatives, dehydration solvents and lyses procedures on fluorescent signals in chloroplasts.

Whole-Mount, Chemical Fixation Treatment	Autofluorescence Background	Tagged Protein Signal
3% FA/0.1% Glutaraldehyde	-	+++
3% FA/0.1% Glutaraldehyde, OsO_4	-	+++
2.5% Glutaraldeyde + 1% acrolein	+++	-
Acrolein vapors + ethylene glycol	+++	-
Dehydration		
Ethanol	+	+
Ethanol + 1% PPD	+++	-
Methanol	+	-
Methanol + 1% PPD	+++	-
Methanol + Tannic Acid	+++	-
Isolated Chloroplast		
Control (Whole Leaf before Isolation)	+	+++
Treatment		
Unlysed chloroplasts	+	++
NP-40 + OG	+++	-
Hypotonic Buffer	+++	-
Sonicator	+++	-
3% FA/0.1% Glutaraldehyde/0.1% Tannic Acid	+++	-

(-) = none; (+) = low; (++) = medium; (+++) = high

Optimization of HPF-FS-Embedding Protocols

To maintain fluorescence and to preserve ultrastructure in the tissue, it was necessary to optimize a HPF-FS-embedding protocol for both the conventional FS and the QFS methods (see Materials and Methods). The tissue was pre-screened prior to HPF to verify expression of the *At*FtsZ2-mYFP protein fusion in chloroplasts of live cells. While HPF is an important first step in the preparation of samples, additional measures are crucial to guarantee that the fluorescent signal is not quenched, that autofluorescence does not pose a problem, and that the quality of ultrastructural preservation is sufficient

for localization of subcellular structures. The use of a cryoprotectant for instance (Figure 15) is necessary in order to minimize trapped air, which can act as insulator and impede freezing efficiency (Dahl and Staehelin, 1989). By soliciting 1-hexadecene as a cryoprotectant, the freezing efficiency was further enhanced by virtue of its beneficial physicochemical properties that lower the temperature of homogenous ice nucleation, raise the recrystallization point, and remove nuclei for crystallization. In addition, 1-hexadecene's hydrophobic nature and low osmotic activity allow it to "bind" (structural) extracellular water which prevents it from crystallizing during HPF (Gilkey and Staehelin, 1986; Lippincott-Schwartz et al., 2003; McDonald et al., 2007). Electron micrographs from HPF and FS *Arabidopsis* tissue indicated that 1-hexadecene did not act as a barrier to penetration of the freeze substitution as was previously observed (Studer et al., 1989a). However, after HPF, it was crucial to rapidly (6-8 s) transfer the sample from the HPF device to LN_2 to ensure that the frozen samples do not warm prior to freeze substitution (FS).

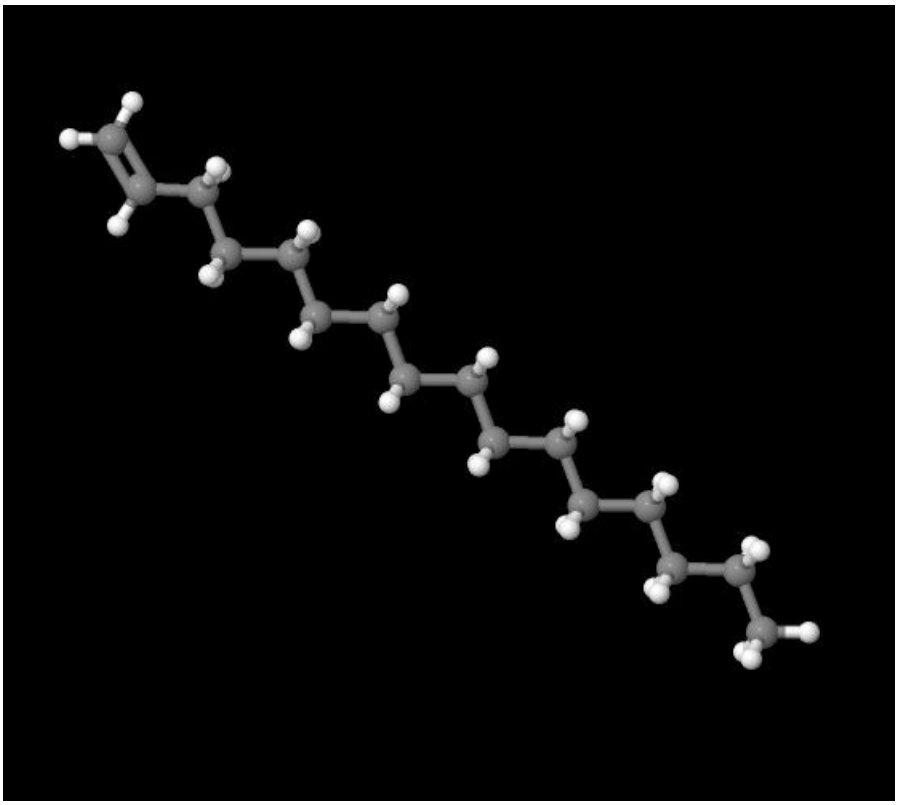

Figure 15. The chemical structure of 1-hexadecene. Reprinted with permission from Chemspider [Internet]. London (UK): Royal Society of Chemistry, Available from: www.chemspider.com/

FS is a critical step in the preparation of samples for investigation at the light and electron microscope levels. During FS, a frozen aqueous solvent is substituted for an organic solvent at temperatures that range from -80 ºC to -95 ºC (Muller, 1980). The organic solvent (i.e. methanol, acetone, ethanol) usually contains a contrasting agent (i.e. osmium tetroxide, uranyl acetate, tannic acid) which enhances the visualization and analysis of intracellular components (Giddings, 2003; Kang, 2010; Kukulski et al., 2011; McDonald et al., 2007; Muller, 1980). Acetone was the organic solvent of choice as

methanol could result in the extraction of lipids during freeze substitution (McDonald, 1994). In one study methanol extracted 15-45% of the cells lipid content during freeze substitution while acetone extracted only 5% of cellular lipids under the same freeze substitution conditions (Weibull, 1984). Acetone was also shown to extract fewer lipids from cells than either ethanol or methanol in a 1:1 mixture with Lowicryl HM20 (Weibull, 1986). To guarantee the exclusion of water from the samples (McDonald et al., 2007) fresh bottles of acetone were used throughout the study. FS can be carried out using commercially available FS equipment or in a homemade device consisting of a Styrofoam® box containing dry ice and a table top shaker (McDonald and Webb, 2011).

Optimization of the HPF-conventional FS-Lowicryl HM20 procedure resulted in the retention of a fluorescent signal in FtsZ-mini-rings (arrowheads) located within the chloroplast (Figure 16C) of a semi-thin section of fixed leaf tissue (Figure 16B) albeit less intense than the signal observed in live leaf tissue (Figure 16A). The signal is generated by FtsZ2-mYFP assemblies that were not quenched during fixation. These assemblies will be further examined using correlative microscopy to unravel the ultrastructure of the chloroplast division ring. Although this conventional FS procedure was successful at maintaining fluorescence, it may not be practical for use in all laboratories because it requires a lengthy infiltration time, a large volume of LN_2 and the use of special FS equipment. In an effort to create a more time-and-cost effective protocol, we adapted the QFS protocol developed by McDonald et al. (2011). This entailed using a 4% (w/v) UA/acetone FS solution and infiltrating the sample gradually in LR White/acetone (Table 5). Under these conditions, semithin (300 nm) tissue

sections revealed fluorescently labeled FtsZ assemblies (Figure 16D) within chloroplasts (Figure 16E). The lack of chloroplast localized FtsZ assemblies in semithin sections of untransformed tissue (Figure 16F and 16G) which serves as a negative control, indicate that the signals observed within the samples were from the FtsZ2-mYFP fusion protein within the chloroplasts. A QFS-rapid infiltration procedure (Table 5) that was employed prior to the QFS-gradual infiltration protocol failed to produce any florescent signal (data not shown). For the QFS protocol, a typical QFS warming curve was generated, which shows the warming rate of the samples (Figure 17).

Discussion

HPF-FS-Embedding and Fluorescence Preservation

We have shown by light microscopy that a fluorescent signal can be maintained in transgenic *Arabidopsis* tissue sections that have been fixed using HPF-FS-embedding (low and high temperatures) protocols developed in our laboratory. To the best of our knowledge, this if the first report a FP signal in *A. thaliana* after HPF-FS-Lowicryl HM20 embedding and after HPF-FS-LR White embedding. The results are significant for several reasons. First, they prove that the cumbersome procedures involved in our HFP-FS-embedding protocol were successful in penetrating the thick cell wall of the

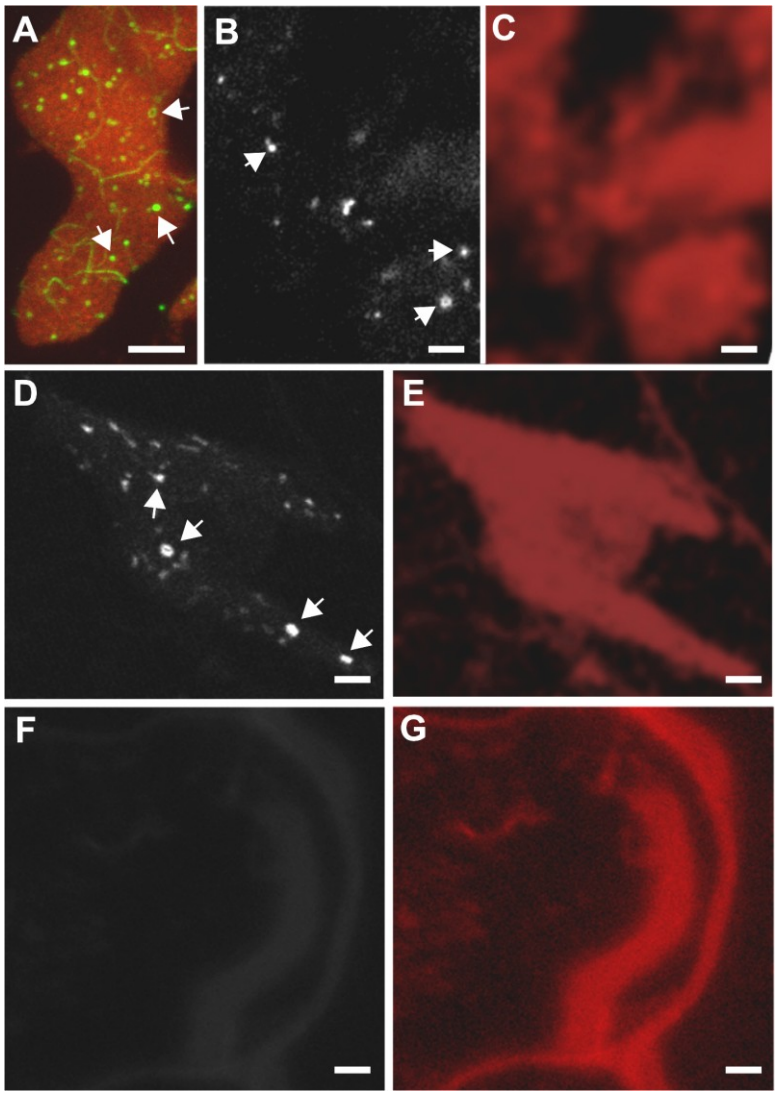

Figure 16. Fluorescence localization of mYFP-tagged FtsZ protein in leaf chloroplasts in whole-mount live tissue and in resin sections after high pressure freezing and freeze substitution. (A) Confocal fluorescence image of live leaf tissue. Green = FtsZ-mYFP, red = chlorophyll autofluorescence delineating the shape of the chloroplast. (B) FtsZ-mYFP fluorescence in a semi-thin section after HPF and conventional FS, embedding in Lowicryl HM-20. (C) the same micrograph with contrast and brightness adjusted to show the weak fluorescence background indicative of chloroplast shape. (D) FtsZ-mYFP fluorescence in a semi-thin section after HPF-QFS, embedding in LR White. (E) Same as in C, showing chloroplast shape. (F) Negative control - tissue from a null mutant plant lacking FtsZ2, processed by HPF – QFS, embedded in LR White. YFP fluorescence channel. (G) Same as in F, showing chloroplast shape. Scale bars 5 µm in (A) and 2 µm in B-G. Arrows indicate FtsZ2-mYFP mini-ring assemblies.

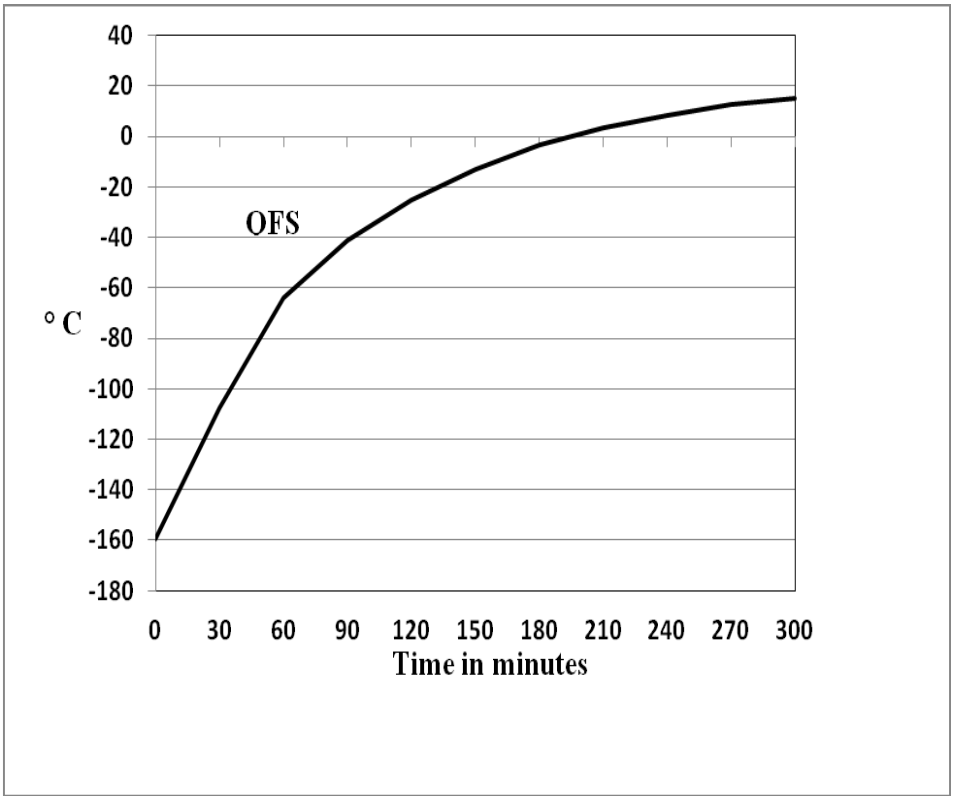

Figure 17. QFS warming curve of high pressure frozen tissue. Samples were freeze substituted in a LN_2 cooled heat block that was placed in a foam box on a shaker until they reached room temperature. Warming time was 300 minutes. The small kink at -65° C is not representative of any interruptions during the warming phase.

plant tissue and fixing and the organelles without deleterious effects. Second, it confirms earlier reports (Dahl and Staehelin, 1989; McDonald et al., 2007; Studer et al., 1989b) that the 1-hexadecene is an effective cryoprotective agent for HPF and it is shows that the use 1-hexadecene does not quench fluorescence of the fluorophores. Third, the results of this research have paved the way for *in vivo* correlative LM-EM studies aimed at elucidating the ultrastructure of Z-ring within chloroplasts. Finally, the protocols developed here can be applied to multiple biological systems.

Our decision to use HPF was guided by current literature which reports that instantaneous cryoimmobilization of samples preserves organelles and other cellular components by instantaneous stabilization (Gilkey and Staehelin, 1986) in a manner that has been proven to be superior to chemical fixative (Kellenberger, 1987). This reproducible procedure minimizes crystal formation by lowering the freezing point of water, by reducing the ice crystal nucleation rate and by retarding ice crystal growth (Dahl and Staehelin, 1989). This stabilization effect was further enhanced by the inclusion of 1-hexadecene. Studer et al. (1989) reported 1-hexadecene greatly improved the yield of well-embedded samples when used in conjunction with the FS organic solvent acetone, due to the fact that it is has better solubility on acetone (Studer et al., 1989b). Hohenberg et al. (1994) claimed that 1-hexadecene is not soluble in acetone at FS temperatures, and proposed that unless physically removed 1-hexadecene could create a barrier to substance exchange during FS. (Hohenberg et al., 1994) did not provide any experimental data or references to support these claims. In contrast, Studer et al. (1989) provided experimental evidence showing that 1-hexadecene has better

solubility in acetone during FS than water. The research findings presented here confirm that 1-hexadecene is soluble in acetone and refute the assertions of Hohenberg.

The Effects of the FS Media and the Embedding Media on Fluorescence

Since HPF immobilizes samples in their native state, autofluorescence did not pose a problem during this portion of the fixation procedure. Acetone is effective at dehydrating and maintaining ultrastructure in an assortment of chemically fixed samples, as it minimizes protein extraction and membrane stripping (Weibull, 1986; Weibull, 1984) . Among the limited number of studies of this nature, uranyl acetate dissolved in acetone is a recently accepted FS media for retaining fluorescence in HPF tissue, as evidenced by its use by Kukulski (2011) and in this study. The present results showed that it neither increased autofluorescence nor quenched FP fluorescence. The findings of another study that the FP fluorescence in zebrafish embryos survived ethanol dehydration are consistent with our findings that fluorescence in whole-mount tissue was retained after dehydration (Luby-Phelps et al., 2003) in ethanol albeit at low levels (Table 4). Based on these results, it can be concluded that increased autofluorescence attributed to ethanol dehydration diminished but did not prevent signal detection. Additionally, the findings of this research which show that fluorescence was maintained in samples infiltrated using either Lowicryl HM20 or LR White is consistent with those others. The HPF-FS-embedding methods described here, provide a basis for studying tissue in a natural state and have the potential to produce valuable knowledge about biological processes and structures.

Materials and Methods

Plant Material and Growth

All *A. thaliana* plants used in the experiments were in the ecotype Columbia (Col-O) background. All seeds were sown on Redi-Earth (SunGro Horticulture, Bellevue, WA). The pots were covered with a humidity lid and stratified at 6º C for 72 hours. Afterwards the pots were transferred to a rooftop greenhouse and grown at a temperature of 72 ºC and a relative humidity of 62%.

An *At*FtsZ2-mYFP transgene was created in our laboratory by cloning and inserting FtsZ2-1cDNA (NM_129183) into a plant transformation vector in front of a mYFP (Zacharias et al., 2002). Afterwards, *Agrobacterium*-mediated transformation of *Arabidopsis* wild-type plants with either *At*FtsZ2-mYFP or *At*FtsZ2-GFP (Vitha et al., 2001) and selection of the herbicide resistant plants was performed as previously described (Clough and Bent, 1998; Osteryoung et al., 1998a). For experiments described here, we chose transgenic plants with high expression levels of the FtsZ-FP. These plants show an abundance of FtsZ mini-ring assemblies that are easily identified in the microscope.

Microscopy

Laser scanning confocal microscopy of fluorescently tagged FtsZ proteins in Arabidopsis leaf tissue was performed using an Olympus FV1000 confocal microscope equipped with a 60x/1.2 water immersion objective and lasers appropriate for the fluorescent proteins (405 nm for mCFP, 488 nm for GFP and mYFP). Prior to imaging a drop of perfluorodecalin (Littlejohn et al., 2010) was placed on a piece of young leaf

tissue to remove air pockets that compromise optical quality from intercellular spaces. Sections from resin-embedded tissue were viewed using a 100x/1.4 oil immersion objective.

Chloroplast Isolation without Fixatives

Chloroplasts were isolated from 3-4 week old *Arabidopsis* plant tissue that was prescreened for the presence of a fluorescent signal. Plant material was kept at 4 °C during the isolation procedure. Plants were homogenized for 7-10 s using a polytron (Kinematica PT10-35) with a small rotor set at approximately 40% of the maximum speed in 10 ml of chloroplast isolation buffer (0.3M sorbitol, 5mM $MgCl_2$, 5mM EGTA, 5mM EDTA, 20mM HEPES/KOH, ph 8.0, 10mM $NaHCO_3$) in 50 ml beaker. The homogenate was filtered through a double layer of Miracloth (Calbiochem, Billerica, MA) into a falcon tube. The plant material in the Miracloth was returned to the beaker, washed with 20 ml of fresh chloroplast isolation buffer and filtered again through fresh Miracloth. The homogenate was centrifuged at 1000xg_{max} for 5 min (brake on) and resuspend the pellet in 350 µl of isolation buffer. An aliquot of the isolated chloroplasts was removed and checked for fluorescence on the confocal microscope. The remainder of the chloroplast suspension was loaded onto a two-step Percoll gradient which was prepared as described (Aronsson and Jarvis, 2002) and centrifuged in a swing-out rotor at 1500xg_{max} for 10 min (brake off). The intact chloroplasts were removed from the gradient using a glass pipette and added to 30 ml of HS buffer (50mM HEPES, 0.3M Sorbitol) and inverted several times to wash off the Percoll. After centrifuging the washed suspension in a swing-out rotor at 1000xg_{max} for 5 minutes, the supernatant was

decanted and the chloroplast remained in the tube. An aliquot was removed and viewed using phase contrast microscopy to verify chloroplast intactness. Next, the intact chloroplasts were aliquoted into three different test tubes. One tube of samples was lysed via syringe aspiration. Another sample was incubated in 0.2% Nonidet for 30 min on ice, 100mM n0octyl-β-D-glycopyranoside (OG) in PBS for 20 min on ice, layered onto a 40% percoll gradient and centrifuged at 13,200xg_{max} for 20 min in a swing-bucket rotor. The insoluble fraction was removed and washed in sucrose free isolation buffer by centrifuging at 7700xg_{max} for 10 minutes. The last aliquot was isolated in a hypotonic isolation buffer solution.

Chloroplast Isolation with Fixatives

Plant tissues were sampled from 3-4 week old *Arabidopsis* plants that were prescreened for the presence of a fluorescent signal using the Zeiss Axiophot microscope. Leaves were extracted from the plant and placed into chloroplast isolation buffer (20mM Tris-HCl pH 7.5, 5mM $MgCl_2$, 5mM KCl, 5mM EGTA) adapted from Yoshida et al. (2006) containing fixative (1% glutaraldehyde, 4% formaldehyde). Leaves were cut into small pieces and processed in the PELCO Biowave Pro Laboratory Tissue Processing System equipped with a Cold Spot temperature control system at 25 ° C and 250 watts for 30 min (2 min on, 2 min off, 2 min on). The tissue was checked for the presence of a fluorescent signal prior to being dividing into 5 separate tubes. Four of the samples were subjected to one of the following one-minute microwave dehydration protocols (1) a graded series of 10%- 90% ethanol containing 1 % (w/v) paraphenylenediamine (PPD) (2) a graded series of 10%- 90% methanol containing 1 %

(w/v) paraphenylenediamine (PPD) (3) a graded series of 10%- 90% ethanol (4) a graded series of 10%- 90% methanol. The fifth sample was placed on a piece of the fixed tissue on a microscope slide containing a drop of isolation buffer without fixative and macerate with a razor blade before covering with a coverslip and view using the Axiophot light microscope.

Additional chloroplast isolation procedures used the isolation buffer described in the preceding paragraph with the following modifications (a) add 300mM D-sorbitol plus 3% formaldehyde and 0.1 % (v/v) glutaraldehyde (b) add 300 mM D-sorbitol + 2.5% (v/v) glutaraldehyde + 1% (v/v) acrolein + 1% (w/v) tannic acid (c). Some of the plant material was also subjected to an anhydrous preparative protocol that consisted of exposure to acrolein vapors and overnight incubation in ethylene glycol.

High Pressure Freezing

3-4 week old transgenic tissue was prescreened using a laser scanning confocal microscope for the presence of a fluorescent signal prior to high pressure freezing. A small piece of leaf tissue from either a plant expressing a fluorescently labeled FtsZ2 protein or from a wild-type plant was extracted from the base of young (20-30 mm) leaves of *Arabidopsis thaliana* plants using either a 2-mm-diameter biopsy punch (Miltex) or a scalpel and loaded into a Type B 0.3mm deep specimen carrier (Technotrade, Manchester, NH) filled with the cryoprotectant, 1-hexadecene. The filled specimen carrier was covered with the flat side of another specimen carrier. Subsequently, the specimen carrier sandwich was immediately loaded into a specimen carrier holder, inserted into the Wohlwend Compact 01 HPF machine (Technotrade,

Manchester, NH) and cryoimmbolized at -190 °C under 2045 bar of pressure. Afterwards, the specimen holder was rapidly removed from the HFP machine and plunged in a LN_2 filled chamber. The specimen carriers containing the frozen hydrated samples were transferred under LN_2 to the pre-chilled cryovials using pre-cooled tweezers and stored in LN_2 until further processed.

Conventional Freeze Substitution

Scalpel-extracted HFP samples were used for this method of freeze substitution (FS). The freeze substitution solution used on the HFP samples was 4% (w/v) uranyl acetate dissolved in glass-distilled acetone (EMS, Hatfield, PA) that was opened immediately prior to use. The freeze substitution procedures are outlined in Table 5.

Quick Freeze-Gradual Substitution

This QFS method is a modification of the protocol that was first described by McDonald and Webb (2011). A heater block was cooled by LN2 in a Styrofoam® shipping box. 2-mm-dimater HPF leaf disks were transferred to LN2 cooled cryovials containing a freeze substitution media composed of 4% (w/v) uranyl acetate in freshly opened glass-distilled acetone. The cryotubes and datalogger probe (Lascar, Erie, PA) were placed in the center rows of the LN_2 submerged heat block and the heat block was transferred to a Styrofoam® box (McDonald, personal communication). The box was placed on a rotary shaker set to 121 rpm and allowed to shake until the temperature on

Table 5. Conventional, QFS-rapid, and QFS-gradual tissue fixation procedures.

Conventional	QFS-rapid	QFS-gradual
Freeze Substitution Substitution (4%UA/Acetone) – 90 °C (76 h) (76 h) – 45 °C (30 h)	Freeze Substitution (4%UA/Acetone) – 169 °C to 23 °C (76 h)	Freeze (4%UA/Acetone) – 169 °C 23 °C
Infiltration (-25 °C) (Lowicryl-HM20/acetone) White/Acetone)	Infiltration (25 °C) (LR White/Acetone)	Infiltration (25°C) (LR
10% (6 h) 25% (16 h) 50% (7.5 h) 75% (14.5 h) 100% (6.5 h) 100% (19 h)	25% (1 h) 50% (2 h) 75% (4 h) 100% (1 h) 100% (15 h) 100% (1 h)	10% (13 h) 20% (3 h) 30% (2 h) 40% (19 h) 50% (2 h) 60% (2 h)
100% (7 h)		70% (3 h) 80% (1 h) 90% (1 h) 100% (15 h) 100% (2 h) 100% (2 h)
UV Polymerization	Embedding	Embedding
– 45 °C (48 h) 20 °C (48 h)	60 °C (24 h)	60 °C (24 h)

the datalogger reached room temperature (Figure 18). Afterwards, the samples were removed from the shaker and the datalogger was stopped. The samples were rinsed in pure acetone, and infiltrated as described in Table 5.

Sectioning

Thick sections (300nm) that were cut on a Reichert-Jung Ultracut E microtome equipped with a diamond knife and mounted onto silane-coated microscope slides for light microscope viewing and thin sections (80 nm-100 nm) that were also cut under the same conditions mentioned above were picked up on uncoated nickel grids prior to electron microscope viewing.

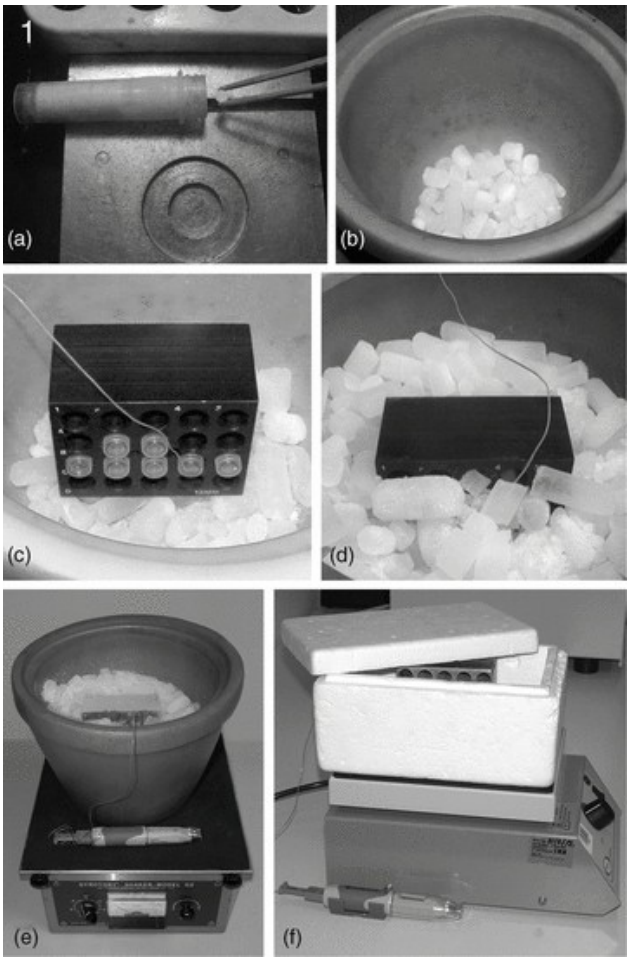

Figure 18. Cryovial set up QFS and SQFS. (a) Cryovials are laid horizontally on an aluminum block in liquid nitrogen that is just below the level of the top of the block. Frozen specimens are transferred in the liquid nitrogen vapour phase to avoid trapping liquid in the cryovial. (b) A layer of dry ice pellets about 1 cm thick is put in the bottom of an ice bucket. (c) The heater block with sample cryovials and temperature probe (attached to the wire) is transferred from liquid nitrogen to the dry ice bucket and arranged so that the vials are nearly horizontal. (d) More dry ice is added around the block. If more rows are filled, then more dry ice can be added. The complete working set-ups: (e) At UCB, an ice bucket is used to hold the dry ice, block and samples. A lid is used during actual processing. (f) At UQ, a smaller shipping container is used, as well as a smaller platform shaker. Here the lid is shown, although for the SQFS procedure it is not used. For scale information, the datalogger is the same in both figures and is 18 cm long from end-to-end. Reprinted with permission from John Wiley and Sons (McDonald and Webb, 2011).

CHAPTER IV

USING CORRELATIVE MICROSCOPY TO EXPLORE FTSZ ASSEMBLY STRUCTURE

Introduction

Correlative light and electron microscopy facilitates the visualization of cellular processes in a myriad of biological systems (Brown et al., 2009; Buser and McDonald, 2010; Jahn et al., 2009; Kukulski et al., 2011; Luby-Phelps et al., 2003; McDonald, 2009; Mironov and Beznoussenko, 2009; Muller-Reichert et al., 2007; Nixon et al., 2009; Robinson and Takizawa, 2009). Merging microscopic approaches to increase analytical capability permits the (i) investigation of dynamic cellular events, (ii) identification and visualization of protein structural design and (iii) elucidation of organelle morphology as this information has the potential to answer many important cell biology questions. Visualization of a fluorescent signal using light microscopy and preservation of the ultrastructure are prerequisites for correlative microscopy. A protocol that meets these requirements through the use of high pressure freezing (HPF)-freeze substitution (FS)-embedding and sectioning was established (see Chapter III).

HPF cryoimmobilizes samples in a native-like state while minimizing ice crystal formation and artifact distortions (Gilkey and Staehelin, 1986; Nicolas, 1991; Robards and Sleytr, 1985) prior to subsequent FS which exchanges cellular water for an organic substance and low temperature embedding in Lowicryl HM20 which is characterized by

a good structural preservation and its compatibility with immunolabeling (Nixon et al., 2009).

Chloroplasts are abundant in the leaf mesophyll of higher plants like *A. thaliana* and green algae where they divide via binary fission to maintain homeostatic levels and produce smaller chloroplasts capable of responding to environmental factors (Jeong et al., 2002; Leech et al., 1981; Osteryoung and Nunnari, 2003; Possingham and Lawrence, 1983). Filamentation temperature sensitive Z (FtsZ) protein is a filament-forming tubulin homolog of prokaryotic origin that localizes to the division site (Bi and Lutkenhaus, 1991) and initiates a cascade of events associated with binary fission in bacteria, higher plants and green algae. For normal chloroplast division, two endosymbiosis derived functionally non-redundant protein coding FtsZ gene families (FtsZ1 and FtsZ2) (Miyagishima et al., 2004; Stokes and Osteryoung, 2003) are necessary (Osteryoung et al., 1998a; Schmitz et al., 2009; Yoder et al., 2007). FtsZ1 contains one family member (FtsZ1-1) and FtsZ2 contains two functionally redundant family members (FtsZ2-1 and FtsZ2-2) (Schmitz et al., 2009). At the onset of division, FtsZ1-1 co-localizes mid-chloroplast with FtsZ2-1 to form the Z-ring (Vitha et al., 2003). The interactions between FtsZ-ring proteins and other accessory proteins such as ARC3(Maple et al., 2007) and ARC6 (Vitha et al., 2003) are instrumental in the formation of the complex division machinery. Although functional information about the division proteins has contributed to an improved understanding of the division machinery, there is a paucity of structural information as it relates to these proteins in chloroplasts.

Studies with bacterial FtsZ show that under different experimental conditions of *in vitro* assembly, FtsZ can assemble into rings, sheets, or tubular structures (Erickson et al., 1996; Redick et al., 2005). It is crucial to ask which, if any, of these structures are present and relevant *in vivo*. Standard fluorescent microscopy imaging provides limited resolution of only 200-300 nm. High resolution electron microscopic imaging of FtsZ assemblies *in situ* remains elusive or is limited to cryo-electron tomography of small bacteria (Li et al., 2007) as this is not straight forward with thick leaf tissue. To answer this question, we employed a sample preparation protocol that was devised that maintains the fluorescence of mYFP after embedding and thin sectioning of *Arabidopsis* leaf tissue, and also preserves the tissue ultrastructure permits transmission electron microscopic detection of FtsZ filaments. This research presents a correlative light microscopy (LM)-electron microscopy (EM) method that allows light-based imaging of FtsZ2-mYPF fluorescent fusion proteins by confocal microscopy, super-resolution microscopy, and EM-based imaging of the FtsZ-ring ultrastructure within the chloroplast of *Arabidopsis thaliana*. This research shows for the first time the *in vivo* ultrastructure of FtsZ in plants expressed at near wild-type levels.

Results

Visualization of *in vivo* FtsZ Assemblies in Chloroplasts Using Light Microscopy

A critical step in the use of multiple modalities for fine structure analysis is the maintanence of a fluorescent signal in the transgenic tissue. Therefore, fluorescence microscopy was used to visualize filaments, and punctate structures in leaf tissue from a

transgenic line overexpressing FtsZ2-mYFP (Figure 19C). The puncta were clearly resolved as circular structures with a mean diameter of 202 ± 66 nm (Figure 19A and 19B) using super-resolution fluorescence imaging based on structured illumination (on an OMX microscope (Applied Precision, Inc., Issaquah, WA)). Leaf tissue samples were then processed by HPF, FS and resin embedding. These correlative microscopy results are significant as they provide details of the puncta that would not be possible through the sole use of one type of microscopic approach.

Fine Structure of the Chloroplasts FtsZ Assemblies

Immunolabeled tissue sections were visualized at the EM level and the diameters of the easily discernible linear and circular structures were measured (Figure 20A). The measurements revealed that the diameters of the linear filaments varied over a wide range. A bimodal distribution histogram was created by plotting the frequency of occurrence vs. diameter (Figure 20B). A major peak ranging between 11 and 14 nm and the minor peak at 3-5 nm were observed in the graph. The major peak tallies were well with the diameters reported for *in vitro* filaments (Smith et al., 2010) while the smaller peak may have been created by a breakdown of filaments into protofilaments. Although measurements of the circular structures were highly variable, the average overall diameter of the rings were 183 ± 50 nm which is in excellent agreement with the diameter determined by superresolution fluorescence microscopy (Figure 19B). The average filament diameter in the EM micrographs within the ring structures measured 11.3 ± 0.6 nm, which is suggestive of the type-II *in vitro* filaments observed earlier (Smith et al., 2010) especially when taking a closer look at the appearance of these 11-

nm *in vivo* filaments as highlighted in Figure 20C. Together, these data are very encouraging and present the first *in vivo* - *in vitro* correlation for FtsZ in higher plants to date.

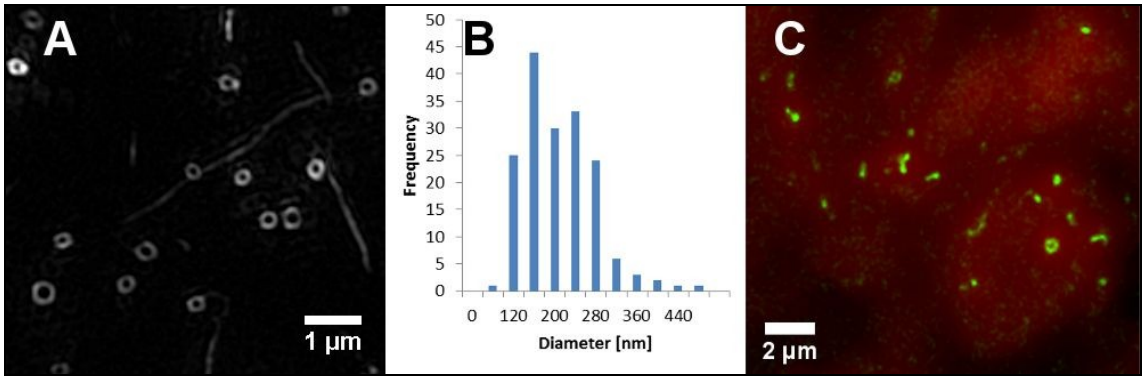

Figure 19. Correlative microscopy of FtsZ2-1-mYFP assemblies in *Arabidopsis* chloroplasts. A) Super-resolution fluorescence micrograph resolves small FtsZ circular assemblies (mini-rings) in fixed leaf tissue. Inset: The mini-ring diameter is measured as a peak-to-peak distance in a line intensity profile across the ring. B) Mini-ring size distribution, n=170. C) Conventional micrograph of FtsZ2-mYFP fluorescence in a thin section from a leaf after high-pressure freezing, freeze substitution and resin embedding. Red color denotes the shape of the chloroplast.

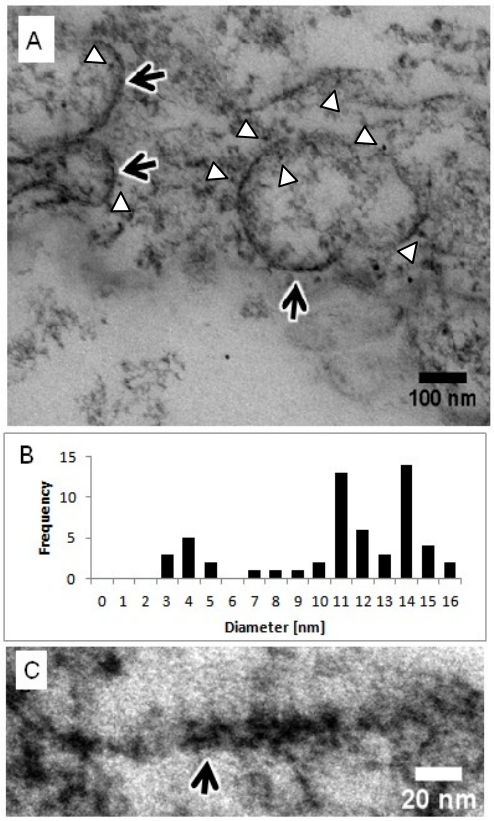

Figure 20. Ultrastructure of FtsZ2-1-mYFP assemblies. A) Depicts circular FtsZ assemblies at the electron microscopy level (highlighted by arrows)**.** 12 nm gold particles are highlighted by arrowheads. B) Distribution of filament thickness; n=52. C) Electron micrograph of a single linear filament (arrow) at higher magnification.

Bundling Patterns of the Z-ring

Electron tomography (ET) methods were used to learn more about the bundling patterns of the Z-ring assemblies that were visualized at the LM and EM levels. ET is applicable for imaging *in situ* subcellular components in biological systems and for determining 3D structures of those components using multiple projections (Lucic et al., 2005; McIntosh et al., 2005) by tilting the specimen relative to the incident electron

beam. Using this technique, it was possible to retrieve high-resolution information of the FtsZ-ring structure in its native environment (Figure 21). The Z-ring appears to be composed of several (2-3) laterally arranged protofilaments. To take full advantage of this technique, components of interest must be identified and segmented which can be challenging especially in densely packed cellular environments. In order to overcome the inherently low contrast of biological specimens, UA was incorporated into the FS media as a contrasting agent.

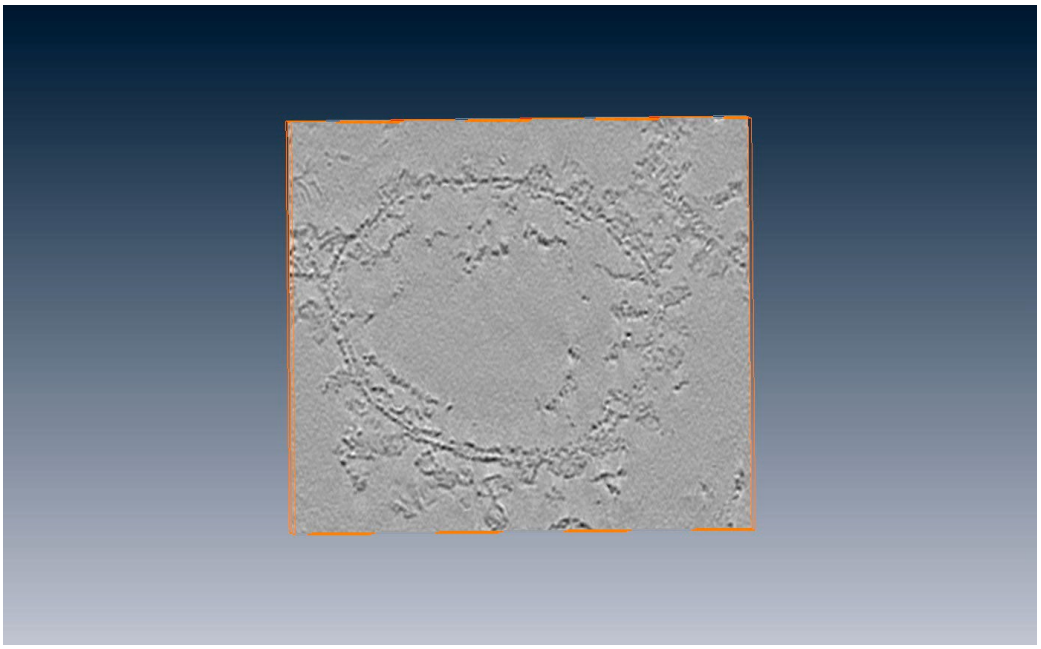

Figure 21. 0° tilt projection of an electron tomographic data set using scanning transmission electron microscopy.

Discussion

Exploring FtsZ Assembly Structures with *in situ* Correlative Microscopy

Recently, the *in vivo* length and curvature of FtsZ protofilaments in *Caulobacter crescentus* was deciphered using cryotomography reconstruction (Li et al., 2007). However, until this research, the macromolecular structure and assembly organization of FtsZ-ring subunits in both plants and bacteria had not been unraveled. The structure of the *in vitro* FtsZ assemblies generated and imaged using electron microscopy was validated by employing correlative LM-EM microscopy to observe and image *in vivo* assemblies.

3D Reconstruction of Electron Tomograms

EM3D software for electron microscope tomography (Stanford, CA) segmentation software will assist in the "isolation" of the filaments from their noisy surroundings and in the creation of stacks of individual slices that will be used to construct a 3D model of the Z-ring. The electron dense anti-GFP gold particles used for immunolabeling (Figure 20A) also served as fiducial markers during the alignment processes is necessary for 3D reconstruction. Segmentation analyses of stacks are currently being conducted.

In the context of this research, LM-EM correlative microscopy was employed to study the FtsZ-ring in fixed *A. thaliana* tissue sections. This correlative method and the specimen preparation protocols leading up to these studies offer many advantages for cell biology because they are universally applicable to other biological systems.

Materials and Methods

Plant Material and Growth

All *A. thaliana* plants used in the experiments were in the ecotype Columbia (Col-O) background. All seeds were sown on Redi-Earth (SunGro Horticulture, Bellevue, WA). The pots were covered with a humidity lid and stratified at 6 ºC for 72 hours. Afterwards the pots were transferred to a rooftop greenhouse and grown at a temperature of 72 ºC and a relative humidity of 62%. The lids were removed after 5 days and the plants were grown for 4 weeks and watered as needed.

Plasmid Constructs

The complementation construct mYFP obtained from Dr. Roger Tsien's Lab (University of California, San Diego) were amplified by PCR using primer 5'-GATGACTAGTAAGGGCGAGGAGCTGTTC (forward) containing a 5' SpeI site and 5'-AAATGTTTACTTGTACAGCTCGTCCATGC (reverse) containing a 3' STOP codon, cloned into pBluescript plasmid and sequenced to confirm that no PCR errors were introduced into the coding sequence. The mYFP were excised using a SpeI-PstI double digest and cloned into SpeI-PmlI digested site in the plant transformation vector, pCAMBIA_BAR 1302 which carries glufosinate ammonium resistance. This produced vectors for C-terminal tagging with mYFP.

Construction of the AtFtsZ-mYFP Transgene

The *At*FtsZ2cDNA sequence was also amplified by PCR using primers 5'-GCATGAATTCTCAGCACCGTAAATGTAGC (forward) and 5'-ATAGGATCCTGGACTCGGGGATAACGAG (reverse) to create an EcoRI forward

restriction site (underlined) and a BamHI reverse restriction site (underlined). The ~2.8-kb *At*FtsZ2 amplicon were inserted in front of the mYFP in the tagging vector. The transformant was sequenced to confirm that no PCR errors were introduced into the coding sequence and to confirm that the insert was in frame with the mYFP coding sequence.

Plant Transformation

The FtsZ2-mYFP construct was introduced into plants via *Agrobacterium*-mediated transformation as described (Clough and Bent, 1998) followed by germination of T_1 seedlings on soil . T1 seedlings were sprayed three times (7, 10, 16 days) with glufosinate herbicide containing 120 mg/liter glufosinate ammonium as the active compound. Leaves from the surviving plants were visualized using fluorescence microscopy.

Microscopy

Laser scanning confocal microscopy of fluorescently tagged FtsZ proteins in arabidopsis leaf tissue was performed using an Olympus FV1000 confocal microscope equipped with a 60x/1.2 water immersion objective and lasers appropriate for the fluorescent proteins (405 nm for mCFP, 488 nm for GFP and mYFP). Prior to imaging a drop of perfluorodecalin (Littlejohn et al., 2010) was placed on a piece of young leaf tissue to remove air pockets and improve image quality.

HPF-FS-processed samples were viewed in a FEI Tecnai™ G2 F20, equipped with a field emission gun (FEG) and a Fischione (Export, PA) ultra-high resolution STEM high angle annular dark field (HAADF) detector. STEM tomography data were acquired

using the FEI Xplore3D™ program and processed and reconstructed in FEI Inspect 3D. The results were rendered using Amira® (San Diego, CA).

High Pressure Freezing

All transgenic tissue was prescreened using a laser scanning confocal microscope for the presence of a fluorescent signal prior to high pressure freezing. A small piece of leaf tissue from either a plant expressing a fluorescently labeled FtsZ2 protein or from a wild-type plant was extracted from the base of young (20-30 mm) leaves of *Arabidopsis thaliana* plants using either a 2mm biopsy punch (Miltex) or a scalpel and loaded into a Type B 0.3mm deep specimen carrier (Technotrade, Manchester, NH) filled with the cryoprotectant, 1-hexadecene (Sigma-Aldrich, Saint Louis, MO). The filled specimen carrier was covered with the flat side of another specimen carrier and immediately loaded into a carrier holder, prior to insertion into a Wohlwend Compact 01 HPF instrument (Technotrade, Seenwald, Switzerland) and cryoimmbolized. Afterwards, the specimen holder was rapidly removed from the HFP machine and plunged into LN_2. Specimen carriers containing the frozen hydrated samples were transferred under LN_2 to the pre-chilled cryovials using pre-cooled tweezers and stored in LN_2 until further processed.

Conventional Freeze Substitution

Scalpel extracted HFP samples were used for this method of freeze substitution (FS). The freeze substitution solution used on the HFP samples was 4% (w/v) uranyl acetate dissolved in glass-distilled acetone that was opened immediately prior to use.

The samples were freeze substituted at -90 ºC for 76 hours using a Reichert-Jung FS machine. Optimization of the protocol revealed that longer FS times were necessary to overcome the barrier created by the thick cell wall of the plant tissue. This time is consistent with freeze substitution times used by others on thick wall samples (Otegui and Staehelin, 2004). The temperature was raised to -45 ºC (5 ºC/hour) and samples were held at this temperature for 30 h before being washed 3 times for 10 minutes in acetone. The samples were infiltrated with increasing concentrations of Lowicryl HM-20 in acetone (10% for 6 h, 25% for 16 h, 50% for 7.5 h, 75% for 14.5 h while raising the temperature to -25 ºC in increments of (5 ºC/hour). Incubation in low concentrations of resin is beneficial as it reduces separation of the cytoplasm from the cell wall and facilitates resin infiltration into the cell wall (Kang, 2010). Three 100% Lowicryl-HM-20 changes occurred after 6.5 h, 19 h, and 7 h. Afterwards the temperature was lowered to -45 ºC in increments of (5 ºC/hour) in order to enhance UV polymerization (Kukulski, personal communication) and samples were incubated for 48 h.

Immunolabeling

Thin sections were blocked on nickel grids with 4 % (v/v) cold water fish gelatin in PBS at 250 watts power on a cycle 2 min On, 2 min Off, 2 min On cycle at 37 °C. The grids were reacted with monoclonal mouse anti-GFP antibody (Millipore, Temecula, CA) diluted in PBS blocker at 250 watts power with a cycle 2 min On, 2 min Off, 2 min On cycle at 37 °C. Two grids were used for each of the following concentrations (i) 1:250, (ii) 1:500 and (iii) 1:1000. Grids were washed 2 X 1 min with PBS and 2 X 1 min with 0.15M NaCl TBS. Block in 4 % (v/v) cold water fish gelatin in 0.15M NaCl TBS at

250 watts power on a cycle 2 min On, 2 min Off, 2 min On cycle at 37 °C. Grids were incubated in a 1:30 dilution of donkey anti-mouse IgG-conjugated to 12 nm colloidal gold (Jackson ImmunoResearch, West Grove, PA) at 250 watts power with a cycle 2 min On, 2 min Off, 2 min On cycle at 37 °C. Grids were washed in 0.15M NaCl TBS 3 X 1 min followed by 3 X 1 min with deionized water. They were reacted with 1 % (v/v) glutaraldehyde for 5 min on the bench before being washed 3 X 1 min with deionized water and dried on a slide warmer. Grids were examined and photographed in a JOEL 1200EX transmission electron microscope operated at an accelerating voltage of 100 kV. Electron micrographs were recorded at calibrated magnifications.

Post Staining

Post staining is an essential step when preparing thin sections for electron microscope viewing because it improves contrast (Ellis, 2007). The samples were stained with uranyl acetate (UA) and Reynold's lead (Pb) citrate (Reynolds, 1963) according to the following protocol. The grid containing the sample was placed sample side down onto a drop of UA in a porcelain micro-well plate. Next, the grid was processed in a PELCO BioWave Pro Laboratory Tissue Processing System equipped with a ColdSpot temperature control system (Sanders, 2002) for 5 s before being washed with water. A drop of lead citrate was added to another well of the micro-well plate. A few sodium hydroxide (NaOH) pellets were placed on the edge of the plate to dissolve the CO_2 and the plate was covered with the top of a large glass dish. The grid was transferred to the lead citrate drop and incubated for 2 minutes at room temperature. Afterwards, the grid

was washed three times in water, dried on a hot plate and stored in a grid box until it was viewed in the JOEL 1200EX electron microscope.

CHAPTER V

CONCLUSIONS AND FUTURE DIRECTIONS

Conclusions

The research findings presented in this dissertation provide a more thorough understanding of chloroplast division. To investigate the Z-ring within chloroplasts of higher plants, we created FtsZ1 and FtsZ2 (-mYFP and -mCFP) fluorescent protein constructs, introduced them into *A. thaliana* wild-type, FtsZ2 KO, FtsZ KD, FtsZ2 double-KO backgrounds and accessory mutant proteins (*arc3, arc6, arc5)* via *Agrobacterium* mediated transformation to create an extensive seed stock collection to be used for future research. Afterwards, FtsZ1 and FtsZ2 complementation experiments were carried out to determine the functionality of the complemented lines. The degree of complementation was assessed by counting and plotting the number of chloroplasts per cell area for both the wild-type and FtsZ1 and FtsZ2 complemented lines and comparing their trendlines. Western blots were also performed on the FtsZ1 and FtsZ2 complementation lines to determine if the expression levels in the transgenic plants were near the endogenous levels observed in wild-type plants.

Studies aimed at contributing to the current model of the FtsZ-ring structure and function during chloroplast division involved measuring FtsZ1 and FtsZ2 subunit dynamics within the Z-ring of the leaf epidermal chloroplasts using FRAP. After a small region of interest in leaf tissue of plants expressing either FtsZ1-mYFP of FtsZ2-mYFP was bleached the tissue was monitored for FtsZ subunit turnover within the Z-ring. A

time series of FRAP experiments was employed to measure the fluorescence recovery in the bleached areas over time. The ($t_{1/2}$) values for FtsZ1-mYFP and FtsZ2-mYFP are 117 ± 62 s and 325 ± 117s, respectively. The vastly different turnover rates also suggest that FtsZ1 and FtsZ2 are assembled into the heteropolymeric Z-ring independently of each other.

Prior to the onset of this research, the *in vivo* FtsZ-ring structure at the EM level in FtsZ containing structures (i.e. bacteria, green algae, and higher plants) was unresolved. The arrangement of the protofilaments in the Z-ring of *Caulobacter crescentus* (Li et al., 2007) was the only EM information available. To resolve this structure at the EM level, wild-type plants expressing the FtsZ2-mYFP construct were preserved in a systematic manner using our optimized HFP-FS-embedding protocols before being sectioned and analyzed using a correlative microscopy approach that involved light, super-resolution and electron microscopy . Our EM results revealed that the overall diameter of the Z-ring within in the chloroplasts of *A. thaliana* is 183 ± 50 nm and it appears that the rings are approximately 2-3 protofilaments thick. The linear filament diameter measurements of 11 and 14 nm are in agreement with the measurements of *in vitro* type-I and type-II filaments (Smith et al., 2010). These findings are a significant contribution to the FtsZ community because they reveal *in vivo* features of the Z-ring for the first time.

Future Directions

The plastid division machinery in chloroplast is complex. Current models indicate that FtsZ1 and FtsZ2 assemble mid-chloroplast into a Z-ring (McAndrew et al., 2001;

Vitha et al., 2006; Vitha et al., 2001) where they initiate a cascade of localization and assembly events between other essential chloroplast division proteins such as ARC3, ARC5, ARC6, PARC6, PDV1 and PDV2. ARC3 functions as an accessory protein when it interacts with FtsZ1 and is involved in the positioning of the chloroplast division site through its interaction with PARC6 probably by destabilizing or disassembling the FtsZ filaments (Glynn et al., 2009; Maple et al., 2007). Vitha et al. reported that the ARC6-FtsZ2 exclusive interactions stabilize the FtsZ1-FtsZ2 assemblies and anchors them to the inner envelope membrane (Maple et al., 2005; Vitha et al., 2003). PDV1 and PDV2 localization to the cytosolic face of the chloroplast and interaction with PARC6 and ARC6, respectively, create a link between the stromal and the cytosolic components of the division machinery (Glynn et al., 2008; Glynn et al., 2009). ARC5, a dynamin related protein is recruited to the division site later in division by PDV1 and PDV2 (Miyagishima et al., 2006) and is thought to play a major role in the abscission of the chloroplasts (Gao et al., 2003). These interactions may affect Z-ring assembly dynamics and rate of Z-ring subunit turnover. Case and point, a recovery rate of an FtsZ protein in the mutant background of a suspected interacting partner that is more rapid than an FtsZ protein in the wild-type background would suggest that the recovery rate of the FtsZ protein in a native-like environment is somehow slowed by its interaction with that protein. Since the FtsZ1 and FtsZ2 Z-ring dynamic turnover rates were determined (Johnson et al., in preparation) during this research, future research should focus on determining the FtsZ1 and FtsZ2 turnover in *arc3, arc6, parc6, arc5, pdv1, and pdv2* mutant backgrounds to ascertain whether interaction between the FtsZ proteins and

other chloroplast division proteins affect the Z-ring subunit turnover rates. Transgenic plants expressing fluorescently tagged FtsZ1 or FtsZ2 at wild-type levels will be selected by immunoblotting with specific anti-FtsZ antibodies (Vitha et al., 2001) and crossed into mutant lines deficient in ARC3, PARC6 or ARC6, or with each other (to obtain plants co-expressing FtsZ1 and FtsZ2 tagged with different-color fluorescent proteins). The double transgenic lines will be selected using antibiotic or herbicide resistance markers (for FtsZ-mCFP or mYFP transgene) and by PCR screening for T-DNA insertion (for *ftsz1*, *ftsz2* KO mutations) and for single nucleotide polymorphism (for *arc3*, *parc6*, *arc6* mutations) (Bui and Liu, 2009). Similar studies in *E. coli* showed an effect on FtsZ dynamics. These studies should also determine if the mutant backgrounds affect the dynamics of both FtsZ1 and FtsZ2 or just one of these proteins. Future, ARC6 dynamic studies will serve both as an internal control since it is an inner membrane protein (Vitha et al., 2003) and is expected to have a slower turnover rate as well as provide information about FtsZ2 since studies have shown that ARC6 and FtsZ2 are interacting partners (Maple et al., 2005).

Continued FtsZ2 dynamic studies will require the use of plants that are expressing FtsZ2 at near wild-type levels as not to inhibit chloroplast division. Several attempts to transform FtsZ2-mYFP into an FtsZ2 double KO plants and FtsZ2-GFP into FtsZ2-1 KD plants were successful but complementation tests with these constructs were unsuccessful. Future studies include creating an insertional fluorescent protein fusion with FtsZ2 by cloning mYFP between between Q436 and M437. Sequence alignment and structural analysis suggested that this position, after the last resolved strand SC6 (in

M. jannaschii FtsZ), but before the C-terminal conserved region, corresponds to YFP insertion site after P334 in *E. coli* FtsZ, which proved functional in bacterial cell division (Osawa and Erickson, 2005).

In *Arabidopsis*, chloroplast division is perturbed by altering the FtsZ1:FtsZ2 ratios (Vitha et al., 2001). For example, the absence of FtsZ2 results in only short scarce FtsZ1 filaments and the absence of FtsZ1 results in long disorganized FtsZ2 filaments (Vitha et al., 2001). This is consistent with the model which shows that the interaction between FtsZ2 and ARC6 are required for stabilization and anchoring of the Z-ring. On the other hand, the absence of FtsZ1 will prevent FtsZ1-ARC3 interactions which destabilize assemblies and result in excessive assembly. This suggests that the FtsZ1: FtsZ2 ratio may be a means to regulate the properties of the Z-ring and the division process. Although it was shown that the total FtsZ1:FtsZ2 ratio in *Arabidopsis* chloroplasts is 1: 2 (McAndrew et al., 2008), to date no data exist about the FtsZ1: FtsZ2 ratio within the Z-ring proper. Therefore *in vivo* quantification of FtsZ1-mCFP (or FtsZ1-EBFP2) and FtsZ2-mYFP (or FtsZ2-mOrange2) being co-expressed or FtsZ2-mCFP (or FtsZ2-EBFP2) and FtsZ1-mYFP (or FtsZ1-mOrange2) being co-expressed in individual FtsZ assemblies should be conducted to ascertain the FtsZ1: FtsZ2 ratio of the Z-ring in chloroplasts of various cell types and at different stages of division to determine if the Z-ring ratios are regulated by cell specific cues. The relative intensity of each signal in FtsZ assemblies as well as in the rest of the plastid should be measured and the proportion of the total protein that is in the Z-ring, as well as FtsZ1: FtsZ2 stoichiometry in the assemblies should be calculated. For calibration of instrument response, dilution

series of the same purified, recombinant fluorescent proteins should be measured in solution using an identical instrument setup. By choosing fluorescent proteins that (mCFP, mOrange2) are well spectrally separated, significant errors in intensity measurements due to fluorescence resonance energy transfer (FRET) are unlikely. If the background fluorescence of chloroplasts pigments is a problem, spectral scanning and unmixing capability of the Olympus FV1000 should be utilized to subtract the non-specific background from the signals of interest.

HPF has been shown to be the preferred cryoimmobilization method for the preservation of samples of up to 0.6 mm (McDonald, 1999) because chemical fixation protocols have resulted in unsatisfactory preservation and artifact formation (Porta and Lopez-Iglesias, 1998). HPF produced consistent results when used in combination with acetone as the FS media. The optimization of this protocol with our thick walled plant cells will allow future research to be conducted on other transgenic plant lines. This research should begin with ultrastructure analysis of transgenic plant tissue expressing FtsZ1 and FtsZ2 at or near endogenous levels as they will provide a baseline for comparison of any changes in FtsZ ultrastructure when FtsZ proteins are expressed in mutant backgrounds (*arc5, arc6,arc3, pdv1and pdv2*). This information could contribute to an improved understanding of chloroplast division and the proteins that are involved. Additionally analysis of HPF-FS-embedded and sectioned tagged accessory proteins has the potential to provide data that could be useful in establishing structure-function relationships. These experiments should not be time-consuming since the seed

stocks were prepared during the course of this research and the protocol was optimized in the confounds of this project.

Correlative microscopy approaches have been useful in obtaining complementary information by combining live imaging with high resolution analysis. This process entails the identification of cellular features at the LM level followed by fine structure analysis of those same features at the EM level. Recently a number of correlative methods have been proposed (Kolotuev et al., 2010; Muller-Reichert et al., 2007). Since well preserved tissue is a critical requirement for this approach, tissue should be fixed via HPF-FS-embedding prior to sectioning. In the context of this research, correlative was defined as imaging tissue sections at the LM and EM that was taken from the same region of the resin block. Future correlative studies should involve placing cut semithin sections of tissue on a finder grid and viewing them using LM and EM tomography. This will ensure high precision in the identification of features. Immunolabelling of these sections using anti-FtsZ antibody concentrations that were optimized during this research will assist with the correlation procedures.

Segmentation results of the electron tomography acquired Z-ring stacks will allow a 3D reconstruction of the assembly and provide a vivid picture of the bundling patterns of the protofilaments within the ring. This information could provide details about subcellular events such as the *in vivo* filament assembly mechanism.

REFERENCES

Addinall, S.G., Bi, E., and Lutkenhaus, J. (1996). FtsZ ring formation in *fts* mutants. J. Bacteriol. **178**, 3877-3884.

Alonso, J.M., Stepanova, A.N., Leisse, T.J., Kim, C.J., and Chen, H. (2003). Genome-wide insertional mutagenesis of *Arabidopsis thaliana*. Science **301**, 653-657.

Anderson, D., Guerios-Filho, F., and Erickson, H. (2004). Assemby dynamics of FtsZ rings in *Bacillus subtilis* and *Escherichia coli* and effects of FtsZ-regulating proteins. J. Bacteriol. **186**, 5775-5781.

Aronsson, H., and Jarvis, P. (2002). A simple method for isolating import-competent *Arabidopsis* chloroplasts. FEBS Lett. **529**, 215-220.

Austin, J.R., 2nd, and Staehelin, L.A. (2011). Three-dimensional architecture of grana and stroma thylakoids of higher plants as determined by electron tomography. Plant Physiol. **155**, 1601-1611.

Bi, E., Dai, K., Subbarao, S., Beall, B., and Lutkenhaus, J. (1991). FtsZ and cell division. Res. Microbiol. **142**, 249-252.

Bi, E., and Lutkenhaus, J. (1991). Ftsz ring structure associated with division in *Escherichia coli*. Nature **354**, 161-164.

Boyes, D.C. (2001). Growth stage–based phenotypic analysis of *Arabidopsis*:a model for high throughput functional genomics in plants. Plant Cell **13**, 1499-1510.

Brown, E., Mantell, J., Carter, D.E., Tilly, G., and Verkade, P. (2009). Studying intracellular transport using high-pressure freezing and correlative light electron microscopy Sem. in Cell & Devel. Biol. **20**, 910-919.

Bui, M., and Liu, Z. (2009). Simple allele-discriminating PCR for cost-effective and rapid genotyping and mapping. Plant Methods **5**, 1-8.

Buser, C., and McDonald, K. (2010). Correlative GFP-immunoelectron microscopy in yeast. Methods Enzymol **470**, 603-618.

Chalfie, M., Tu, Y., Euskirchen, G., Ward, W.W., and Prasher, D.C. (1994). Green fluorescent protein as a marker for gene expression. Science **263**, 802-805.

Chudakov, D.M., Matz, M.V., Lukyanov, S., and Lukyanov, K.A. (2010). Fluorescent proteins and their applications in imaging living cells and tissues. Physiol Rev **90**, 1103-1163.

Clough, S.J., and Bent, A.F. (1998). Floral dip: a simplified method for *Agrobacterium*-mediated transformation of *Arabidopsis thaliana*. Plant J. **16**, 735-743.

Colletti, K.S., Tattersall, E.A., Pyke, K.A., Froelich, J.E., Stokes, K.D., and Osteryoung, K.W. (2000). A homologue of the bacterial cell division site-determining factor MinD mediates placement of the chloroplast division apparatus. Curr. Biol. **10**, 507-516.

Dahl, R., and Staehelin, L.A. (1989). High-pressure freezing for the preservation of biological structure: theory and practice. J Electron Microsc Tech **13**, 165-174.

de Boer, P., Crossley, R., and Rothfield, L. (1992). The essential bacterial cell-division protein FtsZ is a GTPase. Nature **359**, 254-256.

de Boer, P.A.J., Crossley, R.E., and Rothfield, L.I. (1989). A division inhibitor and a topological specificity factor coded for by the minicell locus determine proper placement of the division septum in *E. coli*. Cell **56**, 641-649.

de Pater, S., Caspers, M., Kottenhagen, M., Meima, H., ter Stege, R., and de Vetten, N. (2006). Manipulation of starch granule size distribution in potato tubers by modulation of plastid division. Plant Biotech. J. **4**, 123-134.

Douglas, S.E. (1998). Plastid evolution: origins, diversity, trends. Curr. Opin. Genet. Dev. **8**, 655-661.

Ellis, E.A. (2007). Poststaining grids for transmission electron microscopy: conventional and alternative protocols. Methods Mol. Biol. **369**, 97-106.

Erickson, H.P., Anderson, D.E., and Osawa, M. (2010). FtsZ in bacterial cytokinesis: cytoskeleton and force generator all in one. Microbiology and molecular biology reviews : MMBR **74**, 504-528.

Erickson, H.P., Taylor, D.W., Taylor, K.A., and Bramhill, D. (1996). Bacterial cell division protein FtsZ assembles into protofilament sheets and minirings, structural homologs of tubulin polymers. Proc. Natl. Acad. Sci. USA **93**, 519-523.

Franks, F. (1982). The properties of aqueous solutions at subzero temperatures. In Water-A Comprehensive Teatise, Water and Aqeous Solutions at Subzero Temperatures, Franks, F., ed. (New York: Plenum), pp. 215-238.

Fu, X., Shih, Y.L., Zhang, Y., and Rothfield, L.I. (2001). The MinE ring required for proper placement of the division site is a mobile structure that changes its cellular location during the *Escherichia coli* division cycle. Proc. Natl. Acad. Sci. USA **98**, 980-985.

Fujiwara, M.T., Nakamura, A., Itoh, R., Shimada, Y., Yoshida, S., and Moller, S.G. (2004). Chloroplast division site placement requires dimerization of the ARC11/AtMinD1 protein in *Arabidopsis*. J. Cell Sci. **117**, 2399-2410.

Fujiwara, M.T., Sekine, K., Yamamoto, Y.Y., Abe, T., Sato, N., and Itoh, R.D. (2009). Live Imaging of Chloroplast FtsZ1 Filaments, Rings, Spirals, and Motile Dot Structures in the AtMinE1 Mutant and Overexpressor of *Arabidopsis thaliana*. Plant Cell Physiol. **50**, 1116-1126.

Gao, H., Kadirjan-Kalbach, D., Froehlich, J.E., and Osteryoung, K.W. (2003). ARC5, a cytosolic dynamin-like protein from plants, is part of the chloroplast division machinery. Proc. Natl. Acad. Sci. USA **100**, 4328-4333.

Ghosh, B., and Sain, A. (2008). Origin of contractile force during cell division of bacteria. Physical review letters **101**, 178101.

Ghosh, B., and Sain, A. (2011). Force generation in bacteria without nucleotide-dependent bending of cytoskeletal filaments. Physical review. **83**, 051924.

Giddings, T.H. (2003). Freeze-substitution protocols for improved visualization of membranes in high-pressure frozen samples. J. Microsc. **212**, 53-61.

Gilkey, J.C., and Staehelin, L.A. (1986). Advances in Ultra-Rapid Freezing for the Preservation of Cellular Ultrastructure. Journal of electron microscopy technique **3**, 177-210.

Glynn, J.M., Froehlich, J.E., and Osteryoung, K.W. (2008). Arabidopsis ARC6 coordinates the division machineries of the inner and outer chloroplast membranes through interaction with PDV2 in the intermembrane space. The Plant Cell **20**, 2460-2470.

Glynn, J.M., Miyagishima, S., Yoder, D.W., Osteryoung, K.W., and Vitha, S. (2007). Chloroplast division. Traffic **8**, 451-461.

Glynn, J.M., et al. (2009). PARC6, a novel chloroplast division factor, influences FtsZ assembly and is required for recruitment of PDV1 during chloroplast division in *Arabidopsis*. Plant J. **59**, 700-711.

Goehring, N.W., and Beckwith, J. (2005). Diverse paths to midcell: assembly of the bacterial cell division machinery. Curr Biol **15**, R514-526.

Gutierrez, O.A., Campbell, M.R., and Glover, D.V. (2002). Starch particle volume in single- and double-mutant maize endosperm genotypes involving the soft starch (h) gene. Crop Science **42**, 355-359.

Heim, R., Cubitt, A.B., and Tsien, R.Y. (1995). Improved green fluorescence. Nature **373**, 663-664.

Hell, S.W., Dyba, M., and Jakobs, S. (2004). Concepts for nanoscale resolution in fluorescence microscopy. Current opinion in neurobiology **14**, 599-609.

Hernandez-Boussard, T., Downey, J.R., McDonald, K., and Morton, J.M. (2011). Relationship between patient safety and hospital surgical volume. Health services research **47**, 756-769.

Hess, M.W. (2007). Cryopreparation methodology for plant cell biology. Methods Cell Biol **79**, 57-100.

Hohenberg, H., Mannweiler, K., and Műller, M. (1994). High-pressure freezing of cell suspensions in cellulose capillary tubes. J. Microsc. **175**, 34-43.

Hoppert, M., and Holzenburg, A. (2003). Electron microscopy. In Microscopic Techniques in Biotechnology, Hoppert, M., ed. (Germany: Wiley-VCH Verlag), pp. 201-286.

Hu, Z., Mukherjee, A., Pichoff, S., and Lutkenhaus, J. (1999). The MinC component of the division site selection system in *Escherichia coli* interacts with FtsZ to prevent polymerization. Proc. Natl. Acad. Sci. USA **96**, 14819-14824.

Hu, Z.L., and Lutkenhaus, J. (1999). Topological regulation of cell division in *Escherichia coli* involves rapid pole to pole oscillation of the division inhibitor MinC under the control of MinD and MinE. Mol. Microbiol. **34**, 82-90.

Itoh, R., Fujiwara, M., Nagata, N., and Yoshida, S. (2001). A chloroplast protein homologous to the eubacterial topological specificity factor MinE plays a role in chloroplast division. Plant Physiol. **127**, 1644-1655.

Jahn , K.A., Barton, D.A., Su, Y., Riches, J., and Kable, E.P.W. (2009). Correlative fluorescence and electron microscopy: an elegant tool to study the actin cytoskeleton of whole-mount (breast) cancer cells. J Microscopy **235**, 282-292.

Jaiswal, R., Beuria, T.K., Mohan, R., Mahajan, S.K., and Panda, D. (2007). Totarol inhibits bacterial cytokinesis by perturbing the assembly dynamics of FtsZ. Biochemistry **46**, 4211-4220.

Jeong, W.J., Park, Y.I., Suh, K., Raven, J.A., Yoo, O.J., and Liu, J.R. (2002). A large population of small chloroplasts in tobacco leaf cells allows more effective chloroplast movement than a few enlarged chloroplasts. Plant Physiol. **129**, 112-121.

Kang, B.H. (2010). Electron microscopy and high-pressure freezing of Arabidopsis. Methods Cell. Biol. **96**, 259-283.

Kellenberger, E. (1987). Cryotechniques in biological electron microscopy. In The Response of Biological Macromolecules and Supramolecular Structures to the Physics Of Specimen Cryoprepreparation, Steinbrecht, R. A.,Zierold, K., eds. (Berlin: Springer-Verlag), pp. 35-63.

Kerppola, T.K. (2008). Bimolecular Fluorescence Complementation (BiFC) Analysis as a Probe of Protein Interactions in Living Cells. Annual Review of Biophysics **37**, 465-487.

Kiessling, J., Kruse, S., Rensing, S.A., Harter, K., Decker, E.L., and Reski, R. (2000). Visualization of a cytoskeleton-like FtsZ network in chloroplasts. J. Cell Biol. **151**, 945-950.

Kirk, M., Tonkin, E., Skirton, H., McDonald, K., Cope, B., and Morgan, R. (2011). Storytellers as partners in developing a genetics education resource for health professionals. Nurse Educ. Today **1,** 1-7.

Kiss, J.Z., Staehelin, L. A. (1995). High pressure freezing. In Rapid Freezing, Freeze Fracture, and Deep Etching, Shotton, D. M., ed. (New York: Wiley-Liss), pp. 89-104.

Koksharova, O.A., and Wolk, P.C. (2002). A novel gene that bears a DnaJ motif influences cyanobacterial cell division. J. Bacteriol. **184**, 5524-5528.

Kolotuev, I., Schwab, Y., and Labouesse, M. (2010). A precise and rapid mapping protocol for correlative light and electron microscopy of small invertebrate organisms. Biology of the cell / under the auspices of the European Cell Biology Organization **102**, 121-132.

Kukulski, W., Schorb, M., Welsch, S., Picco, A., Kaksonen, M., and Briggs, J.A. (2011). Correlated fluorescence and 3D electron microscopy with high sensitivity and spatial precision. J. Cell Biol. **192**, 111-119.

Laemmli, U.K. (1970). Cleavage of structural proteins during the assembly of the head of bacteriophage T4. Nature **227**, 680-685.

Larsen, R.A., Cusumano, C., Fujioka, A., Lim-Fong, G., Patterson, P., and Pogliano, J. (2007). Treadmilling of a prokaryotic tubulin-like protein, TubZ, required for plasmid stability in *Bacillus thuringiensis*. Genes Dev. **21**, 1340-1352.

Lee, J.S., et al. (2011). AHR drives the development of gut ILC22 cells and postnatal lymphoid tissues via pathways dependent on and independent of Notch. Nature immunology **13**, 144-151.

Leech, R.M., Thomson, W.W., and Platt-Aloia, K.A. (1981). Observations on the mechanism of chloroplast division in higher plants. New Phytol. **87**, 1-9.

Li, Z., Trimble, M.J., Brun, Y.V., and Jensen, G.J. (2007). The structure of FtsZ filaments *in vivo* suggests a force-generating role in cell division. EMBO J. **26**, 4694-4708.

Lippincott-Schwartz, J., Altan-Bonnet, N., and Patterson, G.H. (2003). Photobleaching and photoactivation: following protein dynamics in living cells. Nat Cell Biol. **Suppl**, S7-14.

Littlejohn, G.R., Gouveia, J.D., Edner, C., Smirnoff, N., and Love, J. (2010). Perfluorodecalin enhances *in vivo* confocal microscopy resolution of *Arabidopsis thaliana* mesophyll. New Phytol. **186**, 1018-1025.

Löwe, J. (1998). Crystal structure determination of FtsZ from *Methanococcus jannaschii*. J. Struct. Biol. **124**, 235-243.

Lu, C., Stricker, J., and Erickson, H.P. (2001). Site-specific mutations of FtsZ - effects on GTPase and in vitro assembly. BMC Microbiol. **1**, 7.

Lu, C.L., Reedy, M., and Erickson, H.P. (2000). Straight and curved conformations of FtsZ are regulated by GTP hydrolysis. J. Bacteriol. **182**, 164-170.

Luby-Phelps, K., Ning, G., Fogerty, J., and Besharse, J.C. (2003). Visualization of identified GFP-expressing cells by light and electron microscopy. J. Histochem. Cytochem. **51**, 271-274.

Lucic, V., Forster, F., and Baumeister, W. (2005). Structural studies by electron tomography: from cells to molecules. Annu Rev Biochem **74**, 833-865.

Lutkenhaus, J. (2007). Assembly dynamics of the bacterial MinCDE system and spatial regulation of the Z ring. Annu Rev Biochem **76**, 539-562.

Ma, L., Zhao, H., and Deng, X.W. (2003). Analysis of the mutational effects of the COP/DET/FUS loci on genome expression profiles reveals their overlapping yet not identical roles in regulating *Arabidopsis* seedling development. Development **130**, 969-981.

Maple, J., Aldridge, C., and Moller, S.G. (2005). Plastid division is mediated by combinatorial assembly of plastid division proteins. Plant J **43**, 811-823.

Maple, J., and Moller, S.G. (2007). Plastid division coordination across a double-membraned structure. FEBS Lett. **581**, 2162-2167.

Maple, J., Vojta, L., Soll, J., and Moller, S.G. (2007). ARC3 is a stromal Z-ring accessory protein essential for plastid division. EMBO reports **8**, 293-299.

Margalit, D.N., et al. (2004). Targeting cell division: Small-molecule inhibitors of FtsZ GTPase perturb cytokinetic ring assembly and induce bacterial lethality. Proc. Natl. Acad. Sci. USA **101**, 11821-11826.

Marston, A.L., and Errington, J. (1999). Selection of the midcell division site in *Bacillus subtilis* through MinD-dependent polar localization and activation of MinC. Mol. Microbiol. **33**, 84-96.

Martin, W., and Herrmann, R.G. (1998). Gene transfer from organelles to the nucleus: how much, what happens, and why? Plant Physiol. **118**, 9-17.

McAndrew, R.S., Froehlich, J.E., Vitha, S., Stokes, K.D., and Osteryoung, K.W. (2001). Colocalization of plastid division proteins in the chloroplast stromal compartment establishes a new functional relationship between FtsZ1 and FtsZ2 in higher plants. Plant Physiol. **127**, 1656-1666.

McAndrew, R.S., et al. (2008). *In vivo* quantitative relationship between plastid division proteins FtsZ1 and FtsZ2 and identification of ARC6 and ARC3 in a native FtsZ complex. Biochem. J. **412**, 367-378.

McDonald, K. (1994). Electron Microscopy and EM Immunocytochemistry. Methods Cell. Biol. **44**, 411-444.

McDonald, K. (1999). High-pressure freezing for preservation of high resolution fine structure and antigenicity for immunolabeling. Methods Mol. Biol. **117**, 77-97.

McDonald, K.L. (2009). A review of high-pressure freezing preparation techniques for correlative light and electron microscopy of the same cells and tissues. J Microsc **235**, 273-281.

McDonald, K.L., Morphew, M., Verkade, P., and Müller-Reichert, T. (2007). Recent advances in high-pressure freezing. In Electron Microscopy: Methods and Protocols, Kuo, J., ed. (New York: Humana Press), pp. 143-173.

McDonald, K.L., and Webb, R.I. (2011). Freeze substitution in 3 hours or less. J Microsc **243**, 227-233.

McDonald, K.P., Ramabhadran, R.O., Lee, S., Raghavachari, K., and Flood, A.H. (2011). Polarized naphthalimide CH donors enhance Cl- binding within an aryl-triazole receptor. Organic letters **13**, 6260-6263.

McFadden, G. (1999a). Chloroplasts. Ever decreasing circles. Nature **400**, 119-120.

McFadden, G.I. (1999b). Endosymbiosis and evolution of the plant cell. Curr. Opin. Plant Biol. **2**, 513-519.

McIntosh, R., Nicastro, D., and Mastronarde, D. (2005). New views of cells in 3D: an introduction to electron tomography. Trends Cell Biol **15**, 43-51.

Mereschkowsky, C. (1905). Über natur un Ursprung der Chromatophoren im Pflanzenreiche. *Biol. Centralbl.* **25:**593-604. English translation in Martin, W., Kowallik, K.V. (1999). Annotated English translation of Mereschkowsky's 1905 paper 'Über Natur und Ursprung der Chromatophoren im Pflanzenreiche'. *Eur. J. Phycol.*, **24:**287-296.

Meryman, H.T. (1971). Cryoprotective agents. Cryobiology **8**, 173-183.

Meyerowitz, E.M. (2001). Prehistory and history of Arabidopsis research. Plant Physiol. **125**, 15-19.

Mironov, A.A., and Beznoussenko, G.V. (2009). Correlative microscopy: a potent tool for the study of rare or unique cellular and tissue events. J Microsc **235**, 308-321.

Miyagishima, S.Y. (2011). Mechanism of plastid division: from a bacterium to an organelle. Plant Physiol. **155**, 1533-1544.

Miyagishima, S.Y., Froehlich, J.E., and Osteryoung, K.W. (2006). PDV1 and PDV2 mediate recruitment of the dynamin-related protein ARC5 to the plastid division site. Plant Cell **18**, 2517-2530.

Miyagishima, S.Y., and Kabeya, Y. (2010). Chloroplast division: squeezing the photosynthetic captive. Curr. Opin. Microbiol. **13**, 738-746.

Miyagishima, S.Y., Nozaki, H., Nishida, K., Nishida, K., Matsuzaki, M., and Kuroiwa, T. (2004). Two types of FtsZ proteins in mitochondria and red-lineage chloroplasts: the duplication of FtsZ is implicated in endosymbiosis. J. Mol. Evol. **58**, 291-303.

Miyawaki, A., and Tsien, R.Y. (2000). Monitoring protein conformations and interactions by fluorescence resonance energy transfer between mutants of green fluorescent protein. Methods Enzymol **327**, 472-500.

Muller-Reichert, T., Srayko, M., Hyman, A., O'Toole, E.T., and McDonald, K. (2007). Correlative light and electron microscopy of early *Caenorhabditis elegans* embryos in mitosis. Methods Cell Biol **79**, 101-119.

Muller, M., Marti, T., Kriz, S. . (1980). Improved Structural Preservation by Freeze substitution. In: Seventh European Congres on Electron Microscopy The Hague, The Netherlands. 720-721.

Nicolas, G. (1991). Advantages of fast-freeze fixation followed by freeze-substitution for the preservation of cell integrity. J. Electron Microsc. Techn. **18**, 395-405.

Nixon, S.J., Webb, R.I., Floetenmeyer, M., Schieber, N., Lo, H.P., and Parton, R.G. (2009). A single method for cryofixation and correlative light, electron microscopy and tomography of zebrafish embryos. Traffic **10**, 131-136.

Oliva, M.A., Huecas, S., Palacios, J.M., Martin-Benito, J., Valpuesta, J.M., and Andreu, J.M. (2003). Assembly of archaeal cell division protein FtsZ and a GTPase-inactive mutant into double-stranded filaments. J. Biol. Chem. **278**, 33562-33570.

Olson, B.J., Wang, Q., and Osteryoung, K.W. (2010). GTP-dependent heteropolymer formation and bundling of chloroplast FtsZ1 and FtsZ2. J. Biol. Chem. **285**, 20634-20643.

Ormo, M., Cubitt, A.B., Kallio, K., Gross, L.A., Tsien, R.Y., and Remington, S.J. (1996). Crystal structure of the *Aequorea victoria* green fluorescent protein. Science **273**, 1392-1395.

Osawa, M., Anderson, D.E., and Erickson, H.P. (2008). Reconstitution of contractile FtsZ rings in liposomes. Science **320**, 792-794.

Osawa, M., and Erickson, H.P. (2005). Probing the domain structure of FtsZ by random truncation and insertion of GFP. Microbiol. **151**, 4033-4043.

Osteryoung, K.W. (2001). Organele fission in eukaryotes. Curr. Opin. Microbiol. **4**, 639-646.

Osteryoung, K.W. (2011). Plastid Biology: Focus on the Defining Organelle of Plants. Plant Physiol. **155**, 1475-1476.

Osteryoung, K.W., and McAndrew, R.S. (2001). The plastid division machine. Annu. Rev. Plant Physiol. Plant Mol. Biol. **52**, 315-333.

Osteryoung, K.W., and Nunnari, J. (2003). The division of endosymbiotic organelles. Early divergence of the FtsZ1 and FtsZ2 plastid division gene families in photosynthetic eukaryotes. Science **302**, 1698-1704.

Osteryoung, K.W., and Pyke, K.A. (1998). Plastid division: evidence for a prokaryotically derived mechanism. Curr. Opin. Plant Biol. **1**, 475-479.

Osteryoung, K.W., Stokes, K.D., Rutherford, S.M., Percival, A.L., and Lee, W.Y. (1998a). Chloroplast division in higher plants requires members of two functionally divergent gene families with homology to bacterial *ftsZ*. Plant Cell **10**, 1991-2004.

Osteryoung, K.W., Stokes, K.D., Rutherford, S.M., Percival, A.L., and Lee, W.Y. (1998b). Chloroplast division in higher plants requires members of two functionally divergent gene families with homology to bacterial *ftsZ*. Plant Cell **10**, 1991-2004.

Osteryoung, K.W., and Vierling, E. (1995). Conserved cell and organelle division. Nature **376**, 473-474.

Otegui, M.S., and Staehelin, L.A. (2004). Electron tomographic analysis of post-meiotic cytokinesis during pollen development in *Arabidopsis thaliana*. Planta **218**, 501-515.

Plattner, H., and Bachmann, L. (1982). Cryofixation: a tool in biological ultrastructural research. Int. Rev. Cytol. **79**, 237-304.

Porta, D., and Lopez-Iglesias, C. (1998). A comparison of cryo- versus chemical fixation in the soil green algae *Jaagiella*. Tissue & cell **30**, 368-376.

Possingham, J.V., and Lawrence, M.E. (1983). Controls to Plastid Division. Int. Rev. Cytol. **84**, 1-56.

Prasher, D.C., Eckenrode, V.K., Ward, W.W., Prendergast, F.G., and Cormier, M.J. (1992). Primary structure of the *Aequorea victoria* green-fluorescent protein. Gene **111**, 229-233.

Pyke, K. (1998). Plastid Division: The Origin of Replication. Plant Cell **10**, 1971-1972.

Pyke, K.A. (1997). The genetic control of plastid division in higher plants. Am. J. Bot. **84**, 1017-1027.

Pyke, K.A. (2007). Plastid development and differentiation. In Topics in Current Genetics: Cell and Molecular Biology of Plastids, Bock, R. ed., (Berlin: Springer), pp. 1-28.

Pyke, K.A. (2009). Plastid Biology. UK: Cambrige University Press.

Pyke, K.A., and Leech, R.M. (1994). A Ggenetic analysis of chloroplast division and expansion in *Arabidopsis thaliana*. Plant Physiol. **104**, 201-207.

Raskin, D.M., and de Boer, P.A.J. (1999a). MinDE-dependent pole-to-pole oscillation of division inhibitor MinC in *Escherichia coli*. J. Bacteriol. **181**, 6419-6424.

Raskin, D.M., and de Boer, P.A.J. (1999b). Rapid pole-to-pole oscillation of a protein required for directing division to the middle of *Escherichia coli*. Proc. Natl. Acad. Sci. USA **96**, 4971-4976.

RayChaudhuri, D., and Park, J.T. (1994). A point mutation converts *Escherichia coli* FtsZ septation GTPase to an ATPase. J. Biol. Chem. **269**, 22941-22944.

Reddy, A.S.N., and Day, I.S. (2001). Kinesins in the *Arabidopsis* genome: A comparative analysis among eukaryotes. BMC Genomics **2**.

Redick, S.D., Stricker, J., Briscoe, G., and Erickson, H.P. (2005). Mutants of FtsZ targeting the protofilament interface: effects on cell division and GTPase activity. J. Bacteriol. **187**, 2727-2736.

Reynolds, E.S. (1963). The use of lead citrate at high pH as an electron-opague stain in electron microscopy. J. Cell Biol. **17**, 208-212.

Robards, A.W., and Sleytr, U.B. (1985). Low temperature methods in biological electron microscopy. In Practical methods in electron microscopy, (New York: Elsevier).

Robinson, J.M., and Takizawa, T. (2009). Correlative fluorescence and electron microscopy in tissues: immunocytochemistry. J Microsc **235**, 259-272.

Rowland, S.L., Fu, X., Sayed, M.A., Zhang, Y., Cook, W.R., and Rothfield, L.I. (2000). Membrane redistribution of the Escherichia coli MinD protein induced by MinE. J. Bacteriol. **182**, 613-619.

Ryder, M., Beattie, J.M., O'Hanlon, R., and McDonald, K. (2011). Multidsciplinary heart failure management and end of life care. Current opinion in supportive and palliative care **5**, 317-321.

Sanders, M.A. (2002). Recent advances in microwave-assisted specimen processing: keeping it cool. Microsc. Microanal. Proc **8**, 158-159.

Saxton, W.M., Stemple, D.L., Leslie, R.J., Salmon, E.D., Zavortink, M., and McIntosh, J.R. (1984). Tubulin dynamics in cultured mammalian cells. J. Cell Biol. **99**, 2175-2186.

Scheffers, D.J., de Wit, J.G., den Blaauwen, T., and Driessen, A.J. (2002). GTP hydrolysis of cell division protein FtsZ: evidence that the active site is formed by the association of monomers. Biochemistry **41**, 521-529.

Schmitz, A.J., Glynn, J.M., Olson, B.J.S.C., Stokes, K.D., and Osteryoung, K.W. (2009). *Arabidopsis* FtsZ2-1 and FtsZ2-2 are functionally redundant, but FtsZ-based plastid division is not essential for chloroplast partitioning or plant growth and development. Mol. Plant **2**, 1211-1222

Shaner, N.C., Campbell, R.E., Steinbach, P.A., Giepmans, B.N., Palmer, A.E., and Tsien, R.Y. (2004). Improved monomeric red, orange and yellow fluorescent proteins derived from Discosoma sp. red fluorescent protein. Nature biotechnology **22**, 1567-1572.

Shaner, N.C., Patterson, G.H., and Davidson, M.W. (2007). Advances in fluorescent protein technology. J. Cell Sci. **120**, 4247-4260.

Shapiro, L., and Losick, R. (2000). Dynamic spatial regulation in the bacterial cell. Cell **100**, 89-98.

Shaw, S.L., Kamyar, R., and Ehrhardt, D.W. (2003). Sustained microtubule treadmilling in rabidopsis cortical arrays. Science **300**, 1715-1718.

Shimada, H., et al. (2004). ARC3, a chloroplast division factor, is a chimera of prokaryotic FtsZ and part of eukaryotic phosphatidylinositol-4-phosphate 5-kinase. Plant Cell Physiol. **45**, 960-967.

Shimomura, O. (1979). Structure of the chromophore of *Aequorea* green fluorescent protein. FEBS Lett. **104**, 220-222.

Shimomura, O., Johnson, F., and Saiga, Y. (1962). Extraction, purification and properties of aequorin, a bioluminescent protein from the luminous hydromedusan, Aequorea. J. Cell. Comp. Physiol **59**, 223-229.

Skaer, H. (1982). Chemical cryoprotection for structural studies. J. Microsc. **125**, 137-147.

Smith, A.G., Johnson, C.B., Vitha, S., and Holzenburg, A. (2010). Plant FtsZ1 and FtsZ2 expressed in a eukaryotic host: GTPase activity and self-assembly. FEBS Lett. **584**, 166-172.

Sprague, B.L., and McNally, J.G. (2005). FRAP analysis of binding: proper and fitting. Trends Cell Biol. **15**, 84-91.

Spriet, C., Trinel, D., Riquet, F., Vandenbunder, B., Usson, Y., and Heliot, L. (2008). Enhanced FRET contrast in lifetime imaging. Cytometry Part A **73A**, 745-753.

Srinivasan, R., Mishra, M., Wu, L., Yin, Z., and Balasubramanian, M.K. (2008). The bacterial cell division protein FtsZ assembles into cytoplasmic rings in fission yeast. Genes Dev. **22**, 1741-1746.

Stokes, K.D., McAndrew, R.S., Figueroa, R., Vitha, S., and Osteryoung, K.W. (2000). Chloroplast division and morphology are differentially affected by overexpression of *FtsZ1* and *FtsZ2* genes in *Arabidopsis*. Plant Physiol. **124**, 1668-1677.

Stokes, K.D., and Osteryoung, K.W. (2003). Early divergence of the *FtsZ1* and *FtsZ2* plastid division gene families in photosynthetic eukaryotes. Gene **320**, 97-108.

Stricker, J., Maddox, P., Salmon, E.D., and Erickson, H.P. (2002). Rapid assembly dynamics of the *Escherichia coli* FtsZ-ring demonstrated by fluorescence recovery after photobleaching. Proc. Natl. Acad. Sci. USA **99**, 3171-3175.

Studer, D., Hennecke, H., Muller, M. (1992). High-pressure freezing of soybean nodules leads to improved preservation of ultrastructure. Planta **188**, 155-116.

Studer, D., Michel, M., and Muller, M. (1989a). High pressure freezing comes of age. Scanning microscopy. Supplement **3**, 253-268.

Studer, D., Michel, M., and Muller, M. (1989b). High pressure freezing comes of age. Scanning microscopy. Supplement **3**, 253-268; discussion 268-259.

Vaughan, S., Wickstead, B., Gull, K., and Addinall, S.G. (2004). Molecular evolution of FtsZ protein sequences encoded within the genomes of archaea, bacteria, and eukaryota. J. Mol. Evol. **58**, 19-29.

Vitha, S., Froehlich, J.E., Koksharova, O., Pyke, K.A., van Erp, H., and Osteryoung, K.W. (2003). ARC6 Is a J-domain plastid division protein and an evolutionary descendant of the cyanobacterial cell division protein Ftn2. Plant Cell **15**, 1918-1933.

Vitha, S., McAndrew, R.S., Kadirjan-Kalbach, D., Osteryoung, K.W., and Holzenburg, A. (2006). Localization and molecular stoichiometry of plastid division proteins FtsZ1 and FtsZ2. Microsc. Microanal. **12**, 456 CD.

Vitha, S., McAndrew, R.S., and Osteryoung, K.W. (2001). FtsZ ring formation at the chloroplast division site in plants. J. Cell Biol. **153**, 111-119.

Wang, Y.L. (1987). Mobility of filamentous actin in living cytoplasm. J. Cell Biol. **105**, 2811-2816.

Weibull, C., Christiansson, A,. (1986). Extraction of proteins and membrane lipids during low temperature embedding of biological material for electron microscopy. J. Microsc. **142**, 79-86.

Weibull, C., Villiger, W., Carlemalm, E. (1984). Extraction of lipids during freeze-substitution of *Acholeplasma laidlawii*-cells for electron microscopy. J. Microsc. **134**, 213-216.

Wong, J.W., Abuhusain, H.J., McDonald, K.L., and Don, A.S. (2012). MMSAT: automated quantification of metabolites in selected reaction monitoring experiments. Analytical chemistry **84**, 470-474.

Yang, Y., Glynn, J.M., Olson, B.J., Schmitz, A.J., and Osteryoung, K.W. (2008). Plastid division: across time and space. Curr. Opin. Plant Biol. **11**, 577-584.

Yoder, D.W., et al. (2007). Effects of mutations in *Arabidopsis* FtsZ1 on plastid division, FtsZ ring formation and positioning, and FtsZ filament morphology *in vivo*. Plant Cell Physiol. **48**, 775-791.

Yoshida, Y., et al. (2006). Isolated chloroplast division machinery can actively constrict after stretching. Science **313**, 1435-1438.

Zacharias, D.A., Violin, J.D., Newton, A.C., and Tsien, R.Y. (2002). Partitioning of lipid-modified monomeric GFPs into membrane microdomains of live cells. Science **296**, 913-916.

APPENDIX A

Table A-I**.** Primers used to design the constructs.

Primer	Sequence	Protein
CJ-1	TAGAATTCGCATGCGCAAAGTCAGT (forward)	FtsZ1-genomic
CJ-2	TATGGATCCTGGAAGAAAAGTCTACGGGGA (reverse)	FtsZ1-genomic
CJ-3	GCATGAATTCTCAGCACCGTAAATGTAGC (forward)	FtsZ2-cDNA
CJ-4	ATAGGATCCTGGACTCGGGGATAACGAG (reverse)	FtsZ2-cDNA
CJ-5	GATGACTAGTAAGGGCGAGGAGCTGTTC (forward)	mCFP, mYFP
CJ-6	AAATGTTTACTTGTACAGCTCGTCCATGC (reverse)	mCFP, mYFP

Restriction sites used for cloning are underlined.

Table A-II. *Arabidopsis thaliana* plant lines used in the research.

Wild-type-ecotypes		Abbreviation
Columbia		Col-0
Wassilewskija		WS-0
Mutants lines	**Locus**	**Description**
SALK_134970	*At*2G36250	FtsZ2-1 T-DNA insertion (knock-down)
SALK_073878	*At*5G55280	FtsZ1-1 T-DNA insertion (null mutant)
SALK_100009	*At*3G19180	*parc6-1* T-DNA insertion (null mutant)
arc6 mutant)	*At*5G42480	accumulation and replication of chloroplast 6 (null
596H04	*At*2G36250	FtsZ2-1 GABI-Kat T-DNA insertion (null mutant)
ftsZ2-1/ftsZ2-2	*At*2G36250/ *At*5G55280	FtsZ2 double knockout (KO) (double mutant)
ftsZ1-1/ftsZ2-1/ftsZ2-2	*At*5G55280.1/ *At*2G36250.1/ *At*3G52750.1	FtsZ1-1 FtsZ2-1 and FtsZ2-2 (triple mutant)

APPENDIX B

Aaron G. Smith, Carol B. Johnson, Stanislav Vitha, and Andreas Holzenburg (2011). "Oligomerization of plant FtsZ1 and FtsZ2 plastid division proteins. Archives of Biochemistry and Biophysics. **513,** 94-101.

Note: Reprinted with permission from Elsevier.

Carol Beatrice Johnson contributed the following: assisted with protein purification, the immunoblots and contributed editorial assistance to the final manuscript.

Archives of Biochemistry and Biophysics 513 (2011) 94–101

Contents lists available at ScienceDirect

Archives of Biochemistry and Biophysics

journal homepage: www.elsevier.com/locate/yabbi

Oligomerization of plant FtsZ1 and FtsZ2 plastid division proteins

Aaron G. Smith [a,b], Carol B. Johnson [a,c], Stanislav Vitha [a], Andreas Holzenburg [a,b,c,*]

[a] Microscopy and Imaging Center, Texas A&M University, College Station, TX 77843-2257, USA
[b] Department of Biochemistry and Biophysics, Texas A&M University, College Station, TX 77843-2128, USA
[c] Department of Biology, Texas A&M University, College Station, TX 77843-3258, USA

ARTICLE INFO

Article history:
Received 4 April 2011
and in revised form 22 June 2011
Available online 14 July 2011

Keywords:
FtsZ
Electron microscopy
Structure
Chloroplast division
Assembly mechanism

ABSTRACT

FtsZ was identified in bacteria as the first protein to localize mid-cell prior to division and homologs have been found in many plant species. Bacterial studies demonstrated that FtsZ forms a ring structure that is dynamically exchanged with a soluble pool of FtsZ. Our previous work established that *Arabidopsis* FtsZ1 and FtsZ2-1 are capable of *in vitro* self-assembly into two distinct filament types, termed type-I and type-II and noted the presence of filament precursor molecules which prompted this investigation. Using a combination of electron microscopy, gel chromatography and native PAGE revealed that (i) prior to FtsZ assembly initiation the pool consists solely of dimers and (ii) during assembly of the *Arabidopsis* FtsZ type-II filaments the most common intermediate between the dimer and filament state is a tetramer. Three-dimensional reconstructions of the observed dimer and tetramer suggest these oligomeric forms may represent consecutive steps in type-II filament assembly and a mechanism is proposed, which is expanded to include FtsZ assembly into type-I filaments. Finally, the results permit a discussion of the oligomeric nature of the soluble pool in plants.

Introduction

The Filamentous temperature sensitive Z (FtsZ)[1] protein has been identified as the first protein to localize to the mid-cell in bacteria during a division event [1]. FtsZ contains a tubulin signature motif, GGGTG(T/S)G (S = G or C) that allows for binding of GTP [2,3] and a separate T7 loop region that is highly conserved in all FtsZ and required for GTP hydrolysis [4,5]. Extensive *in vitro* research has demonstrated the GTPase activity of prokaryotic FtsZ [6,7] and its self-assembly into several types of filamentous assemblies depending on the experimental conditions used. A monomeric population of FtsZ undergoes linear antiparallel assembly into 4.3 nm wide single-stranded protofilaments [8,9]. There are significant differences between FtsZ from different prokaryotes. In contrast to the most frequently studied FtsZ from *Escherichia coli* and *Bacillus subtilis*, *Mycobacterium tuberculosis* FtsZ has substantially lower GTPase activity and assembly dynamics, forms thicker bundles (53 ± 11 nm) [10] and lateral dimers that assemble longitudinally and/or laterally into larger structures [11].

Plant chloroplasts evolved from a cyanobacterial endosymbiont and, during evolution, the single prokaryotic FtsZ gene from the endosymbiont gave rise to two functionally distinct FtsZ families, FtsZ1 and FtsZ2 [12,13]. The FtsZ1 and FtsZ2 families in the model plant *Arabidopsis thaliana* share 51% sequence identity to *E. coli* FtsZ [14,15] and retain the tubulin signature motif, have a highly conserved N-terminus and localize to a Z-ring at mid-chloroplast [14,16]. The FtsZ1 family has a single member, *At*FtsZ1-1, while the FtsZ2 family has two members with redundant functions, *At*FtsZ2-1 and *At*FtsZ2-2 [12,14,17]. A number of additional components of the chloroplast division machinery has been identified, and their roles and interactions are being elucidated. The assembly of FtsZ1 and FtsZ2 at the division site and their specific interactions with positive and negative regulators is crucial for normal chloroplast division [18,19]. However, the biochemical and structural properties of FtsZ1 and FtsZ2 and their assembly mechanism remain poorly understood. Only recently Olson et al. [18,20] and a report from our laboratory [21] demonstrated differential GTPase activity of FtsZ1 and FtsZ2 and evidence of *in vitro* assembly. Results from our ongoing *in vivo* analysis of FtsZ indicated that similar to bacterial Z-ring, *Arabidopsis* FtsZ1 and FtsZ2 also undergo dynamic exchange of subunits within the Z-ring (C.B. Johnson et al., in preparation). The existence of this turnover activity prompted an investigation into the state of the FtsZ soluble pool using electron microscopy (EM), native PAGE and gel chromatography of (i) precursor molecules occurring in the presence of GTP under assembly conditions and (ii) particles occurring in the

* Corresponding author at: Microscopy and Imaging Center, Texas A&M University, College Station, TX 77843-2257, USA. Fax: +1 979 847 8933.
E-mail address: holzen@mic.tamu.edu (A. Holzenburg).

[1] *Abbreviations used:* FtsZ, filamentous temperature sensitive Z; EM, electron microscopy; EDTA, ethylenediaminetetraacetic acid; NaMES, 2-(*N*-morpholino)ethanesulfonic acid; EGTA, ethylene glycol tetraacetic acid; MEMK, 100 mM MES, 1 mM EGTA, 5 mM Mg acetate, pH 6.5; FSC, Fourier shell correlation.

0003-9861/$ - see front matter © 2011 Elsevier Inc. All rights reserved.
doi:10.1016/j.abb.2011.07.001

absence of nucleotides and assembly procedures *in vitro*. The data described here characterize for the first time the structures of oligomeric states present during assembly of *Arabidopsis* FtsZ at 2.5 nm resolution.

Materials and methods

Protein purification

A detailed explanation of the FtsZ1 and FtsZ2 plasmid constructs used in this work has been described previously [21]. *Pichia* X-33 strains expressing FtsZ1 or FtsZ2 were grown in 250 ml cultures using buffered methanol complex medium (1% (w/v) yeast extract, 2% (w/v) peptone, 100 mM potassium phosphate (pH 6.0), 1.34% (w/v) yeast nitrogen base, 4×10^{-5}% (w/v) biotin, and 1% (v/v) methanol) and supplemented with 3% (v/v) methanol every 12 h for a total growth time of 60 h at 30 °C. Cell lysates were prepared by centrifuging the culture and resuspending in 10 ml of breaking buffer (50 mM sodium phosphate (pH 7.4), 1 mM phenylmethylsulfonyl fluoride, 1 mM EDTA, and 5% (v/v) glycerol). An equal volume of 0.5 μm glass beads were added and the sample was vortexed for eight 30 s cycles interspersed by 30 s on ice. The proteins were purified under native conditions using Ni–NTA agarose beads (Invitrogen, Carlsbad, CA) as follows. Cell lysates were poured over a 10 ml Ni–NTA column to selectively purify the tagged protein. After addition of the lysate, it was allowed to bind under gentle agitation for 30 min at 4 °C. Subsequently, four washes were performed with 8 ml of native wash buffer (50 mM sodium phosphate, 0.5 M sodium chloride, and 20 mM imidazole, pH 8.0) and collected by gravity filtration. Finally, the protein was eluted using native elution buffer (50 mM sodium phosphate, 0.5 M sodium chloride, and 250 mM imidazole, pH 8.0) and collected in 1-ml fractions. Subsequently, fractions determined to contain the respective FtsZ protein by SDS–PAGE were dialyzed against a buffer comprised of 50 mM 2-(*N*-morpholino)ethanesulfonic acid (NaMES), 100 mM potassium chloride, 1 mM ethylene glycol tetraacetic acid (EGTA) and 2.5 mM magnesium acetate (pH 6.5) using SnakeSkin® pleated dialysis tubing (Pierce, Rockford, IL) with a 10,000 molecular weight cutoff. Protein concentrations were determined using a NanoDrop 1000 (Thermo Scientific, Rockford, IL), the bicinchoninic acid protein assay (Pierce, Rockford, IL) [22] or by the Bradford method [23]. Collected fractions were subjected to SDS–PAGE and Western blotting to identify pure aliquots for assembly reactions. When homogenous populations were desired, purified protein was subjected to gel permeation chromatography using a Superdex-200 column running on an ÄKTA FPLC™ system (GE Healthcare, Piscataway, NJ). The column was equilibrated with a buffer containing 50 mM NaMES (pH 6.5), 100 mM KCl, 1 mM EGTA, and 2.5 mM magnesium acetate. For calibration purposes, the following standards were used: thyroglobulin (elution volume 10.11 ml, R_S = 8.5 nm, M_r = 669 kDa), apoferritin (elution volume 11.62 ml, R_S = 6.1 nm, M_r = 443 kDa), beta-amylase (elution volume 13.09 ml, R_S = 5.1 nm, M_r = 200 kDa), alcohol dehydrogenase (elution volume 13.85 ml, R_S = 4.6 nm, M_r = 150 kDa), albumin (elution volume 15.1 ml, R_S = 3.55 nm, M_r = 66 kDa) and carbonic anhydrase (elution volume 16.39 ml, R_S = 2.01 nm, M_r = 29 kDa).

FtsZ assembly reactions and electron microscopy

Assembly reactions (20 μl total) were carried out with 0.6 mg of protein and 100 mM MES, 1 mM EGTA, 5 mM Mg acetate, pH 6.5 (MEMK) assembly buffer [21,24], supplemented with 2 mM GTP. Samples were placed on ice for 10 min followed by 10 min at 37 °C. Samples were adsorbed onto carbon-coated grids or carbon-coated formvar grids (copper G 400 mesh) for up to 5 min and negatively stained with 2% (w/v) uranyl acetate. Uranyl acetate has been shown to fix the structure of protein molecules within 10 ms and prior to removing its aqueous environment [25,26]. The preparation therefore reasonably reflects the situation in solution. Specimens were observed in a Jeol 1200 EX TEM operated at an accelerating voltage of 100 kV. Images were captured at calibrated magnifications using an optically coupled 3 k slow scan CCD camera (model 15C, SIA, Duluth, GA) and Maxim DL imaging software.

Image processing

Images typically sampled at 0.51 nm/pixel at the specimen level were processed with CRISP to evaluate initial image quality [27]. Suitable micrographs (absence of drift, astigmatism, etc.) were further processed within the framework of the EMAN software package [28]. Images of selected particles were bandpass-filtered and aligned by reference-free alignment [29]. Classes of particles representing identical orientations were determined by multivariate statistical analysis and hierarchical ascendant classification using complete linkage. Resolution was assessed by using the standard Fourier shell correlation (FSC) criterion [30,31]. The angular refinement process was stopped when no further increase of resolution was observed. The three-dimensional reconstructions were visualized and manipulated using the Chimera software package [32]. Threading of *At*FtsZ1 and *At*FtsZ2 was carried out using the Phyre2 server [33] with *M. tuberculosis* FtsZ (pdb accession code 1rlu) as a template. The Electron Microscopy Data Bank accession code for the homodimer reconstruction is EMD-1910 and the tetramer reconstruction accession code is EMD-1911.

To obtain an averaged projection of the antiparallel dimer a different approach needed to be taken. Given the low abundance of characteristic projections, individual particles were selected and processed using Fourier peak filtering performed on an array of images essentially as described by Ottensmeyer et al. [34] and numerically extended by Misell [58]. Fourier operations were executed using the software package CRISP [27].

Native gel electrophoresis

Discontinuous native gel electrophoresis was carried out according to a protocol developed at the Wolfson Centre for Applied Structural Biology at The Hebrew University of Jerusalem (http://wolfson.huji.ac.il/). Basic-native gels were run in buffer containing 0.38 M glycine, 0.05 M Trizma and pH adjusted to 8.9 with 2 M NaOH. Loading buffer consisted of two parts 100% (v/v) glycerol, one part (v/v) 0.5 M Tris–HCl pH 6.8, one part (v/v) dH_2O and trace amounts of bromophenol blue. In some cases 2 μl of 2% (w/v) ammonium molybdate (pH 7.0) was added following assembly reactions to stabilize intermediates. Ten percent resolving and 4% separating gels were cast and FtsZ protein was loaded into the wells. Gels were initially ran at 50 V and increased to 100 V after the protein front entered the resolving gel. Staining used 50% (v/v) methanol, 40% (v/v) dH_2O, 10% (v/v) acetic acid and 0.25% (w/v) Coomassie Brilliant Blue R and gels were shaken in stain for 1 h. Destaining solution consisted of 15% (v/v) methanol, 10% (v/v) acetic acid and 75% (v/v) dH_2O and was carried out with several changes until bands were readily visible. Precision Plus protein markers (Bio-Rad Hercules, CA) were used as standards for the native PAGE experiments.

Determination of FtsZ critical concentration

FtsZ proteins were subjected to an assembly protocol as above with MEMK buffer containing GTP. Afterwards the samples were

spun at 26 psi for 30 min in an Airfuge® Ultracentrifuge (Beckman Coulter, Fullerton, CA) using an A-100/30 rotor. Following centrifugation, supernatant fractions were carefully removed and fresh assembly buffer was used to resuspend the pellet fractions. Samples were subjected to SDS–PAGE as described previously [21] using a 7% separating gel. Densitometry was performed using ImageJ, a freeware available from http://rsb.info.nih.gov/ij, on Coomassie-stained gel images.

Results

FtsZ1 and FtsZ2 under non-assembly conditions are homodimers

To better understand the population of *Arabidopsis* FtsZ that participates in Z-ring assembly, the oligomeric state of non-assembled FtsZ1 and FtsZ2 particles were determined *in vitro*. Previous results demonstrated that *Arabidopsis* FtsZ assembles into two filament types (type-I and type-II) in the presence of GTP with one of them (type-II) displaying discrete subunits that when assumed to be a prolate ellipsoid yielded a volume of 41.5 kDa which is in agreement with a monomer [21,35]. No filaments were observed in the absence of the assembly procedure and nucleotides (non-assembly condition) [21].

FtsZ1 and FtsZ2 were purified to homogeneity and analyzed for purity by subsequent SDS–PAGE analysis [21]. Protein in the absence of assembly procedures and nucleotides was then subjected to gel permeation chromatography using a Superdex-200 column to separate potential different oligomeric states of FtsZ. Only one major peak was observed on the gel chromatograph for each FtsZ protein and the peak corresponded to approximately 78 kDa for FtsZ1 and approximately 80 kDa for FtsZ2 (Fig. 1) which are close to the calculated molecular mass of dimers suggesting that the molecules are homodimers prior to assembly. This result suggests that *Arabidopsis* FtsZ can dimerize in the absence of added GTP as was shown for bacterial FtsZ [36]. A smaller peak (approximately 3 kDa) was present in both chromatographs and most likely represents residual imidazole carried over from previous purification steps (Fig. 1). The ~78 kDa and ~80 kDa protein peaks were collected over two fractions. In order to determine if protein subjected to chromatography remained biologically active, fractions representing the 78 kDa and 80 kDa proteins were used in assembly reactions in the presence of GTP and/or GDP. Type-I and type-II filaments (see above) were present in these reactions suggesting the proteins remained active following chromatography. The relative ratio of the two filament types differed depending on whether GTP or GDP was included in the reaction and this trend is highlighted in Table 1. Experiments with the dimeric FtsZ1 and FtsZ2 fractions under non-assembly conditions over a wide range of concentrations (from 25 to 500 μg/ml FtsZ) and in the absence of nucleotides did not yield filaments as judged by TEM.

Native gel electrophoresis was used as an independent method to confirm the oligomeric state of unassembled FtsZ proteins. The basic native PAGE gel (Fig. 2) displays a broadened band around the 80 kDa mark which is in agreement with the major peak from the gel chromatograph. No other bands were observed except for one at high molecular weight that most likely represents the assembled FtsZ [21]. Taken together, these results reinforce the idea that FtsZ1 and FtsZ2 are dimers prior to assembly and that the dimer is the principal early building block used in filament formation.

Electron microscopy and image analysis of FtsZ under non-assembly conditions

Following Superdex-200 column fractionation and TEM data acquisition, particles were selected using a semi-automatic routine [28] as it led to a larger data set and eliminated the possibility of user bias. Following particle selection, all data were normalized and low-pass filtered presenting the initial data set (Fig. 3 top panel) that was subsequently aligned by reference-free alignment into class averages (Fig. 3 middle panel) [29]. Initial reconstructions were created using a subset of class averages without imposed symmetry. Iterative refinement was carried out until no further increase of resolution was observed. Examination of the back-projections used to create the final reconstructions revealed that these projections showed features that agreed with those present in the class averages (Fig. 3 bottom panel).

The validity of the three-dimensional reconstructions were evaluated by several methods. Asymmetric triangles are useful in determining whether a sufficient number of projections are present during reconstruction with the vertices of the triangle representing orthogonal views. The asymmetric triangle presented in Fig. 4A demonstrates that many views of the particle are reflected in the reconstruction and that the three-dimensional space has been well sampled. FSC curves help determine whether reconstructions converge as similar FSC curves between iterations are a mark of convergence and provide an approximate resolution. Resolution for the final dimer reconstruction is approximately 2.5 nm and was obtained from a data set containing 12,360 particles. The curves for eight iterations of unassembled FtsZ1 are shown in Fig. 4B. Similar results were generated using the FtsZ2 reconstruction. The reconstruction after the eighth iterative round of refinement displayed an arc-shaped structure with two protomers separated by a wide gap (Fig. 5). Volume measurements estimate the molecular mass of the reconstruction at approximately 85 kDa as shown. It is interesting to note that with bacterial FtsZ the same type of arc-shaped parallel dimers have been observed in *M. tuberculosis* [11]. The chromatography, electrophoresis and EM data together strongly support the existence of parallel dimers in solution thus corroborating the mycobacterial crystal data [11].

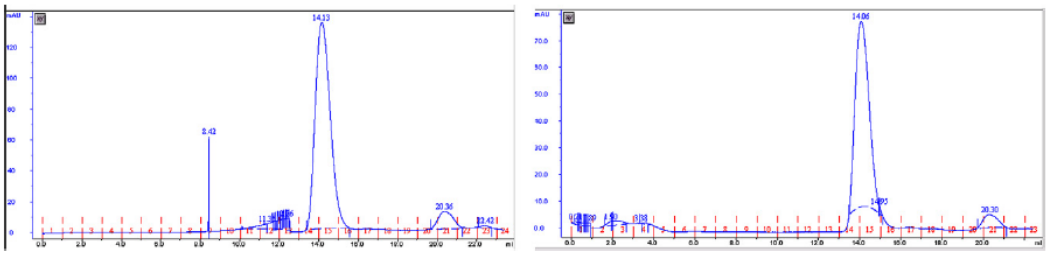

Fig. 1. Gel filtration chromatography of nucleotide-free FtsZ1. Left panel is an elution profile of FtsZ1. The mobility of the front (right) peak corresponds to ~3 kDa, the rear (left) peak is estimated as ~79 kDa, using molecular mass standards. Right panel is an elution profile of FtsZ2. The mobility of the front (right) peak corresponds to ~3 kDa, the rear (left) peak is estimated as ~81 kDa, using molecular mass standards.

Table 1
Distribution and diameter measurements of type-I and type-II filaments with GTP and GDP containing MEMK buffer and under assembly conditions.

	Type-I (%)[a]	Type-II (%)[a]
FtsZ 1+2 (GTP)	38	62
FtsZ 1 (GTP)	27	73
FtsZ 2 (GTP)	41	59
FtsZ1+2 (GDP)	71	29
FtsZ 1 (GDP)	66	34
FtsZ 2 (GDP)	58	42
Filament diameter[b]	14.4 nm ± 0.8	11.2 nm ± 0.3

Standard deviation for type-II filaments in GTP is 6.01.
Standard deviation for type-I filaments in GDP is 5.35.
[a] $n = 100$.
[b] $n = 70$.

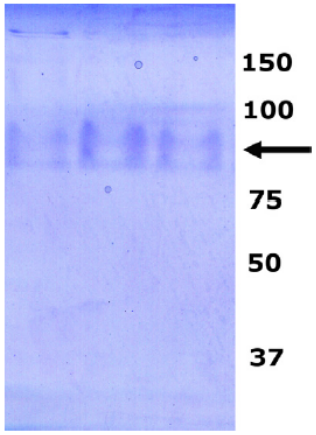

Fig. 2. Basic native PAGE of FtsZ proteins. Native gel showing bands for FtsZ1 (left lane) and FtsZ2 (middle and right lanes) at approximately 80 kDa (arrow) which corresponds to a dimer. The broadness of the band suggests that two distinct populations of similar sizes may be represented. Molecular weight marker positions are given in kDa.

It should be noted that the 85 kDa reconstruction presented here is of an even smaller mass than the recently studied 144 kDa tetrameric Kir prokaryotic channel leading to a structure at 2.4 nm resolution [37]. Aligning the sequences of *Arabidopsis* FtsZ1 and FtsZ2 to mycobacterial FtsZ resulted in a predicted model (Supplement Fig. 1) that showed considerable hydrophilic surfaces in the hinge region of the arc-shaped dimer. It is possible that these surfaces in conjunction with their positioning close to a cleft would lead to a local accrual of negative stain in the hinge region and subsequently account for the "slim" appearance of the intersubunit connection (Fig. 5).

In any case, this connection is the only one point where the monomers contact each other and this part of the protein is likely to contain the FtsZ self-interaction domain. Separate studies using *E. coli* FtsZ suggest that the self-interaction domain is contained between amino acid residues 175 to 323 [38] or residues 100 to 326 [39]. This region is well conserved between bacterial and *Arabidopsis* FtsZ. It should be noted that the tubulin signature motif, essential for nucleotide binding, is located upstream of the region described by Di Lallo and colleagues [38]. A report utilizing *Staphylococcus aureus* FtsZ showed that a nine amino acid region (residues 202–210) of FtsZ and a single residue, L270, are necessary for self-interaction [40]. Three amino acids are conserved in both *Arabidopsis* FtsZ families in the 202–210 region and are also conserved in *E. coli* FtsZ and the L270 residue is conserved in FtsZ2 but not FtsZ1 (Supplement Fig. 2). These results lend support to the idea that homodimers are a building block of the FtsZ filament assembly mechanism in the presence of GTP.

The most abundant FtsZ assembly precursor molecule en route to type-II filament assembly is a tetramer

Preceding the analysis of filament assembly precursors, the dependence of the onset of assembly on protein concentration was determined by sedimentation analysis (see Supplement Fig. 3). This parameter, the critical concentration, amounted to 82.75 μg/ml (≈1.95 μM), which is comparable to that for bacterial FtsZ measured using light scattering [41] (2.5 μM), sedimentation [42] (1.5 μM) or isothermal calorimetry [43] (0.3 μM).

Native PAGE of assembly reactions revealed that there are intermediate oligomeric forms between the homodimer and assembled filaments (Fig. 6). It should be noted that these oligomeric forms

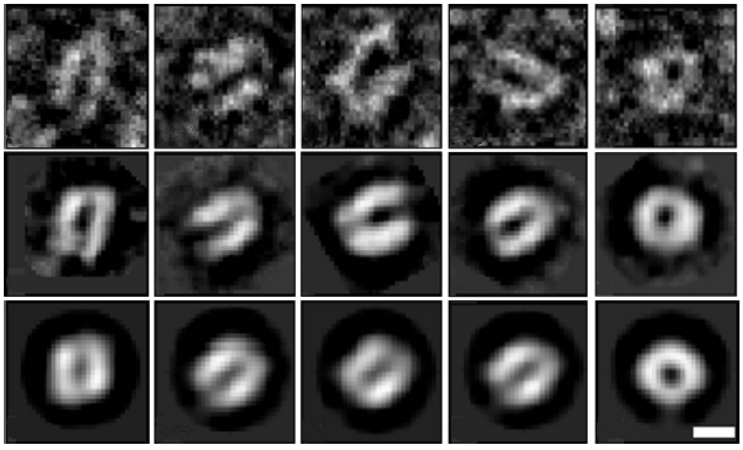

Fig. 3. Image analysis of the FtsZ1 unassembled particles. Top row: raw particles. Middle row: representative class averages harboring the raw particles presented in the top row as members. Bottom row: back-projections from the final three-dimensional reconstruction. Scale bar corresponds to 10 nm.

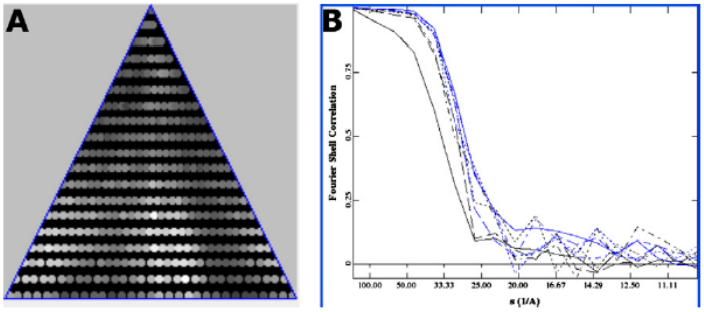

Fig. 4. Asymmetric triangle and FSC curves for FtsZ1 unassembled particles. (A) Asymmetric triangle from the final round of refinement, (B) FSC curves for eight iterative cycles. Estimated resolution for the final reconstruction is approximately 2.6 nm.

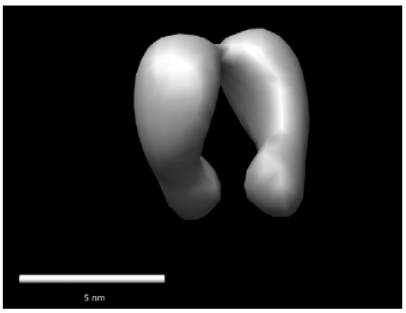

Fig. 5. FtsZ1 unassembled reconstruction. Rendering of the final three-dimensional reconstruction with C2 symmetry imposed.

were only visualized in reactions where ammonium molybdate was added after FtsZ assembly. Ammonium molybdate, in this instance, acted as fixative effectively stopping the assembly reaction and thus preserving a population of oligomeric FtsZ that could enter into the gel. Gel permeation chromatography in the absence of a fixative did not detect a tetrameric population. This observation suggests that the tetramer may be a transiently occurring precursor.

FtsZ1 and FtsZ2 assembly reactions were conducted in the presence of 2 mM GTP, adsorbed onto grids, negatively stained and processed as described for the FtsZ unassembled particles. Initial reconstructions were calculated without imposing symmetry as well as with C4 symmetry imposed (Fig. 7 top and middle panels). Back projections used in the final reconstruction were contained in the class averages (Fig. 7 bottom panel) demonstrating the consistency of the single particle analysis. Iterative refinement was carried out separately with each initial reconstruction yielding similar results. The quality of the data and analysis is also reflected by the asymmetric triangle and the FSC curves for eight iterations of refinement after which no further gain in resolution was observed (Supplement Fig. 4).

The final three-dimensional reconstruction was calculated in C4 with an included mass of 175 kDa which agrees well with the molecule being a tetramer. The molecule measures approximately $12 \times 12 \times 12$ nm with a significant protein deficit of ~5 nm across the base of the structure (Fig. 8). Four protomers are connected at the base where the protein density is contiguous. Each protomer extends from the base approximately 6 nm and measures 4 nm across. In this projection, the center-to-center distance between the protomers measures 5.7 nm. A similar value is observed with

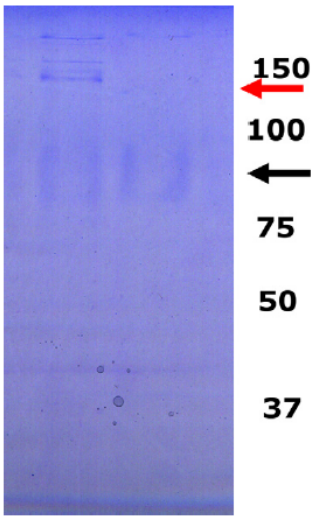

Fig. 6. Native gel of assembly reaction. Left lane shows assembly reaction in the presence of GTP and 2 μl 2% (w/v) ammonium molybdate as a fixative. Additional oligomeric intermediates are present as slower migrating bands. Right lane shows bands for an assembly reaction without ammonium molybdate and no additional intermediates are observed. Migration of molecular mass markers is indicated in kDa. The black arrow corresponds to 75 kDa and the red arrow to 150 kDa. (For interpretation of the references to color in this figure legend, the reader is referred to the web version of this article).

regards to the subunit separation in type-II filaments, which is approximately 6 nm. Taken these data together with earlier observations a tetrameric footprint is discernible within type-II filaments (cf. [21]) which could be interpreted as tetramers assembling into type-II filaments (Fig. 9A). Reconstructions imposing the higher D4 symmetry, which would produce an octamer, did not produce back-projections consistent with the class averages. An octamer could therefore be excluded as the most prevalent assembly intermediate.

Discussion

The current model of chloroplast division implies the presence of a stromal FtsZ pool [44], but the state of assembly or oligomerization of FtsZ in this pool or is not known. The results presented here are the first to examine the composition of the soluble FtsZ

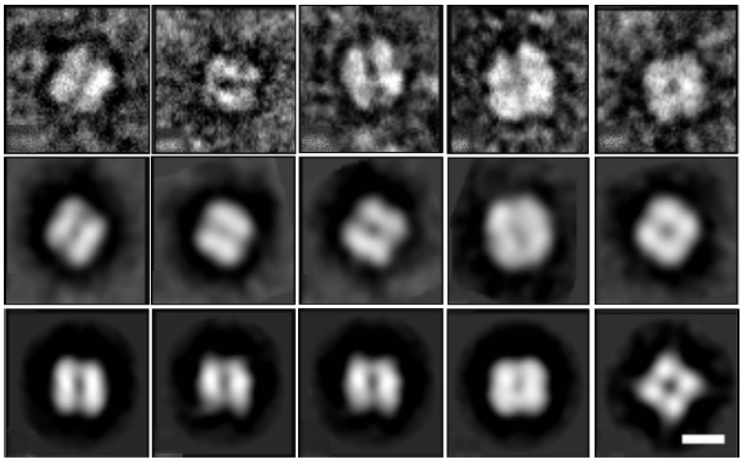

Fig. 7. Image analysis of the FtsZ1 assembly particles. Top row: raw particles. Middle row: representative class averages harboring the raw particles presented in the top row as members. Bottom row: back-projections from the final three-dimensional reconstruction. Scale bar corresponds to 10 nm.

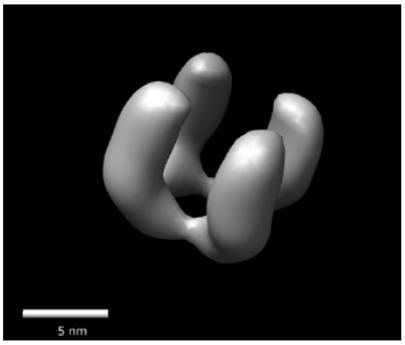

Fig. 8. FtsZ1 assembly intermediate reconstruction. Rendering of the final three-dimensional reconstruction with C4 symmetry imposed.

pool *in vitro*. These experiments investigated the oligomeric state of *Arabidopsis* FtsZ prior to assembly events and following initiation of assembly. Native PAGE and gel chromatography results demonstrate that the smallest identifiable building block of FtsZ assembly is a dimer and native PAGE and image analysis suggest that a tetramer is present under assembly conditions. Additional oligomeric states were not detected in the data sets used for the reconstructions presented here. However, particles that possess dimensions consistent with monomeric FtsZ particles were detected in assembly reactions using GDP (Supplement Fig. 5). Under assembly conditions, image processing with the EMAN software revealed tetramers to be the most widely available oligomeric species in FtsZ assembly reactions. This raises the questions as to whether the dimer and tetramer are consecutive steps in the assembly pathway and what is the ultimate fate of the tetramer during filament assembly.

It is noteworthy that in none of the reactions under assembly conditions has monomeric FtsZ been detected by EM, native PAGE or gel permeation chromatography. This is in stark contrast to bacterial FtsZ, for which a monomeric population was reported *in vitro*

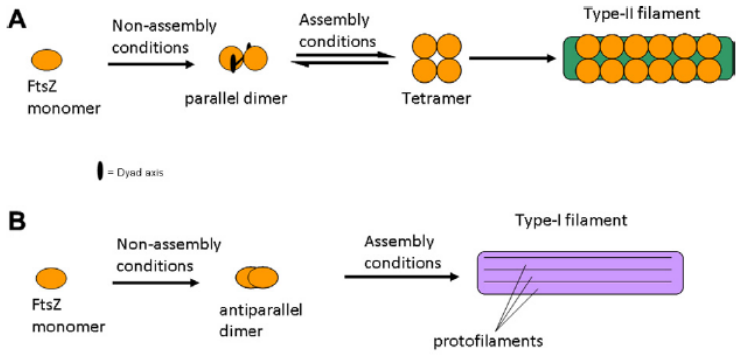

Fig. 9. Hypothetical FtsZ assembly mechanisms in a GTP environment. Schematic representation of FtsZ assembling into (A) type-II or (B) type-I filaments. In this model the type-II filaments are exclusively assembled from tetramers preceded by parallel dimers while type-I filaments are assembled as a result of the formation of antiparallel dimers into protofilaments.

[8] based on sedimentation equilibrium centrifugation. Those authors also propose the linear assembly of monomers into 4.3 nm wide single-stranded protofilaments. Chen et al. [45] reported rapid dimer formation *in vitro* for *M. tuberculosis* FtsZ and suggested that the assembly involves (i) monomer activation, (ii) formation of weak dimer nucleus and (iii) elongation. The presence of FtsZ monomers, dimers and tetramers was also demonstrated by *in vivo* crosslinking in *B. subtilis* [46], suggesting that dimer formation is an essential step of FtsZ assembly not only in *in vitro* but also *in vivo*. Consistent with prior polymerization kinetics data, Lan et al. [47] proposed a simple bundling kinetic model of FtsZ assembly that introduces lateral interactions (perpendicular to filament direction) leading to formation of laterally associated dimers.

The absence of a distinct population of FtsZ monomers in our experiments could be due to their pronounced instability. It has, for instance, been argued that the simple association of two identical monomeric protein molecules into a dimer confers thermodynamic benefits, i.e. freedom for rotational motion and mutual vibration of the monomers in the dimer in conjunction with a possible gain in entropy ($\Delta S_{solvent}$) (based on the loss of protein surface area available for binding water molecules) and a decrease in binding enthalpy (ΔH) [48–50]. This implies that the formation of dimers is highly favored as compared to remaining a monomer. Such a scenario is in line with the two-state reaction model proposed by Neet and Timm who suggest that stable monomers do not exist in significant concentrations at equilibrium [50,51]. In a similar vein, forming a larger ordered assembly would offer the same or even more pronounced overall negative free energy (ΔG) values. Following on from this, it is conceivable that the soluble pool undergoes prompt self-assembly into protofilaments and filaments. If this were true, one would expect to see filaments that exhibit an inter-protofilament spacing in the order of 4 nm based on the findings published for bacterial FtsZ. Upon closer inspection of FtsZ type-I filaments which appear overall void of finer structural details, striations occurring at 4-nm periodicities have been noted. It is therefore plausible that type-I filaments consist of protofilament bundles and that each protofilament resulted from a linear self-association starting with the formation of antiparallel dimers in which there is significant overlap between the monomeric units (Fig. 9B).

The existence of parallel and antiparallel dimers would also be compatible with the broad band observed in the native PAGE (Fig. 2) hinting at the presence of protein populations of similar mass but with different electrophoretic mobilities. Such differences are due to variations in the charge to mass ratio regimes and could be conferred by e.g. differences in subunit interactions which would support the existence of two types of dimers.

The parallel dimers (lateral association) are distinct from the antiparallel (longitudinal association) and do not engage in dovetailing along the 6-nm axis as demonstrated by the given reconstruction (Fig. 5). Through this different association, the antiparallel dimers would have more solvent-accessible surface area available for interaction, which would argue for a quick turnover into protofilaments and filaments. This would in turn explain the low abundance of antiparallel dimers under assembly conditions. This reasoning is also echoed by the low abundance (1–2%) of characteristic antiparallel projections in the electron microscopy data sets. In addition, all class averages of homodimer reconstructions favored the parallel dimer. An average of a rare projection displays some skewing of the two monomers in the antiparallel dimer which enables the dovetailing upon assembly into a protofilament (Supplement Fig. 5).

Plants and algae encode two conserved FtsZ families, FtsZ1 and FtsZ2, which arose by gene duplication after endosymbiosis [12,13] and are both required for normal plastid division [14,17,52]. FtsZ2 closely resembles its cyanobacterial ancestor, while FtsZ1 lost a conserved C-terminal core domain [12,53,54] known to mediate interactions with proteins involved in Z-ring stabilization and tethering to the membrane in both prokaryotes (FtsA, [55]) and plants (ARC6, [56]). The loss of this domain may play a role in FtsZ assembly and differences in the relative rate of assembly between the two FtsZ families. Previous data have shown that both FtsZ1 and FtsZ2 assembly reactions promote the same types of filaments [20,21]. This suggests that both proteins may employ comparable assembly mechanisms. *In vivo*, their assembly rates and/or stability of the assemblies may be modulated by regulatory proteins of the division machinery: FtsZ1 has been shown to interact with a destabilizing factor ARC3 [57], and FtsZ2 with the stabilizing factor ARC6 [56]. Results from recent fluorescence recovery after photobleaching studies are consistent with this model and showed that the *in vivo* turnover of FtsZ2 is substantially slower than that of FtsZ1 (C.B. Johnson et al., in preparation).

The results described in this report demonstrate that both FtsZ1 and FtsZ2 form homodimers prior to assembly. These experiments investigated FtsZ1 and FtsZ2 assembly separately though the proteins are known to colocalize in FtsZ rings *in vivo* [16]. Olson et al. concluded that FtsZ1 and FtsZ2 are able to form heteropolymers *in vitro* where the catalytic loop of one FtsZ molecule interacts with the GTP-binding pocket of the other FtsZ [20]. Whether these heteropolymers are built from FtsZ1 and FtsZ2 homodimers described in this report or whether FtsZ1–FtsZ2 heterodimers are also formed and used for filament incorporation remains to be elucidated. It is, however, intriguing that two types of filaments can be formed from either FtsZ1 or FtsZ2 and that the fate appears to be decided at the level of dimerization. Future studies aiming at a more complete understanding of the assembly process will include filament reconstructions in the presence of nucleotide analogs.

Acknowledgments

The authors wish to thank Dr. Christos Savva for providing guidance concerning the EMAN software and Dr. Ryland Young's laboratory for use of the ÄKTA FPLC™ system. The support by the Office of the Vice-President for Research is greatly acknowledged.

Appendix A. Supplementary data

Supplementary data associated with this article can be found, in the online version, at doi:10.1016/j.abb.2011.07.001.

References

[1] E. Bi, J. Lutkenhaus, Nature 354 (1991) 161–164.
[2] J. Löwe, J. Struct. Biol. 124 (1998) 235–243.
[3] M.G. Rossman, D. Moras, K.W. Olsen, Nature 250 (1974) 194–199.
[4] K. Dai, A. Mukherjee, Y. Xu, J. Lutkenhaus, J. Bacteriol. 176 (1994) 130–136.
[5] J. Löwe, L.A. Amos, EMBO J. 18 (1999) 2364–2371.
[6] P. de Boer, R. Crossley, L. Rothfield, Nature 359 (1992) 254–256.
[7] H.P. Erickson, Trends Cell Biol. 7 (1997) 362–367.
[8] G. Rivas, A. Lopez, J. Mingorance, M.J. Ferrandiz, S. Zorrilla, A.P. Minton, M. Vicente, J.M. Andreu, J. Biol. Chem. 275 (2000) 11740–11749.
[9] D.W. Adams, J. Errington, Nat. Rev. Microbiol. 7 (2009) 642–653.
[10] R. Jaiswal, D. Panda, J. Biochem. 146 (2009) 733–742.
[11] A.K. Leung, E. Lucile White, L.J. Ross, R.C. Reynolds, J.A. DeVito, D.W. Borhani, J. Mol. Biol. 342 (2004) 953–970.
[12] S.Y. Miyagishima, H. Nozaki, K. Nishida, M. Matsuzaki, T. Kuroiwa, J. Mol. Evol. 58 (2004) 291–303.
[13] K.D. Stokes, K.W. Osteryoung, Gene 320 (2003) 97–108.
[14] K.W. Osteryoung, K.D. Stokes, S.M. Rutherford, A.L. Percival, W.Y. Lee, Plant Cell 10 (1998) 1991–2004.
[15] K.W. Osteryoung, E. Vierling, Nature 376 (1995) 473–474.
[16] S. Vitha, R.S. McAndrew, K.W. Osteryoung, J. Cell Biol. 153 (2001) 111–119.
[17] A.J. Schmitz, J.M. Glynn, B.J.S.C. Olson, K.D. Stokes, K.W. Osteryoung, Mol. Plant (2009) (doi:10.1093/mp/ssp1077).

[18] J.M. Glynn, Y. Yang, S. Vitha, A.J. Schmitz, M. Hemmes, S.Y. Miyagishima, K.W. Osteryoung, Plant J. 59 (2009) 700–711.
[19] J. Maple, S.G. Møller, Ann. Bot. 99 (2007) 565–579.
[20] B.J. Olson, Q. Wang, K.W. Osteryoung, J. Biol. Chem. 285 (2010) 20634–20643.
[21] A.G. Smith, C.B. Johnson, S. Vitha, A. Holzenburg, FEBS Lett. 584 (2010) 166–172.
[22] P.K. Smith, R.I. Krohn, G.T. Hermanson, A.K. Mallia, F.H. Gartner, M.D. Provenzano, E.K. Fujimoto, N.M. Goeke, B.J. Olson, D.C. Klenk, Anal. Biochem. 150 (1985) 76–85.
[23] M.M. Bradford, Anal. Biochem. 72 (1976) 248–254.
[24] H.P. Erickson, J. Cell Biol. 148 (2000) 1103–1106.
[25] A.J. Martin-Galiano, R.M. Buey, M. Cabezas, J.M. Andreu, J. Biol. Chem. (2010) (doi:10.1074/jbc.M110.117127).
[26] J.L. Camberg, J.R. Hoskins, S. Wickner, Proc. Natl. Acad. Sci. 106 (2009) 10614–10619.
[27] S. Hovmöller, Ultramicroscopy 41 (1992) 121–135.
[28] S.J. Ludtke, P.R. Baldwin, W. Chiu, J. Struct. Biol. 128 (1999) 82–97.
[29] P. Penczek, M. Radermacher, J. Frank, Ultramicroscopy 40 (1992) 33–53.
[30] G. Harauz, M. van Heel, Optik 73 (1986) 146–156.
[31] W.O. Saxton, W. Baumeister, J. Microsc. Oxford 127 (1982) 127–138.
[32] E.F. Pettersen, T.D. Goddard, C.C. Huang, G.S. Couch, D.M. Greenblatt, E.C. Meng, T.E. Ferrin, J. Comput. Chem. 25 (2004) 1605–1612.
[33] L.A. Kelley, M.J. Sternberg, Nat. Protoc. 4 (2009) 363–371.
[34] F.P. Ottensmeyer, J.W. Andrew, D.P. Bazettjones, A.S.K. Chan, J. Hewitt, J. Microsc. Oxford 109 (1977) 259–268.
[35] A. Holzenburg, P.C. Jones, T. Franklin, T. Pali, T. Heimburg, D. Marsh, J.B. Findlay, M.E. Finbow, Eur. J. Biochem. 213 (1993) 21–30.
[36] T.M. Sossong, M.R. Brigham-Burke, P. Hensley, K.H. Pearce, Biochemistry 38 (1999) 14843–14850.
[37] E. Leal-Pinto, Y. Gomez-Llorente, S. Sundaram, Q.Y. Tang, T. Ivanova-Nikolova, R. Mahajan, L. Baki, Z. Zhang, J. Chavez, I. Ubarretxena-Belandia, D.E. Logothetis, J. Biol. Chem. 285 (2010) 39790–39800.
[38] G. Di Lallo, D. Anderluzzi, P. Ghelardini, L. Paolozzi, Mol. Microbiol. 32 (1999) 265–274.
[39] X. Wang, J. Huang, A. Mukherjee, C. Cao, J. Lutkenhaus, J. Bacteriol. 179 (1997) 5551–5559.
[40] K. Yan, T.M. Sossong, D.J. Payne, Biochem. Biophys. Res. Commun. 284 (2001) 515–518.
[41] A. Mukherjee, J. Lutkenhaus, J. Bacteriol. 181 (1999) 823–832.
[42] A. Mukherjee, J. Lutkenhaus, EMBO J. 17 (1998) 462–469.
[43] M.R. Caplan, H.P. Erickson, J. Biol. Chem. 278 (2003) 13784–13788.
[44] J.M. Glynn, S. Miyagishima, D.W. Yoder, K.W. Osteryoung, S. Vitha, Traffic 8 (2007) 451–461.
[45] Y. Chen, D.E. Anderson, M. Rajagopalan, H.P. Erickson, J. Biol. Chem. 282 (2007) 27736–27743.
[46] S.O. Jensen, L.S. Thompson, E.J. Harry, J. Bacteriol. 187 (2005) 6536–6544.
[47] G. Lan, A. Dajkovic, D. Wirtz, S.X. Sun, Biophys. J. (2008).
[48] I.Z. Steinberg, H.A. Scheraga, J. Biol. Chem. 238 (1963) 172–181.
[49] C. Chothia, J. Janin, Nature 256 (1975) 705–708.
[50] C.J. Tsai, S.L. Lin, H.J. Wolfson, R. Nussinov, Protein Sci. 6 (1997) 53–64.
[51] K.E. Neet, D.E. Timm, Protein Sci. 3 (1994) 2167–2174.
[52] D.W. Yoder, D. Kadirjan-Kalbach, B.J.S.C. Olson, S.Y. Miyagishima, S.L. DeBlasio, R.P. Hangarter, K.W. Osteryoung, Plant Cell Physiol. 48 (2007) 775–791.
[53] K.W. Osteryoung, R.S. McAndrew, Annu. Rev. Plant Physiol. Plant Mol. Biol. 52 (2001) 315–333.
[54] K.W. Osteryoung, J. Nunnari, Science 302 (2003) 1698–1704.
[55] X.L. Ma, W. Margolin, J. Bacteriol. 181 (1999) 7531–7544.
[56] J.M. Glynn, J.E. Froehlich, K.W. Osteryoung, Plant Cell 20 (2008) 2460–2470.
[57] J. Maple, L. Vojta, J. Soll, S.G. Møller, EMBO Rep. 8 (2007) 293–299.
[58] D.L. Misell, Image Analysis, Enhancement and Interpertation, North Holland Publishing, Amsterdam, 1978.

APPENDIX C

Aaron G. Smith, Carol B. Johnson, Stanislav Vitha, and Andreas Holzenburg (2010). Plant FtsZ1 and FtsZ2 expressed in a eukaryotic host: GTPase activity and self-assembly. FEBS Letter. **584**, 166-172.

Reprinted with permission from Elsevier.

Carol Beatrice contributed the following: transformation of *P. pastoris* strains X33, GS115 and KM71H, growth of *Pichia* X33 strains, preparation of cell lysates, JEOL 1200 transmission electron microscope observations, and contributed editorial assistance throughout manuscript preparation.

FEBS Letters 584 (2010) 166–172

FEBS Letters

journal homepage: www.FEBSLetters.org

Plant FtsZ1 and FtsZ2 expressed in a eukaryotic host: GTPase activity and self-assembly

Aaron G. Smith [a,b], Carol B. Johnson [a,c], Stanislav Vitha [a], Andreas Holzenburg [a,b,c,*]

[a] Microscopy and Imaging Center, Texas A&M University, College Station, TX 77843-2257, USA
[b] Department of Biochemistry and Biophysics, Texas A&M University, College Station, TX 77843, USA
[c] Department of Biology, Texas A&M University, College Station, TX 77843, USA

ARTICLE INFO

Article history:
Received 9 October 2009
Revised 6 November 2009
Accepted 11 November 2009
Available online 16 November 2009

Edited by Ulf-Ingo Flügge

Keywords:
FtsZ
Electron microscopy
Self-assembly
GTP
Plastid division
Arabidopsis thaliana

ABSTRACT

Plants and algae contain the FtsZ1 and FtsZ2 protein families that perform specific, non-redundant functions in plastid division. In vitro studies of chloroplast division have been hampered by the lack of a suitable expression system. Here we report the expression and purification of FtsZ1-1 and FtsZ2-1 from *Arabidopsis thaliana* using a eukaryotic host. Specific GTPase activities were determined and found to be different for FtsZ1-1 vs. FtsZ2-1. The purified proteins readily assembled into previously unreported assembly products named type-I and -II filaments. In contrast to bacterial FtsZ, the *Arabidopsis* proteins do not form bundled sheets in the presence of Ca^{2+}.

1. Introduction

Chloroplasts and other types of plastids evolved from cyanobacterial endosymbiotic ancestors [1–3] and their division requires proteins that are homologous to bacterial FtsZ. In contrast to most prokaryotes, which have a single form of FtsZ, plants and algae contain two structurally distinct FtsZ protein families, FtsZ1-1 from *Arabidopsis thaliana* (FtsZ1) and FtsZ2-1 from *A. thaliana* (FtsZ2), that play essential and non-redundant roles in plastid division [4] and are colocalized in FtsZ rings in the chloroplast stroma underneath the envelope membrane [5–7]. Recently, a previously identified FtsZ protein from the moss *Physcomitrella patens* was re-classified as a member of a new FtsZ family, FtsZ3, and it was suggested that FtsZ3 arose after the divergence of bryophytes [8]. Vascular plants apparently do not contain FtsZ3 [8]. *A. thaliana* contains two FtsZ2 family members with redundant functions, *At*FtsZ2-1 and *At*FtsZ2-2, of which the latter is less abundant [9] and therefore only *At*FtsZ2-1 was included in this study.

The assembly of both FtsZ1 and FtsZ2 into the FtsZ ring is a crucial step in plastid division. The two FtsZ proteins integrate the effect of antagonistic regulatory factors (disassembly vs. stabilization of FtsZ polymers) [10,11] via specific interactions of FtsZ1 with accumulation and replication of chloroplasts 3 (ARC3) and FtsZ2 with ARC6, and coordinate assembly of the other components of the division machinery located on both the inner (stromal) and outer (cytoplasmic) sides of the chloroplast envelope [10,12,13]. Even though the mechanism of plastid division is becoming overall better understood and the functional differences between FtsZ1 and FtsZ2 are being revealed, the biochemical properties of FtsZ1 and FtsZ2, structure of FtsZ assemblies and the assembly mechanism remain unknown. To date, in vitro studies have been hampered by the lack of suitable amounts of functional, soluble purified protein from bacterial expression systems. The reason for this is threefold: (i) an unfavorable codon bias of plant FtsZs leads to low expression levels, (ii) toxicity to the host cell, and (iii) the formation of inclusion bodies. Here we describe the expression of *A. thaliana FtsZ1-1* and *FtsZ2-1* in the eukaryotic host *Pichia pastoris*, demonstrate specific GTPase activities of the purified recombinant proteins and show that they are capable of assembling into filamentous structures.

Abbreviations: FtsZ, filamentous temperature sensitive Z; ARC, accumulation and replication of chloroplasts; FtsZ1, FtsZ1-1 from *Arabidopsis thaliana*; FtsZ2, FtsZ2-1 from *Arabidopsis thaliana*

* Corresponding author. Address: Microscopy and Imaging Center, Texas A&M University, College Station, TX 77843-2257, USA. Fax: +1 979 847 8933.
E-mail address: holzen@mic.tamu.edu (A. Holzenburg).

0014-5793/$36.00
doi:10.1016/j.febslet.2009.11.044

2. Materials and methods

Detailed procedures are given in the Supplemental data.

2.1. Plasmid constructs

The following convention is adhered to: FtsZ1 stands for *At*FtsZ1-1 and FtsZ2 for *At*FtsZ2-1. FtsZ1 wild-type cDNA (Genbank accession U39877) 180 nt to end and FtsZ2 cDNA (NM_129183) fragment containing 20–1435 nt of the coding sequence were amplified corresponding to the predicted mature protein without the chloroplast targeting sequence. An initiation ATG as part of a yeast consensus sequence was introduced by PCR [14].

Each PCR product was cloned in-frame into the pPICZ B expression vector (Invitrogen) which added a c-myc and 6× his tag to the C-terminus. The resulting expression constructs were then isolated and used for transformation of *P. pastoris* strains X33, GS115, and KM71H with the Easy Select *Pichia* expression kit (Invitrogen).

2.2. FtsZ gene expression and purification of recombinant proteins

Pichia X33 strains expressing *FtsZ1* or *FtsZ2* were grown in 200 mL cultures using buffered methanol complex medium supplemented with 3% (v/v) methanol every 12 h for a total growth time of 60 h at 30 °C. Cell lysates were prepared and purified under native conditions using nickel–nitriloacetic acid (Ni–NTA) agarose beads (Invitrogen). Fractions determined to contain the respective FtsZ protein by SDS–PAGE were dialyzed and their concentrations determined by NanoDrop 1000 (Thermo Scientific), the BCA protein assay (Pierce) [15] or the Bradford method [16]. Collected fractions were subjected to SDS–PAGE and Western blotting to identify pure aliquots for assembly reactions.

2.3. Western and dot blots

Fractions were separated by SDS–PAGE (10% separating and 4% stacking gels) using a Mini-PROTEAN 3 system (Bio-Rad) [17]. Protein was transferred onto 0.2 μm nitrocellulose, blocked for 1 h with 2% (v/v) cold water fish gelatin (Sigma) followed by an overnight incubation at 4 °C with mouse monoclonal anti-c-myc antibody (Invitrogen), three washes for 10 min each, and a 45-min incubation with mouse anti-rabbit alkaline phosphatase conjugate (Invitrogen) followed by four 10 min washes. Developing was carried out in the presence of 5% (w/v) aqueous BCIP solution (5-Br–4-Cl–3-indolyl-phosphate, Research Products International), and 10 μL of 7.5% (w/v) NBT (nitroblue tetrazolium, Research Products International) in 100% (v/v) methanol at 21 °C.

2.4. GTPase assay

GTPase activity was measured using a continuous, regenerative GTPase assay [18] at 37 °C with 50 μL reaction volumes (4 μM FtsZ) in a 384-well plate (Greiner Bio-One). Absorbances at 340 nm were monitored using a Synergy™ HT Multi-Mode Microplate Reader (BioTek Instruments, Inc.). Data were plotted using Microsoft Excel and corrected against a sample containing no protein. GTPase activities given are derived from triplicate experiments. In control reactions, GTP was substituted by GMPCPP, which is hydrolyzed at a much slower rate than GTP [19].

2.5. FtsZ assembly reactions and electron microscopy

Assembly reactions were carried out with either MEMK [20] or HEPESAc buffers [21]. Reactions contained 0.6 mg of FtsZ protein per mL and either 2 mM GTP, 2 mM GMPPNP (non-hydrolyzable GTP analog) or no nucleotide and assembly conditions consisted of a 10 min incubation on ice followed by 10 min at 37 °C. For electron microscopic analysis 2–5 μL of the reaction mixture was adsorbed onto a freshly glow-discharged carbon-coated Formvar grid, washed briefly in water and negatively stained with a 2% (w/v) aqueous solution of uranyl acetate (pH 4.5). Specimens were observed in a JEOL 1200 EX transmission electron microscope operated at an acceleration voltage of 100 kV. Electron micrographs were recorded at calibrated magnifications.

3. Results

3.1. A. thaliana FtsZ1 and FtsZ2 can be heterologously expressed in a eukaryotic system

The FtsZ constructs in the *P. pastoris* expression vectors were designed to contain only the predicted mature FtsZ protein, without the N-terminal chloroplast targeting sequence as predicted by ChloroP [22]. Three *Pichia* strains bearing FtsZ (X33, GS115, KM71H) were constructed and tested for expression. Only the X33 strain supported expression at levels appropriate for further processing. Positive transformants were identified by immunoblotting with an anti-c-myc antibody (Fig. 1 lanes o–u and Supplementary Fig. 1 lanes k–o).

The purest fractions eluted from the Ni–NTA affinity column (Fig. 1, lanes j–l and Supplementary Fig. 1, lane i) were dialyzed, concentrated to 1–3 mg/mL and used for subsequent experiments. These fractions were resolved as a single band on a stained gel and were detected as a single band of the same molecular mass on immunoblots probed with anti-c-myc antibody (Fig. 1, lanes q–s and Supplementary Fig. 1, lane n). In control cell lysates from a non-transformed X33 *Pichia* strain that were subjected to an identical purification procedure, no detectable protein was obtained after elution from the affinity column on a Coomassie-stained gel and likewise, no signal was detected in immunoblots probed with anti-c-myc antibody (data not shown). This indicated that the purification procedure was specific for the protein of interest, and that the purified FtsZ was free of *Pichia* contaminants.

3.2. FtsZ1 and FtsZ2 have GTPase activity in vitro

Plant FtsZs were expected to be GTPases due to a conserved GTPase domain and overall similarity to prokaryotic FtsZs. To characterize GTPase activity of plant FtsZ1 and FtsZ2 and differences therein, a continuous GTPase assay was used [18]. A continuous assay avoids the possibility of substrate depletion and ensures an accurate representation of data in case of a lag phase [18,23].

The individual FtsZ proteins and the co-assembly each displayed a GTPase activity (Fig. 2A–C). The specific activity of preparations containing both FtsZ1 and FtsZ2 at equimolar concentrations (16.5 ± 0.3 nmol GTP hydrolyzed/min/mg protein) was significantly lower than a simple average (~40 nmol GTP hydrolyzed/min/mg protein) of the individual activities (FtsZ1: 66 ± 1.5 nmol GTP hydrolyzed/min/mg protein; FtsZ2: 12 ± 0.5 nmol GTP hydrolyzed/min/mg protein). This suggests that FtsZ1 + FtsZ2 interactions may regulate GTPase activity of the assemblies. GTP was replaced by the analog GMPCPP, which is hydrolyzed several times slower [19] and the measured GTPase activity dropped significantly (Fig. 2A–C). When the K^+ component of the GTPase buffering system was replaced with Na^+, the GTP hydrolysis fell to essentially zero (data not shown). The same effect was reported for archaeal FtsZ GTPase activity [24].

Overall the results show that plant FtsZ1 and FtsZ2 exhibit GTPase activities comparable to that reported for bacterial/archaeal FtsZ [25–27], which ranges from ~13 nmol/min/mg of protein

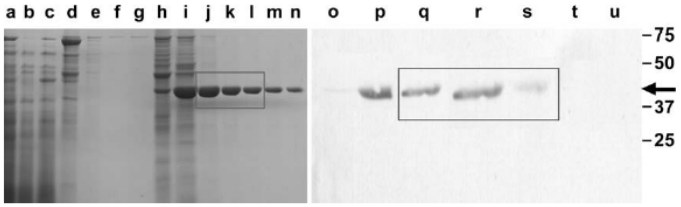

Fig. 1. Purification of recombinant FtsZ1 expressed in *Pichia pastoris*. Coomassie-stained FtsZ1 SDS–PAGE (a–n) and Western blot (o–u) probed with anti-c-myc antibody. (a) Diluted whole cell lysate, (b) flowthrough, (c–g) wash fractions (h–n) eluate fractions 1–7, and (o–u) Western blot corresponding to eluate fractions 1–7. Molecular mass marker positions are given in kDa. The arrow indicates the FtsZ1 band. The box indicates fractions that were used for dialysis and subsequent experiments.

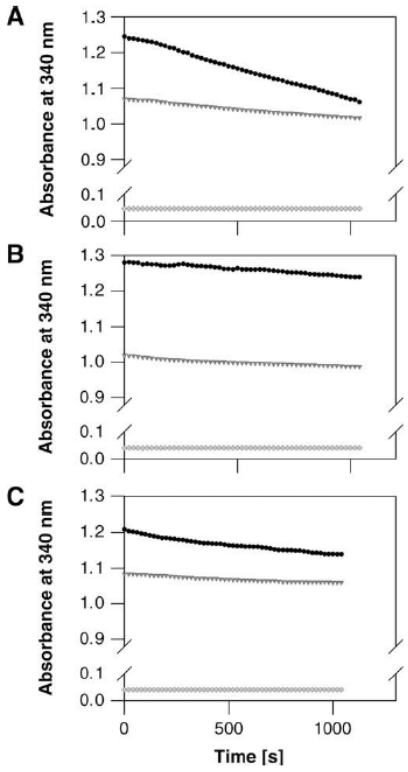

Fig. 2. GTPase activity of FtsZ1-1 from *Arabidopsis thaliana* (FtsZ1) and FtsZ2-1 from *Arabidopsis thaliana* (FtsZ2). Enzyme-coupled assay monitoring NADH oxidation vs. time for (A) FtsZ1, (B) FtsZ2, and (C) FtsZ1 + FtsZ2 in the presence of GTP (top black line). Two controls were carried; FtsZ in the presence of GMPCPP (middle gray line) to show significance of GTP and an empty well control (bottom gray line) to ensure experimental compatibility between different experimental set-ups (i.e. this report vs. Ingerman and Nunnari [18]). Readings were taken every 20 s for at least 15 min. The slope was subsequently used to calculate GTPase activity as described (see Supplemental data).

in *Mycobacterium tuberculosis* (5 μM FtsZ) [28] to ~90 nmol/min/mg of protein in *E. coli* (4 μM FtsZ) [27].

3.3. FtsZ1 and FtsZ2 are able to assemble independently and in combination with each other into filamentous structures in the presence of GTP

In order to determine whether heterologously expressed and purified FtsZ is able to assemble into higher order structures, purified FtsZs were tested in GTP-containing buffer systems that had previously proven successful with bacterial FtsZ, MEMK [20] and HEPESAc [21]. The presence of assemblies was monitored by electron microscopy. Both buffer systems yielded similar results and led to the formation of filamentous structures typically ranging from ~100 nm to several μm in length. Results obtained with the MEMK buffer system are shown. The presence of Ca^{2+} in the assembly buffer did not yield any additional forms of assemblies, which is in contrast to bacterial FtsZ which was reported to form Ca^{2+}-induced filament sheets [29].

Filaments were observed when FtsZ1 and FtsZ2 were both present at an equimolar ratio (Fig. 3A) and also in preparations containing only FtsZ1 (Fig. 3B) or FtsZ2 (Fig. 3C). When the purified protein was placed onto a grid without performing the assembly procedure (no GTP in the buffer and no incubation at 37 °C) and was immediately fixed and stained, no filaments formed and only single particles were present (Fig. 4A and Supplementary Fig. 2). This indicated that the filaments observed after assembly are specifically caused by the assembly procedure and that the recombinant protein is active. Using the same procedure in the presence of the non-hydrolyzable GTP analog GMPPNP again resulted in the absence of filaments and only single particles were observed. This control suggests that the purified protein is free of polymeric contaminants and that hydrolysis of guanine nucleotides is required for plant FtsZ polymerization in vitro.

When analyzing the filamentous structures observed, two morphologically distinct types of filaments, termed type-I and -II, could be readily discerned (Figs. 3A–C and 4B–D). Type-I filaments (Fig. 4B) were smoothly delineated and type-II filaments (Fig. 4C and D) displayed discrete, easily identifiable densities that appeared to constitute the subunits – i.e. the smallest repeating units – from which the filaments had assembled. Each of these filament subunits are elliptical in projection with the long axis measuring 6.1 ± 0.2 nm and the short axis 4 ± 0.2 nm. Assuming a prolate ellipsoid as the 3D subunit shape and a partial specific volume (υ) of 0.74 mL/g [30,31], the molecular mass (m) can be estimated according to the formula m (Da) = volume of the protein (mL) × Avogadro's number × $1/\upsilon$ [30]. Using this approach, one arrives at a molecular mass of 41.5 kDa per subunit which is in agreement with the molecular mass of either recombinant FtsZ1 (41.5 kDa) or FtsZ2 (42.5 kDa) used in this work. The molecular dimensions also agree well with the X-ray data for bacterial FtsZ where the bulk of the protein along the three principal axes measures ~3.5 × 4 × 6 nm [32].

The appearance of two distinct filaments in preparations containing FtsZ proteins independently and in combination led us to investigate the distribution of the two filament types. Type-II filaments were predominant in all preparations albeit at different ratios. FtsZ1 preparations (70% type-II, n = 100) yielded the highest proportion while FtsZ2 preparations (54% type-II, n = 100) were only slightly biased towards type-II filaments. As expected, the equimolar mixture of FtsZ proteins gave an intermediate value

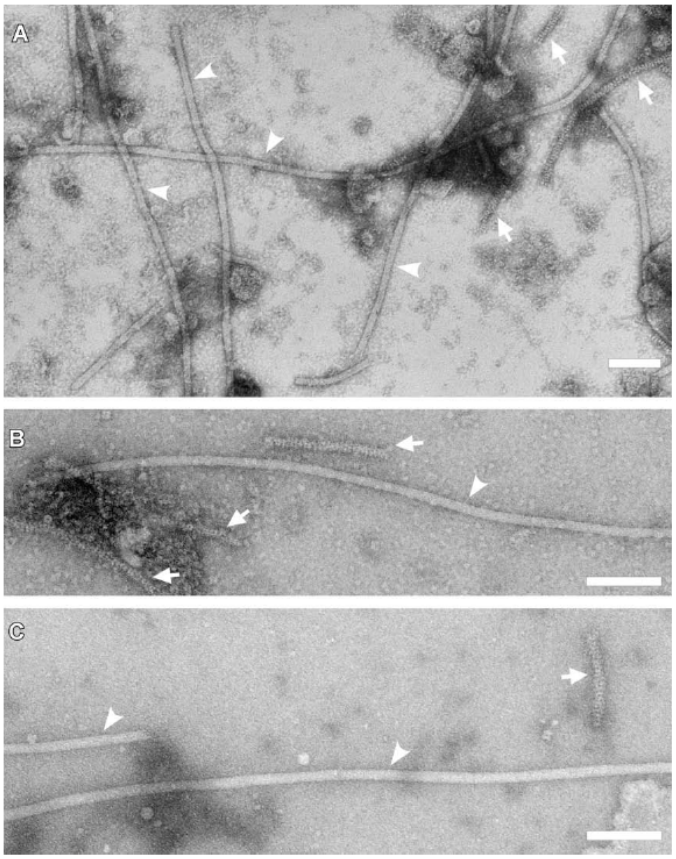

Fig. 3. Electron micrographs of negatively stained FtsZ1 and FtsZ2 assemblies in the presence of GTP. For all panels, arrowheads highlight type-I filaments and arrows highlight type-II filaments. (A) Filaments from a reaction containing FtsZ1 + FtsZ2 in an equimolar mixture, (B) filaments from a reaction containing only FtsZ1, and (C) filaments from a reaction containing only FtsZ2. The background displays filament precursors. Scale bars correspond to 100 nm.

(61% type-II, $n = 100$). Different types of filament precursor particles were observed (Fig. 4A), however, determining their quaternary structures is currently challenged by the high degree of particle heterogeneity.

4. Discussion

The chloroplast division machinery is a complex system composed of both pro- and eukaryotic-origin components and coordinated across the double envelope membranes [13,33,34]. Many prokaryotic cell division proteins have been lost after the endosymbiotic event and new ones evolved to perform novel functions in the chloroplast. The evolution two FtsZ families in plants and their specific interactions with different components of the division machine exemplify this process. However, along with this divergence, there is also a surprising conservation of some interactions and functions between proteins involved in bacterial cell and plant chloroplast division. For instance, plant FtsZ1 and FtsZ2 proteins expressed in *E. coli* assemble into filaments, are localized to the bacterial division site, and their overproduction blocks bacterial cell division [35, and S. Vitha, unpublished] and may even restore bacterial cell division in *ftsZ* mutants [36]. The *Arabidopsis* MinD protein is apparently able to interact with the bacterial FtsZ protein and can rescue *E. coli* Δ*MinCD* mutation [37]. The eukaryotic-origin PARC6 protein [11,38], also known as CDP1 [39] interacts with the chloroplast division protein ARC3, but also blocks cell division when overproduced in *E. coli*. This conservation offers opportunities for studying the properties and interactions of the chloroplast division proteins, but also brings an unwanted complication when purification of recombinant chloroplast division proteins is attempted from a bacterial expression system. Therefore, heterologous expression of higher plant FtsZ was carried out in *Pichia*. There is no endogenous FtsZ in yeast that could result in a contamination of the recombinant FtsZ. Furthermore, *FtsZ* expression is well tolerated in *Pichia*, i.e. the growth is not disrupted and the recombinant protein is neither misfolded nor sequestered into inclusion bodies as often observed with bacterial expression systems [40,41]. The absence of the oligopeptide sequence recognized by the anti-c-myc antibody in the *Pichia* proteome permitted a specific detection of the epitope-tagged recombinant protein. Several lines of evidence indicate that epitope-tagged FtsZ is fully functional: In bacteria, for instance, His-tagged FtsZ constructs can complement the *ftsZ* null allele [42] and assembly dynamics of GFP-tagged FtsZ in *B. subtilis* and *E. coli* is comparable to that ob-

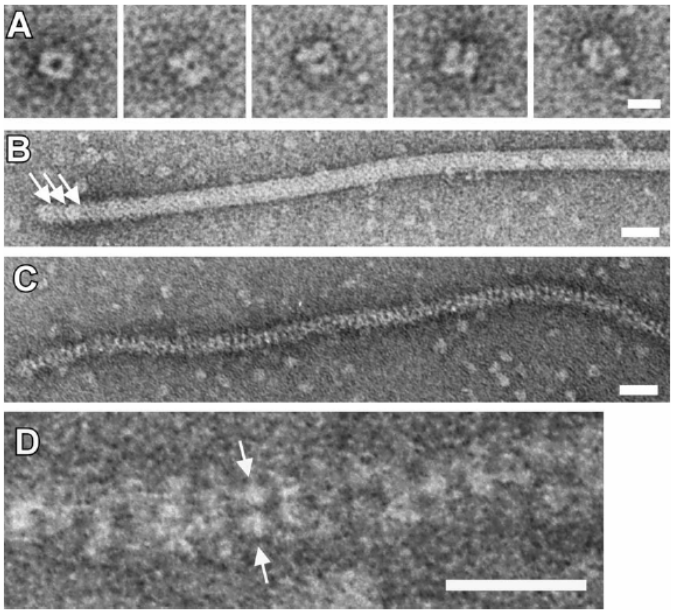

Fig. 4. Electron microscopic analysis of negatively stained in vitro FtsZ1 + FtsZ2 + GTP assemblies. (A) Oligomeric filament precursors in different orientations. (B) Type-I filament displaying helical (arrows) ends. (C) Morphology of type-II filaments including a section of the filament at high magnification (D), readily revealing individual subunits (arrows). Scale bars correspond to 20 nm except for (A) for which it is 10 nm.

tained in vitro with untagged proteins [43]. GFP-tagged *A. thaliana* FtsZ1 and FtsZ2 are capable of assembling into filaments and rings at the chloroplast division site [5], exhibit dynamic turnover in vivo and FtsZ1-GFP can restore chloroplast division in an *ftsZ1* null mutant (personal communication, S. Vitha and C.B. Johnson).

The in vivo macromolecular structure of FtsZ is little understood in either prokaryotes or plant chloroplasts and it remains to be seen to what detail the in vitro polymers reflect the scenario in vivo. An elegant cryo-EM tomography analysis of FtsZ in *Caulobacter crescentus* recently revealed overall length, curvature and localization of FtsZ filaments but did not resolve the filament structure at the macromolecular level [44]. The results in this report demonstrate that *Arabidopsis* FtsZs assemble into two types of filaments that were not previously identified. It is interesting and perhaps not surprising that the observed type-I and -II filaments have not been seen with the single FtsZ bacterial/archaeal in vitro systems and instead other morphologies were reported [24,40,41] that are not echoed by *A. thaliana* FtsZ1 and FtsZ2. Measurements on type-II filaments revealed optically separate building blocks that could correspond to FtsZ monomers (see Section 3). Similar measurements have been used to good effect with filamentous assemblies of the type-II secretion protein of *Pseudomonas aeruginosa* [45].

Both FtsZ1 and FtsZ2 proteins were predicted to be GTPases. It is believed that at least some GTPase activity is needed for their assembly, since in *Arabidopsis*, a G267R mutation of the highly conserved glycine in the predicted GTP-hydrolytic T7 loop of FtsZ1 [46] results in FtsZ1 being unable to form filaments in vivo or coassemble with FtsZ2 [47]. This mutant is likely to be defective in GTPase activity, since mutations in the T7 loop of bacterial FtsZ inhibit GTP hydrolysis activity, cannot complement null mutations [42,48], inhibit bacterial cell division and prevent polymerization both in vitro and in vivo [49]. The in vitro results presented in this report suggest that interaction with guanine nucleotides is necessary for FtsZ1 and/or FtsZ2 assembly since reactions performed without GTP or with a non-hydrolyzable analog (GMPPNP) did not yield any assemblies, which is in agreement with earlier reports on bacterial FtsZ which demonstrated that GMPPNP is a poor substrate for bacterial FtsZ [50,51] and glutathione *S*-transferase tagged *E. coli* FtsZ does not polymerize when GTP is replaced by GMPPNP [52]. However, a more recent study on bacterial FtsZ demonstrated GMPPNP-dependent assemblies – albeit in the presence of crowding agents [53]. While further work is needed to address the relevance of guanine nucleotide binding vs. turnover, the "no-nucleotide" control demonstrates that the filaments observed in the presence of GTP are the result of an active FtsZ protein assembly. Both purified FtsZ1 and FtsZ2 exhibited GTPase activity with the activity of FtsZ1 being ~5 times higher than that of FtsZ2. This is significant, since whether plant FtsZs have any GTPase activity at all, and what the specific activities are, was not previously known. It was suggested that FtsZ1 and FtsZ2 may have evolved to create different GTPase properties within the Z-ring depending on how the monomers assemble [34]. Our results are consistent with this prediction and provide an impetus to investigate the role of the different GTPase activities observed for plant FtsZ1 and FtsZ2.

Type-I filaments for both FtsZ1 and FtsZ2 assemblies presented here appear somewhat similar to those shown by El-Kafafi et al. [54] for *Nicotiana tabacum* recombinant FtsZ1 while for FtsZ2 only globular aggregates were reported. This aggregation may be due to the inclusion of a chloroplast targeting sequence. In contrast, the present studies were conducted using the mature form of FtsZ without the predicted chloroplast transit peptide. Whether both type-I and -II filaments exist in vivo, their stoichiometry and relevance to the overall assembly and function of the FtsZ ring structure is currently under investigation. Both types of filaments may

be required to maintain the FtsZ ring structure in plant chloroplasts and the different molecular arrangements within type-I and -II filaments may affect their ability to interact with other components of the division machinery. Future experiments aimed at studying the interactions of ARC6 and ARC3 with type-I and -II filaments will test this hypothesis.

Acknowledgment

The authors would like to thank E. Ann Ellis and Dr. Christos Savva for helpful discussions and expert technical assistance, Dr. Rosemary McAndrew for discussions in the early stages of the project, the preparation of *Pichia* strain stocks and the purification of cDNA plasmids, and Dr. Matthew Sachs for the gift of GMPPNP. The support of the OVPR is greatly acknowledged. The authors declare that they have no conflict of interest.

Appendix A. Supplementary data

Supplementary data associated with this article can be found, in the online version, at doi:10.1016/j.febslet.2009.11.044.

References

[1] McFadden, G. (1999) Chloroplasts. Ever decreasing circles. Nature 400, 119–120.
[2] Martin, W. and Herrmann, R.G. (1998) Gene transfer from organelles to the nucleus: how much, what happens, and why? Plant Physiol. 118, 9–17.
[3] Douglas, S.E. (1998) Plastid evolution: origins, diversity. Trends Curr. Opin. Genet. Dev. 8, 655–661.
[4] Osteryoung, K.W., Stokes, K.D., Rutherford, S.M., Percival, A.L. and Lee, W.Y. (1998) Chloroplast division in higher plants requires members of two functionally divergent gene families with homology to bacterial *ftsZ*. Plant Cell 10, 1991–2004.
[5] Vitha, S., McAndrew, R.S. and Osteryoung, K.W. (2001) FtsZ ring formation at the chloroplast division site in plants. J. Cell Biol. 153, 111–119.
[6] Kuroiwa, H., Mori, T., Takahara, M., Miyagishima, S. and Kuroiwa, T. (2002) Chloroplast division machinery as revealed by immunofluorescence and electron microscopy. Planta 215, 185–190.
[7] McAndrew, R.S., Froehlich, J.E., Vitha, S., Stokes, K.D. and Osteryoung, K.W. (2001) Colocalization of plastid division proteins in the chloroplast stromal compartment establishes a new functional relationship between FtsZ1 and FtsZ2 in higher plants. Plant Physiol. 127, 1656–1666.
[8] Martin, A., Lang, D., Heckmann, J., Zimmer, A.D., Vervliet-Scheebaum, M. and Reski, R. (2009) A uniquely high number of *ftsZ* genes in the moss *Physcomitrella patens*. Plant Biol. 11, 744–750.
[9] Schmitz, A.J., Glynn, J.M., Olson, B.J.S.C., Stokes, K.D. and Osteryoung, K.W. (2009). *Arabidopsis* FtsZ2-1 and FtsZ2-2 are functionally redundant, but FtsZ-based plastid division is not essential for chloroplast partitioning or plant growth and development. Mol. Plant, doi:10.1093/mp/ssp077.
[10] Maple, J., Vojta, L., Soll, J. and Møller, S.G. (2007) ARC3 is a stromal Z-ring accessory protein essential for plastid division. EMBO Rep. 8, 293–299.
[11] Vitha, S., Froehlich, J.E., Koksharova, O., Pyke, K.A., van Erp, H. and Osteryoung, K.W. (2003) ARC6 Is a J-domain plastid division protein and an evolutionary descendant of the cyanobacterial cell division protein Ftn2. Plant Cell 15, 1918–1933.
[12] Glynn, J.M., Froehlich, J.E. and Osteryoung, K.W. (2008) *Arabidopsis* ARC6 coordinates the division machineries of the inner and outer chloroplast membranes through interaction with PDV2 in the intermembrane space. Plant Cell 20, 2460–2470.
[13] Glynn, J.M., Miyagishima, S., Yoder, D.W., Osteryoung, K.W. and Vitha, S. (2007) Chloroplast division. Traffic 8, 451–461.
[14] Romanos, M.A., Scorer, C.A. and Clare, J.J. (1992) Foreign gene expression in yeast: a review. Yeast 8, 423–488.
[15] Smith, P.K., Krohn, R.I., Hermanson, G.T., Mallia, A.K., Gartner, F.H., Provenzano, M.D., Fujimoto, E.K., Goeke, N.M., Olson, B.J. and Klenk, D.C. (1985) Measurement of protein using bicinchoninic acid. Anal. Biochem. 150, 76–85.
[16] Bradford, M.M. (1976) A rapid and sensitive method for the quantitation of microgram quantities of protein utilizing the principle of protein-dye binding. Anal. Biochem. 72, 248–254.
[17] Laemmli, U.K. (1970) Cleavage of structural proteins during the assembly of the head of bacteriophage T4. Nature 227, 680–685.
[18] Ingerman, E. and Nunnari, J. (2005) A continuous, regenerative coupled GTPase assay for dynamin-related proteins in: Methods Enzymol. (Balch, W.E., Der, C.J. and Hall, A., Eds.), pp. 611–619, Academic Press, New York.
[19] Hyman, A.A., Salser, S., Drechsel, D.N., Unwin, N. and Mitchison, T.J. (1992) Role of GTP hydrolysis in microtubule dynamics – Information from a slowly hydrolyzable analog, GMPCPP. Mol. Biol. Cell 3, 1155–1167.
[20] Erickson, H.P. (2000) Dynamin and FtsZ: missing links in mitochondrial and bacterial division. J. Cell Biol. 148, 1103–1106.
[21] Osawa, M., Anderson, D.E. and Erickson, H.P. (2008) Reconstitution of contractile FtsZ rings in liposomes. Science 320, 792–794.
[22] Emanuelsson, O., Nielsen, H. and von Heijne, G. (1999) ChloroP, a neural network-based method for predicting chloroplast transit peptides and their cleavage sites. Protein Sci. 8, 978–984.
[23] Margalit, D.N., Romberg, L., Mets, R.B., Hebert, A.M., Mitchison, T.J., Kirschner, M.W. and RayChaudhuri, D. (2004) Targeting cell division: small-molecule inhibitors of FtsZ GTPase perturb cytokinetic ring assembly and induce bacterial lethality. Proc. Natl. Acad. Sci. USA 101, 11821–11826.
[24] Oliva, M.A., Huecas, S., Palacios, J.M., Martin-Benito, J., Valpuesta, J.M. and Andreu, J.M. (2003) Assembly of archaeal cell division protein FtsZ and a GTPase-inactive mutant into double-stranded filaments. J. Biol. Chem. 278, 33562–33570.
[25] Mukherjee, A., Dai, K. and Lutkenhaus, J. (1993) *Escherichia coli* cell division protein FtsZ is a guanine nucleotide binding protein. Proc. Natl. Acad. Sci. USA 90, 1053–1057.
[26] de Boer, P., Crossley, R. and Rothfield, L. (1992) The essential bacterial cell-division protein FtsZ is a GTPase. Nature 359, 254–256.
[27] Mukherjee, A., Saez, C. and Lutkenhaus, J. (2001) Assembly of an FtsZ mutant deficient in GTPase activity has implications for FtsZ assembly and the role of the Z ring in cell division. J. Bacteriol. 183, 7190–7197.
[28] Gupta, P., Anand, S.P., Srinivasan, R., Rajeswari, H., Indi, S. and Ajitkumar, P. (2004) The C-terminally truncated MtFtsZ-ΔC169 mutant of *Mycobacterium tuberculosis* FtsZ shows GTPase and GTP-induced, GTP-specific polymerization activities *in vitro*. Microbiology 150, 3906–3908.
[29] Löwe, J. and Amos, L.A. (1999) Tubulin-like protofilaments in Ca^{2+}-induced FtsZ sheets. EMBO J. 18, 2364–2371.
[30] Holzenburg, A., Jones, P.C., Franklin, T., Pali, T., Heimburg, T., Marsh, D., Findlay, J.B. and Finbow, M.E. (1993) Evidence for a common structure for a class of membrane channels. Eur. J. Biochem. 213, 21–30.
[31] Harris, J.R. and Holzenburg, A. (1989) Transmission electron-microscopic studies on the quaternary structure of human erythrocyte catalase. Micron. Microsc. Acta 20, 223–238.
[32] Löwe, J. (1998) Crystal structure determination of FtsZ from *Methanococcus jannaschii*. J. Struct. Biol. 124, 235–243.
[33] Miyagishima, S., Takahara, M., Mori, T., Kuroiwa, H., Higashiyama, T. and Kuroiwa, T. (2001) Plastid division is driven by a complex mechanism that involves differential transition of the bacterial and eukaryotic division rings. Plant Cell 13, 2257–2268.
[34] Maple, J. and Møller, S.G. (2007) Plastid division coordination across a double-membraned structure. FEBS Lett. 581, 2162–2167.
[35] Wang, D., Kong, D.-D., Ju, C.-L., Hu, Y., He, Y.-K. and Sun, J.-S. (2002) Localization of two GFP-tagged tobacco plastid division protein NtFtsZs in *Escherichia coli*. J. Integ. Plant Biol. 44, 931–935.
[36] Gaikwad, A., Babbarwal, V., Pant, V. and Mukherjee, S.K. (2000) Pea chloroplast FtsZ can form multimers and correct the thermosensitive defect of an *Escherichia coli ftsZ* mutant. Mol. Gen. Genet. 263, 213–221.
[37] Zhang, M., Hu, Y., Jia, J., Gao, H. and He, Y. (2009) A plant MinD homologue rescues *Escherichia coli* HL1 mutant (*ΔMinDE*) in the absence of MinE. BMC Microbiol. 9, 101.
[38] Glynn, J.M., Yang, Y., Vitha, S., Schmitz, A.J., Hemmes, M., Miyagishima, S.Y. and Osteryoung, K.W. (2009) PARC6, a novel chloroplast division factor, influences FtsZ assembly and is required for recruitment of PDV1 during chloroplast division in *Arabidopsis*. Plant J. 59, 700–711.
[39] Zhang, M., Hu, Y., Jia, J., Li, D., Zhang, R., Gao, H. and He, Y. (2009) CDP1, a novel component of chloroplast division site positioning system in *Arabidopsis*. Cell Res. 19, 877–886.
[40] Löwe, J. and Amos, L.A. (2000) Helical tubes of FtsZ from *Methanococcus jannaschii*. Biol. Chem. 381, 993–999.
[41] Erickson, H.P., Taylor, D.W., Taylor, K.A and Bramhill, D. (1996) Bacterial cell division protein FtsZ assembles into protofilament sheets and minirings, structural homologs of tubulin polymers. Proc. Natl. Acad. Sci. USA 93, 519–523.
[42] Redick, S.D., Stricker, J., Briscoe, G. and Erickson, H.P. (2005) Mutants of FtsZ targeting the protofilament interface. Effects on cell division and GTPase activity. J. Bacteriol. 187, 2727–2736.
[43] Chen, Y.D. and Erickson, H.P. (2005) Rapid *in vitro* assembly dynamics and subunit turnover of FtsZ demonstrated by fluorescence resonance energy transfer. J. Biol. Chem. 280, 22549–22554.
[44] Li, Z., Trimble, M.J., Brun, Y.V. and Jensen, G.J. (2007) The structure of FtsZ filaments *in vivo* suggests a force-generating role in cell division. EMBO J. 26, 4694–4708.
[45] Durand, E., Bernadac, A., Ball, G., Lazdunski, A., Sturgis, J.N. and Filloux, A. (2003) Type II protein secretion in *Pseudomonas aeruginosa*: the pseudopilus is a multifibrillar and adhesive structure. J. Bacteriol. 185, 2749–2758.
[46] Stokes, K.D. and Osteryoung, K.W. (2003) Early divergence of the *FtsZ1* and *FtsZ2* plastid division gene families in photosynthetic eukaryotes. Gene 320, 97–108.
[47] Yoder, D.W., Kadirjan-Kalbach, D., Olson, B.J.S.C., Miyagishima, S.Y., DeBlasio, S.L., Hangarter, R.P. and Osteryoung, K.W. (2007) Effects of mutations in

Arabidopsis FtsZ1 on plastid division, FtsZ ring formation and positioning, and FtsZ filament morphology in vivo. Plant Cell Physiol. 48, 775–791.
[48] Scheffers, D.J., de Wit, J.G., den Blaauwen, T. and Driessen, A.J. (2002) GTP hydrolysis of cell division protein FtsZ: evidence that the active site is formed by the association of monomers. Biochemistry 41, 521–529.
[49] Addinall, S.G., Small, E., Whitaker, D., Sturrock, S., Donachie, W.D. and Khattar, M.M. (2005) New temperature-sensitive alleles of *ftsZ* in *Escherichia coli*. J. Bacteriol. 187, 358–365.
[50] White, E.L., Ross, L.J., Reynolds, R.C., Seitz, L.E., Moore, G.D. and Borhani, D.W. (2000) Slow polymerization of *Mycobacterium tuberculosis* FtsZ. J. Bacteriol. 182, 4028–4034.
[51] Scheffers, D.J., den Blaauwen, T. and Driessen, A.J. (2000) Non-hydrolysable GTP-γ-S stabilizes the FtsZ polymer in a GDP-bound state. Mol. Microbiol. 35, 1211–1219.
[52] Lockhart, A. and Kendrick-Jones, J. (1998) Interaction of the N-terminal domain of MukB with the bacterial tubulin homologue FtsZ. FEBS Lett. 430, 278–282.
[53] Popp, D., Iwasa, M., Narita, A., Erickson, H.P. and Maeda, Y. (2009) FtsZ condensates: an *in vitro* electron microscopy study. Biopolymers 91, 340–350.
[54] El-Kafafi, S., Mukherjee, S., El-Shami, M., Putaux, J.L., Block, M.A., Pignot-Paintrand, I., Lerbs-Mache, S. and Falconet, D. (2005) The plastid division proteins, FtsZ1 and FtsZ2, differ in their biochemical properties and sub-plastidial localization. Biochem. J. 387, 669–676.

APPENDIX D

Smith, A. G., Jayaram, J., Johnson, C. B., Ellis, E. A., Vitha, S., Collisson, E. W. and Holzenburg, A. (2009) Improved protein detection using cold microwave technology. Methods in Molecular Biology **536**, 533-43.

Reprinted with permission from Springer.

Carol Beatrice contributed the following: microwave western and dot blot quantification, and contributed editorial assistance though the final manuscript.

Chapter 54

Improved Protein Detection Using Cold Microwave Technology

Aaron G. Smith, Jyothi Jayaram, Carol B. Johnson, E. Ann Ellis, Stanislav Vitha, Ellen W. Collisson, and Andreas Holzenburg

Summary

Protein screening/detection is an essential tool in many laboratories. Owing to the relatively large time investments that are required by standard protocols, the development of methods with higher throughput while maintaining an at least comparable signal-to-noise ratio would be highly beneficial to many researchers. This chapter describes how cold microwave technology can be used to enhance the rate of molecular interactions and provides protocols for dot blots, western blots, and ELISA procedures permitting a completion of all incubation steps (blocking and antibody steps) within 45 min.

Key words: Cold microwave technology, Microwave, Protein detection, Dot blot, Western blot, ELISA

1. Introduction

Protein screening is a time-intensive, yet indispensable technique required on a routine basis in many laboratories. Conventional protein detection and blotting protocols call for extensive incubation times *(1)* in order to optimize antigen–antibody interactions in conjunction with appropriate visualization tools (**Table 1**). Most of these interactions can be significantly improved through the use of microwave technology. This technology greatly enhances the rate of antibody–antigen interaction, thereby significantly reducing incubation times. Microwave-assisted (MWA) research had its origins in histological studies over 30 years ago *(2)*, but

Biji T. Kurien and R. Hal Scofield (eds.), *Methods in Molecular Biology, Protein Blotting and Detection, vol. 536*

DOI: 10.1007/978-1-59745-542-8_54

Table 1
Comparison of the conventional and the MWA dot and western blot protocols

	Conventional	MWA
Blocking	Overnight at 4°C (or 2 h at 21°C)	6-min cycle
Primary antibody	Overnight at 4°C	6-min cycle
Wash (TBS + 2% Tween)	4 Times for 10 min each (21°C)	4 Times for 1 min each
Secondary antibody	1 h at 21°C	6-min cycle
Wash (TBS + 2% Tween)	2 Times for 10 min each (21°C)	2 Times at 1 min each
Wash (TBS)	2 Times for 10 min each (21°C)	2 Times at 1 min each

The 6-min cycle consists of 2 min on, 2 min off, and 2 min on at 37°C and a calibrated power of 220 W. Wash steps are at 37°C and a calibrated power of 220 W

remained enigmatic until a thorough examination into the variables allowed for improved sample reproducibility *(3)*. Since that time, a wealth of diverse protocols have been developed using MWA such as decalcification of bone *(4)*, resin polymerization for electron microscopy *(5)*, and antibody labeling of fixed biological tissue *(6)*.

However, previous western blotting and ELISA MWA studies *(7–9)* were compromised by the use of a heterogeneous microwave field and uncalibrated power settings. In essence, these conventional MWA protocols were based on using a microwave apparatus that exerted uncontrolled heat radiation in addition to microwave radiation (**Table 2**). It is thought that pure microwave radiation is different from microwave heating *(10–12)*. While the latter may cause a linear acceleration of molecules, the former could be thought of as introducing high-frequency molecular inversions (flipping). To eliminate or control the heat component, Ted Pella, Inc., developed the ColdSpot® technology *(13)*, which allows for meticulous control of sample temperature during MWA applications. The MWA protocols described in this chapter are therefore referred to as using cold-microwave technology. Protocols assisted by cold-microwave technology employ identical chemistry when compared with conventional techniques and may therefore be adapted for a wide range of other screening/visualization applications.

The most dramatic effect incurred by using cold-microwave technology is significant timesaving, cutting blot development or ELISA processing times down from ≥24 h to 45 min.

Table 2
Comparison of the conventional and MWA ELISA protocols

	Conventional	MWA
Antibody	RT for 2 h	6-min cycle
Blocking	Overnight at 4°C	6-min cycle
Wash	Twice at RT	1-min cycle
Antigen	2 h at RT	6-min cycle
Wash	Four times	1-min cycle
Biotinylated antibody	30 min at RT	6-min cycle
Wash	Thrice	1-min cycle
Streptavidin–HRPO conjugate	30 min	6-min cycle
Wash	Five times	1-min cycle
Substrate	20 min at RT	20 min at RT

The 6-min cycle consists of 2 min on, 2 min off, and 2 min on at 30°C and a wattage setting of 250 W. Wash steps are done at the same microwave settings for 1 min.

2. Materials

2.1. SDS-Polyacrylamide Gel Electrophoresis (SDS-PAGE) and Electrophoretic Transfer

1. Mini-PROTEAN 3 system (Bio-Rad, Hercules, CA, USA) used for protein separation.
2. 0.2-µm Nitrocellulose (Bio-Rad, Hercules, CA, USA) was used for electrophoretic transfer at 1 A for 50 min in 25 mM Tris–glycine/20% methanol (pH 8.3) using a Genie blotter (IdeaScientific, Minneapolis, MN, USA).

2.2. MWA Dot Blotting Protein Detection

1. PELCO BioWave® Pro Laboratory Tissue Processing System equipped with PELCO ColdSpot® Pro (Ted Pella, Inc., Redding, CA) to increase rate of antibody–antigen interactions (**Fig. 1**).
2. PELCO SteadyTemp™ (Ted Pella, Redding, CA) load cooler for maintaining the temperature of the Coldspot®.
3. Polypropylene Petri dishes (50-mm diameter × 12-mm deep (Ted Pella, Redding, CA, USA).
4. 10× Tris-buffered saline (TBS): 200 mM Tris, pH 7.6 and 1.37 M NaCl. Dilute in water to make 1× TBS.
5. Blocking buffer: 0.2% Tween-20 and 2% cold water fish gelatin (Sigma, St. Louis, MO, USA) diluted in 1× TBS.

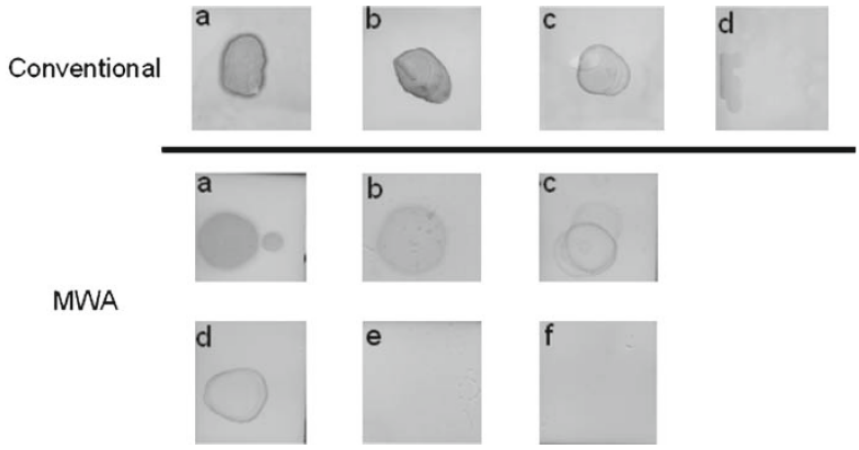

Fig. 1. Conventional and MWA dot blots in comparison. Samples from a conventional dot blot (*top row*) show whole cell lysate (**a**), peak fractions containing different amounts of the assayed protein (**b**, **c**), and a late fraction (after peak elution) as a negative control (**d**). Samples from the MWA dot blot (*middle and bottom rows*) show whole cell lysate run at 37°C (**a**) and 21°C (**b**), peak fractions containing different amounts of the assayed protein (**c**, **d**), and two negative controls, that is, a late fraction (after peak elution) (**e**) and a nonreactive protein (**f**). This figure appeared in *(12)*, Copyright © 2008 by Elsevier, Inc.

6. TBST (TBS-Tween-20) buffer: 1× TBS containing 0.2% Tween-20.
7. Next follows a suitable visualization reaction, e.g., the alkaline phosphatase reaction. Reagents for this reaction are as follows:
   (a) 10× chromogenic reaction buffer: 1 M NaCl, 50 mM $MgCl_2$, 1 M Tris–HCl, pH 8.8, store at RT, good for ~6 months.
   (b) NBT solution (3.75% w/v nitro blue tetrazolium in 100% methanol) (Research Products International, Mount Prospect, IL, USA): Store at −20°C and protect from light.
   (c) BCIP solution (5% w/v 5-Br-4-Cl-3-indolyl-phosphate in water) (Research Products International): Store at −20°C and protect from light.
9. Primary and secondary incubation steps using, e.g., anti c-myc as primary and alkaline phosphatase goat-anti mouse as secondary (Invitrogen, Carlsbad, CA, USA).

2.3. MWA Western Blotting Protein Detection

1. PELCO BioWave® Pro Laboratory Tissue Processing System equipped with PELCO ColdSpot® Pro to increase rate of antibody–antigen interactions.
2. PELCO SteadyTemp™ load cooler for maintaining the temperature of the ColdSpot.
3. Miniblotting containers (9.0 cm × 6.4 cm × 2.1 cm, Research Products International).

4. 10× TBS: 200 mM Tris, pH 7.6 and 1.37 M NaCl. Dilute in water to make 1× TBS.
5. Blocking buffer: 0.2% Tween-20 and 2% cold water fish gelatin diluted in 1× TBS.
6. TBST (TBS-Tween-20) wash buffer: 1× TBS and 0.2% Tween-20.
7. Next follows a suitable visualization reaction, such as, e.g., the alkaline phosphatase reaction. Reagents for this reaction are as follows:
   (a) 10× chromogenic reaction buffer: 1 M NaCl, 50 mM $MgCl_2$, 1 M Tris–HCl, pH 8.8, store at room temperature (RT), good for ~6 months.
   (b) NBT solution: 3.75% w/v.
   (c) BCIP solution: 5% w/v.
8. Primary and secondary incubation steps using, e.g., anti c-myc as primary and alkaline phosphatase goat-anti mouse as secondary.
9. Prestained molecular weight markers: Precision Plus protein standards (Bio-Rad).
10. Denton DV-502 vacuum pump stand (Denton Vacuum USA, Moorestown, NJ, USA) for glow discharging.

2.4. MWA ELISA

1. PELCO BioWave® Pro Laboratory Tissue Processing System equipped with PELCO ColdSpot® Pro to increase rate of antibody–antigen interactions.
2. PELCO SteadyTemp™ load cooler for maintaining the temperature of the ColdSpot®.
3. Immulon 2HB strips (Thermolab systems, Franklin, MA, USA) that can each support 12 wells.
4. 10× phosphate buffered saline (PBS): 56 mM Na_2HPO_4, 10.6 mM KH_2PO_4 and 1.54 M NaCl. Dilute in water to make 1× PBS, pH 7.2.
5. PBST (PBS-Tween-20) wash buffer: 1× PBS and 0.05% Tween-20.
6. Bovine serum albumin.
7. Triton X-100.
8. Dulbecco's Modified Eagle's Medium (DMEM) and fetal bovine serum (FBS) for antibody dilution (Gibco/BRL, Gaithersburg, MD, USA).
9. Detection reagents used: Primary FIV-2D4 monoclonal antibody *(14)* to coat the ELISA plates and capture the antigen. Biotinylated monoclonal anti-mouse secondary antibody-FIV-4F2. Hybridomas for the monoclonal antibodies were

obtained from American Type Culture Collection. Streptavidin–horseradish peroxidase conjugate for final detection (KPL Protein Research Products, Gaithersburg, MD).

10. 3,3′,5,5′-Tetramethylbenzidine (TMB) (KPL Protein Research Products, Gaithersburg, MD, USA) as a substrate for horseradish peroxidase.
11. TMB stop solution (KPL).

3. Methods

The protocols described here were developed using a readily available protein as antigen and alkaline phosphatase (dot and western blots) or horseradish peroxidase (ELISA) in conjunction with appropriate primary and secondary antibodies (*see* **Subheading 2**) for visualization. The protocols were used on both epitope tag-specific and sequence-specific antibodies. The results were comparable in both cases. This protocol is open for variations in terms of the utilization of other visualization reagents.

3.1. SDS-PAGE and Electrophoretic Transfer

1. SDS-PAGE was carried out according to Laemmli *(15)* (*see* Chapter "Non-electrophoretic bi-directional transfer of a single SDS-PAGE gel with multiple antigens to obtain twelve immunoblots").
2. Electrophoretic transfer was carried out according to Towbin et al. *(16)* (*see* Chapter "Detection of La/SS-B by Western Blot Using Nanogold-Tagged Antibodies and Silver Enhancement").

3.2. MWA Dot Blotting Protein Detection

1. Cut a piece of membrane suitable for use and place in a polypropylene Petri dish.
2. Spot the membrane with 2–5 µL of protein to be assayed (~1 mg/mL) and allow 15–20 min for sample binding.
3. Place the membrane in Petri dish and cover with 1–2 mL of blocking buffer.
4. Place the dish into microwave for a 6-min cycle (2 min on, 2 min off, 2 min on). The microwave was set to 250 W corresponding to a calibrated output wattage of 220 W and the ColdSpot® was set to 37 °C. These settings were used for all MWA steps (*see* **Notes 1** and **2**).
5. Pour off blocking buffer and immediately replace with primary antibody solution (antibody diluted in blocking buffer) (*see* **Note 3**). Incubate for a 6-min cycle (2 min on, 2 min off, 2 min on) in the microwave.

6. Pour off primary antibody solution and wash four times with TBST for 1 min each in the microwave.
7. Pour off TBST and immediately replace with secondary antibody solution (antibody diluted blocking buffer) for a 6-min cycle (2 min on, 2 min off, 2 min on).
8. Pour off secondary antibody solution and wash two times with TBST for 1 min each in microwave.
9. Pour off TBST and wash two times with 1× TBS for 1 min each (microwave).
10. Develop the blot as you would for conventional protocol (*see* **Note 4**).

3.3. MWA Western Blotting Protein Detection

1. Glow-discharge (*see* **Notes 5** and **6**) a miniblotting container.
2. After electrophoretic transfer, place membrane in the glow-discharged container and cover with 5 mL of blocking buffer (*see* **Notes 7** and **8**).
3. Place the container into microwave for a 6-min cycle (2 min on, 2 min off, 2 min on). The microwave was set to 250 W corresponding to a calibrated output wattage of 220 W, and the ColdSpot® was set to 37 °C. These settings were used for all MWA steps (*see* **Notes 1** and **2**).
4. Pour off the blocking buffer and immediately replace with primary antibody solution (antibody and blocking buffer). Incubate for a 6-min cycle (2 min on, 2 min off, 2 min on) in the microwave.
5. Pour off primary antibody solution and wash four times with TBST for 1 min each in the microwave.
6. Pour off TBST and immediately replace with secondary antibody solution (antibody and blocking buffer). Incubate for a 6-min cycle (2 min on, 2 min off, 2 min on) in the microwave.
7. Pour off secondary antibody solution and wash two times with TBST for 1 min each in the microwave.
8. Pour off TBST and wash two times with 1× TBS for 1 min each in the microwave.
9. Develop the blot as you would for conventional protocol.

3.4. MWA ELISA

1. Coat Immulon 2HB ELISA strips with 50-µL mouse monoclonal anti-FIV antibody (FTLV-2D4 MAb) at a concentration of 20 µg/mL (made in PBS pH 7.2) (*see* **Note 9**).
2. Add 300 µL of a 3% (w/v) BSA in PBS, pH 7.2 to the plates and block in the microwave for a 6-min cycle (2 min on, 2 min off, 2 min on). The microwave was set to 250 W and 30°C, and these settings were used for all subsequent MWA steps.

3. Wash the plate twice for 1 min with PBS containing 0.05% (v/v) Tween-20 (PBST).
4. Add 10 µL of Triton-X 100 per well and subsequently add 100 µL of various dilutions of the protein solution diluted in growth buffer to the wells.
5. Wash the plate four times for 1 min with PBST.
6. Add 100 µL of primary antibody diluted in PBS containing 3% FBS and incubate in microwave for a 6-min cycle (2 min on, 2 min off, 2 min on).
7. Wash the plate three times with PBST.
8. Add 100 µL of a 1:1,000 dilution of secondary antibody diluted in PBS containing 3% FBS and incubate in microwave for a 6-min cycle (2 min on, 2 min off, 2 min on).
9. Wash the plate five times for 1 min with PBST.
10. Incubate for 20 min with TMB solution.
11. Terminate the reaction with TMB stop solution after incubating the reaction for 20 min at RT (*see* **Note 10**).
12. Read O.D. at 405 nm.

4. Notes

1. MWA steps are carried out without a lid on the Petri dish or blotting container.
2. Calibrated output wattage settings are obtained as follows: Place a glass beaker containing exactly 1 L of water inside the cavity while the ColdSpot® is disconnected and incubate for 2 min at a nominal power setting of 250 W while monitoring the temperature using a digital temperature gauge. The temperature difference prior to and after the incubation (ΔT) multiplied by 35 gives the true output wattage.
3. In our experience, an approximately twofold higher antibody concentration was necessary to attain signal intensities similar to those obtained with conventional methods. For example, a 1:2,500 dilution was used for MWA blots vs. a 1:5,000 dilution used in the conventional protocol.
4. Blot development was not carried out using the microwave in order to prevent overdevelopment and introduction of unnecessary background. However, an approximately twofold background reduction is observed when conventional development is combined with all other steps carried out in the MWA mode.

5. Glow-discharging (in air) for 10 s at reduced atmospheric pressure using, e.g., the vacuum pump stand Denton DV-502 (Denton Vacuum USA) renders the surface of the containers hydrophilic and allows the use of smaller reagent volumes. Volumes used in this protocol are half of those used for non-glow-discharged containers. Containers that have been treated in such a manner should be used within 20 min as they are extremely susceptible to air-borne contaminants.
6. There are several methods of rendering surfaces more hydrophilic. However, glow-discharging in air ensures that a desired degree of hydrophilicity is achieved without introducing any additional chemicals. Since glow-discharging takes place at low vacuum levels requiring only, e.g., a rotary pump, an inexpensive home-built system could be a worthwhile investment and be substantially cheaper than buying a commercial system *(17)*.
7. Because of the short incubation times employed in this protocol, the prestained protein standards are retained on the western blot membrane (**Fig. 2**). This needs to be viewed in contrast to conventional blots where the standards are lost.
8. Membrane must remain submerged during MWA steps, or rampant background is observed during blot development.

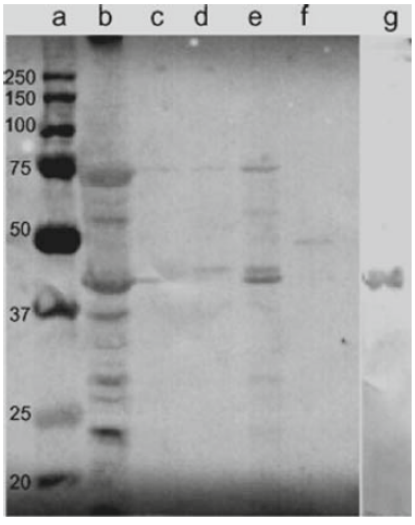

Fig. 2. MWA western blot. *Lanes* a–g have been individually loaded as follows: (**a**) prestained protein standards (highlighted in kDa), (**b**) whole cell lysate, (**c**) late fraction (after peak elution), (**d**, **e**) peak fractions containing different amounts of the assayed protein, (**f**) nonreactive protein as negative control (with a mass of 12.5-kDa), (**g**) conventional western blot (positive control). This figure appeared in *(12)*,

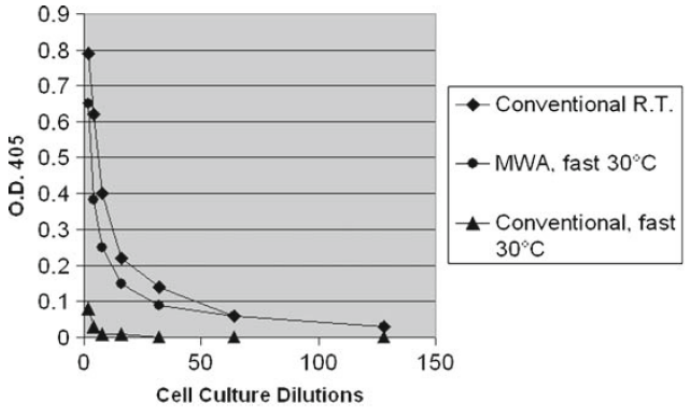

Fig. 3. Comparison of signal intensities for conventional ELISA (*diamonds*), MWA ELISA (*circles*), and a conventional protocol using times from MWA (*triangles*). Results presented here are after background subtraction from negative control (DMEM without antigen). The values presented here are the averages of three independent readings.

9. The Immulon 2HB strips gave us a graded decrease in signal with increasing dilutions of the antigen (Fig. 3). Similar results were not obtained when the ELISA was performed with 96-well microtiter ELISA plates from Sumitomo Bakelite Co. Ltd.
10. The stop solution was added after 20-min incubation of the enzyme with the substrate. As a general rule, add the stop solution immediately after a color reaction develops in the negative control.

References

1. Finney, M. (1998) Nonradioactive methods for visualization of protein blots. In: Pound J.D., ed. *Immunochemical Protocols*, Humana Press, Totowa, NJ, 207–216.
2. Mayers, C.P. (1970) Histological fixation by microwave heating. *J Clin Pathol.* 23, 273–275.
3. Giberson, R.T. and Demaree, R.S., Jr. (1995) Microwave fixation: Understanding the variables to achieve rapid reproducible results. *Microsc Res Tech.* 32, 246–254.
4. Madden, V.J. and Henson, M.M. (1997) Rapid decalcification of temporal bones with preservation of ultrastructure. *Hear Res.* 111, 76–84.
5. Demaree, R.S., Jr., Giberson, R.T., and Smith, R.L. (1995) Routine microwave polymerization of resins for transmission electron microscopy. *Scanning* 17 (Suppl 5), 25–26.
6. Chicoine, L. and Webster, P. (1998) The effect of microwave irradiation on antibody labeling efficiency when applied to ultrathin cryosections through fixed biological material. *Microsc Res Tech.* 42, 24–32.
7. Van Dorp, R., Kok, P.G., Marani, E., Boon, M.E., and Kok, L.P. (1991) ELISA incubation time can be reduced by 2.45-GJz microwaves. *J Clin Lab Immunol.* 34, 87–96.
8. Li, W., Murai, Y., Okada, E., Matsui, K., Hayashi, S., Horie, M., and Takano, Y. (2002) Modified and simplified western blotting protocol: Use of intermittent microwave irradiation (IMWI) and 5% skim milk to improve binding specificity. *Pathol Int.* 52, 234–238.
9. Toyokuni, S., Kawaguchi, W., Akatsuka, S., Makoto, M., and Hiai, H. (2003) Intermittent microwave irradiation facilitates antigen–antibody reaction in western blot analysis. *Pathol Int.* 53, 259–261.
10. Galvez, J.J., Giberson, R.T., and Cardiff, R.D. (2004) Microwave mechanisms – the energy/heat dichotomy. *Microsc Today* 12, 18–23.

11. Sanders, M.A., Anderson, T.E., and Giberson, R. (2006) Microwave methods – evidence to support a microwave effect. *Microsc Microanal Proc.* 12 (Suppl 2), 296 CD.
12. Smith, A.G., Johnson, C.B., Ellis, E.A., Vitha, S., and Holzenburg, A. (2008) Protein screening using cold microwave technology. *Anal Biochem.* 375, 313–317.
13. Sanders, M.A. (2002) Recent advances in microwave-assisted specimen processing: Keeping it cool. *Microsc Microanal Proc.* 8 (Suppl 2), 158–159.
14. Tilton, G.K., Connor, T.P., Jr., Seymour, C.L., Lawrence, K.L., Cohen, N.D., Andersen, P.R., and Tonelli, Q.J. (1990) Immunoassay for detection of feline Immuno-deficiency virus core antigen. *J Clin Microbiol.* 29, 898–904.
15. Laemmli, U.K. (1970) Cleavage of structural proteins during the assembly of the head of bacteriophage T4. *Nature* 227, 680–685.
16. Towbin, H., Staehelin, T., and Gordon, J. (1979) Electrophoretic transfer of proteins from polyacrylamide gels to nitrocellulose sheets: Procedure and some applications. *Proc Natl Acad Sci USA* 76, 4350–4354.
17. Aebi, U. and Pollard, T.D. (1987) A glow discharge unit to render electron microscope grids and other surfaces hydrophilic. *J Electron Microsc Tech.* 7, 29–33.

APPENDIX E

Smith, A.G., Johnson, C.B., Ellis E.A., Vitha, S., and Holzenburg A. (2008). Protein screening using cold microwave technology. Anal Biochem. **375**, 313-317.

Reprinted with permission from Elsevier.

Carol Beatrice contributed the following: FtsZ1 protein expression, FtsZ1 protein purification, glow discharging, blot quantification, and contributed editorial assistance though the final manuscript.

Available online at www.sciencedirect.com
ScienceDirect
Analytical Biochemistry 375 (2008) 313–317
ANALYTICAL BIOCHEMISTRY
www.elsevier.com/locate/yabio

Protein screening using cold microwave technology

Aaron G. Smith [a,b], Carol B. Johnson [a,c], E. Ann Ellis [a], Stanislav Vitha [a], Andreas Holzenburg [a,b,c,*]

[a] Microscopy and Imaging Center, Texas A&M University, College Station, TX 77843, USA
[b] Department of Biochemistry and Biophysics, Texas A&M University, College Station, TX 77843, USA
[c] Department of Biology, Texas A&M University, College Station, TX 77843, USA

Received 28 November 2007
Available online 19 January 2008

Abstract

Protein detection is a common yet time-intensive task in many laboratories. Here we report a protocol that makes use of cold microwave technology to reduce the total processing time to less than 1 h with dot and Western blot applications while yielding lower background noise at similar signal strength when compared with conventional protocols. With dot blots, the time savings was accompanied by a decrease in reagent use. With Western blots, the visibility of prestained markers was maintained, in stark contrast to conventional procedures. Experiments kept at a constant temperature of 21 °C support the existence of a microwave radiation effect, whereas an additional thermal effect is noted when the temperature is increased to 37 °C from ambient. Microwave-assisted dot blotting is suggested as an effective way of facilitating large-scale screening of expressed proteins.

Keywords: Cold microwave technology; Microwave; Protein detection; Dot blot; Western blot

Protein blotting [1,2] has become an essential technique in many laboratories. Protein detection routinely takes places by blotting after separation on an acrylamide gel. Alternatively, protein mixtures can be spotted directly on the membrane in a dot blot [3]. Standard blotting protocols require a minimum of several hours, but many suggest several days for maximum signal detection [4]. The time involved presents a logistical problem when, for example, screening multiple strains for optimal protein expression. A faster protocol that does not require use of more reagents and yields comparably reliable results would be advantageous to labs expressing and purifying proteins on a routine basis. To meet this need, we have developed a protocol using cold microwave technology that allows comparable detection of signal to conventional protocols in less than 1 h posttransfer or spotting.

Microwave-assisted (MWA)[1] research was first realized in histological studies more than three decades ago [5]. Reproducibility problems were common in early studies and lingered until a closer examination of potential variables allowed resolution of these difficulties [6]. MWA users were challenged to reproduce work partly due to inhomogeneities in the strength of the microwave field and uncontrolled heating [7–9]. The ColdSpot technology (developed by Ted Pella) creates uniform microwave irradiation and allows a rigorous temperature control of the sample [10]. For these reasons, it has been used in the MWA protocols presented in the current study. Since its inception, many optimization trials have taken place, and recent reports in the literature show that a 6-min cycle (2 min on, 2 min off, and 2 min on) at $\leqslant$ 250 W was found to be suitable for most MWA applications [10,11]. MWA

* Corresponding author. Address: Microscopy and Imaging Center, Texas A&M University, College Station, TX 77843, USA Fax: +1 979 847 8933.
E-mail address: holzen@mic.tamu.edu (A. Holzenburg).

[1] *Abbreviations used:* MWA, microwave-assisted; ELISA, enzyme-linked immunosorbent assay; PMSF, phenylmethylsulfonyl fluoride; Ni–NTA, nickel–nitriloacetic acid; BCIP solution, 5-Br-4-Cl-3-indolyl-phosphate; NBT, nitroblue tetrazolium.

0003-2697/$ - see front matter © 2008 Elsevier Inc. All rights reserved.
doi:10.1016/j.ab.2008.01.019

protocols have been used extensively for diverse procedures such as decalcification of bone [12], resin polymerization for electron microscopy [13], and antibody labeling of fixed biological tissue [14]. Although MWA protocols potentially could be developed for use in other immunochemical endeavors, the current study focuses on Western and dot blot applications. To this end, it should be pointed out that earlier MWA protocols, such as the enzyme-linked immunosorbent assay (ELISA) protocol described by Van Dorp and coworkers [15] and the Western blot analyses reported by Li and coworkers [16] and Toyokuni and coworkers [17], used a microwave environment that does not provide a homogeneous, temperature-controlled microwave field at calibrated power settings (watts). Therefore, the latter studies could not discount the involvement of microwave heat in addition to microwave energy [18] and need to be seen in contrast to the cold microwave approach reported in the current study. In addition, the reports by Li and coworkers [16] and Toyokuni and coworkers [17] described extended blocking and antibody incubation steps resulting in longer protocols.

Materials and methods

Protein expression

FtsZ1 from *Arabidopsis thaliana* was transformed into the yeast *Pichia pastoris* using the Easy Select *Pichia* expression kit (Invitrogen). Protocols were carried out as described in the user manual using plasmid pPICZB bearing FtsZ1 and *Pichia* strain X-33. Transformants were selected with YPD plates supplemented with 18.2% (w/v) sorbitol and zeocin at 100 μg/ml. Integration and expression were verified by PCR analysis and blotting.

Protein purification

Pichia strains expressing FtsZ1 were grown in 200-ml cultures using buffered methanol–complex medium (1% [w/v] yeast extract, 2% [w/v] peptone, 100 mM potassium phosphate [pH 6.0], 1.34% [w/v] yeast nitrogen base, 4×10^{-5}% [w/v] biotin, and 1% [v/v] methanol) and supplemented with 3% (v/v) methanol every 12 h for a total growth time of 60 h. Cell lysates were prepared by centrifuging the culture and resuspending in 10 ml of breaking buffer (50 mM sodium phosphate [pH 7.4], 1 mM phenylmethylsulfonyl fluoride (PMSF), 1 mM EDTA, and 5% [v/v] glycerol). An equal volume of 0.5 μm glass beads was added, and the sample was vortexed for eight cycles of 30 s vortexing and 30 s on ice. FtsZ1 was purified under native conditions using nickel–nitriloacetic acid (Ni–NTA) agarose beads (Invitrogen). Then 8 ml of cell lysate was added to a column and allowed to bind for 30 min with gentle agitation at 4 °C. Four washes were performed with 8 ml of native wash buffer (50 mM sodium phosphate, 0.5 M NaCl, and 60 mM imidazole [pH 8.0]) and collected by gravity filtration. Protein was eluted using 8 ml of native elution buffer (50 mM sodium phosphate, 0.5 M NaCl, and 250 mM imidazole [pH 8.0]) and collected in 1-ml fractions.

Western and dot blot protocols

For Western blotting, the proteins were first separated by SDS–PAGE (10% separating and 4% stacking gels) using a Mini-PROTEAN 3 system (Bio-Rad) [19] and the Precision Plus protein standards (Bio-Rad). The protein was transferred onto 0.2 μm nitrocellulose at 1 A for 50 min in 25 mM Tris–glycine/20% methanol (pH 8.3) using a Genie blotter (Idea Scientific). The conventional protocol entailed blocking for 1 h at 21 °C with cold water fish gelatin (Sigma), overnight incubation at 4 °C with primary antibody (anti-c-myc, Invitrogen), a 45-min incubation with secondary antibody at 21 °C (mouse anti-rabbit alkaline phosphatase, Invitrogen), and developing at 21 °C with 10 ml of reaction buffer (100 mM NaCl, 5 mM $MgCl_2$, and 100 mM Tris–HCl [pH 8.8]), 60 μl of 5% (w/v) aqueous BCIP solution (5-Br-4-Cl-3-indolyl-phosphate, Research Products International), and 10 μl of 7.5% (w/v) NBT (nitroblue tetrazolium, Research Products International) in 100% (v/v) methanol. Individual washes of membranes were carried out for 10 min in TBS (50 mM Tris and 200 mM NaCl [pH 7.4]) or TBS plus 2% Tween 20 (Research Products International). The protocol using cold microwave technology involved identical reagents but made use of a PELCO BioWave Pro Laboratory Tissue Processing System equipped with a ColdSpot temperature control system. Processing temperature was set at 37 or 21 °C (temperature cutoff at 42 or 25 °C, respectively), and blocking and antibody incubations were cycled for 6 min (2 min on, 2 min off, and 2 min on) using a calibrated power output of 220 W (see below). Washing step times were reduced to 1 min each. Development of the blots was carried out as described above. Dot blots were done by placing 2- to 5-μl droplets of a 0.2-mg/ml protein sample onto a 0.2-μm nitrocellulose membrane (Bio-Rad). Subsequent steps followed either the conventional or cold microwave protocols described above. Polypropylene dishes (50 mm diameter × 12 mm deep, Ted Pella) were used for MWA dot blots, and miniblotting containers ($9.0 \times 6.4 \times 2.1$ cm, Research Products International) were used for Western blotting.

Microwave calibration

Wattage was calibrated by placing a glass beaker containing 1 L of water inside the cavity without the ColdSpot and incubating for 2 min at a nominal power setting of 250 W. The temperature difference prior to and after the incubation (ΔT) multiplied by 35 gave the true wattage output. For precise temperature measurements, the temperature sensor of the BioWave was employed.

Glow discharging

To minimize the volumes required for the above protocols, containers were rendered hydrophilic by glow discharging (in air) for 10 s at reduced atmospheric pressure using a Denton DV-502 vacuum pump stand (Denton Vacuum USA).

Blot quantification

Integrated densities in the dot and Western blots were quantified using ImageJ routines [20]. Briefly, the digitized data were converted to 8-bit grayscale images, uniform background features were subtracted using a 25-pixel rolling ball algorithm, and the densities were inverted to yield pixel values near zero. The speckled background features observed with the conventional dot blots were assessed using the Digital Map routine within the CRISP image processing software package [21]. Two representative background areas were cropped, and their density distributions were evaluated for maximum and minimum values. The change in density variations (Δ) were compared between the MWA and conventional dot blot background areas and were found to amount to $\Delta = 18$ and $\Delta = 42$, respectively, suggesting that the MWA protocol provides approximately twofold lower background noise.

Results and discussion

In general, the primary advantages of using cold microwave technology are (i) significant time savings, (ii) improved reagent reactivity, (iii) reduced background, and (iv) enhanced infiltration when used in conjunction with embedding protocols [22]. More important, all of the above advantages can be attained without the involvement of interfering chemicals. The protocol described here was developed for the FtsZ1 protein from *A. thaliana* [23] expressed in the yeast *P. pastoris* (see Materials and methods).

Conventional dot blotting (Fig. 1) was carried out by spotting samples onto nitrocellulose, drying for 30 min, blocking for 60 min, primary antibody incubation overnight, and a final incubation with the alkaline phosphatase-conjugated secondary antibody for 45 min (see Materials and methods). MWA dot blots were cycled for 6 min (2 min on, 2 min off, and 2 min on) at 220 W for all blocking and antibody incubation steps, and developing the MWA blots was carried out at 21 °C. Control dot blots processed exactly as described for the MWA blots, but in the absence of microwave radiation, did not produce a detectable signal (data not shown). Preparation of immunochemical samples for microscopy has been carried out routinely at 37 °C to facilitate an improved signal/noise ratio [24]. To investigate whether the temperature used during the MWA protocols would have a similar determining effect, MWA dot blots were carried out at 37 and 21 °C (Fig. 1). Higher temperature led to an increase in signal intensity, but the specificity of the antibody and level of background appeared to remain constant. For Western blotting, SDS–PAGE was performed according to standard protocols (see Materials and Methods). After transferring the protein, the results of a conventional protocol were compared with those of an MWA protocol using identical reagents. The results for a typical MWA Western blot (including all blocking and antibody incubation steps) that was cycled for 6 min (2 min on, 2 min off, and 2 min on) at 37 °C and 220 W are shown in Fig. 2. Developing the MWA Western blot was carried out at as described for the MWA dot blot. To determine whether MWA blots can deliver true positives accurately, a negative control was carried, that is, a variant of lambda holin S105 containing a His tag [25]. The anti-myc primary antibody did not detect S105 in dot blots (Fig. 1) and did not produce any noticeable background in the size range of the S105 protein (Fig. 2), indicating that the observed signals are not due to nonspecific interactions. The conventional Western blot with blocking and antibody incubation steps identical to the conventional dot blot showed results that were indistinguishable from those with the MWA protocol (Fig. 2). However, it was noted that, owing to the very short blocking times allowed by the MWA protocol, the prestained protein standards were readily visible throughout the entire blotting procedure. This is in contrast to the prolonged blocking steps employed in conventional Western blots and previous MWA protocols [16,17] that do not retain the standards. Quantification of dot blot (Table 1) and Western blot (Table 2) data supports the notion that the uniform background-corrected, integrated signal intensities in both the conventional and MWA Western and dot blots are comparable. However, due to prolonged handling time with the conventional blots, speckled background features partially camouflaged the observed signal, resulting in an increased noise level by a factor of approximately 2 (see Materials and methods).

To economize on the materials/reagents used, volume and microwave compatibility were considered when choosing the correct vessels for the antibody incubations. Polypropylene dishes (Ted Pella) were used for MWA dot blots, and miniblotting containers (Research Products International) were used for Western blotting. Both of these were reused a minimum of five times without showing any effects on the results. Although MWA dot blots required 1 ml of total volume per step, which was less than the amount used for conventional dot blots (2 ml), overall antibody use was equal due to a twofold higher antibody concentration in the MWA protocols. Even higher antibody concentrations may be necessary for proper detection of protein from low-expressing strains. Originally, MWA Western blots required a larger volume (20 ml) than did conventional protocols (3 ml). This difference is due to the fact that the heat-sealed

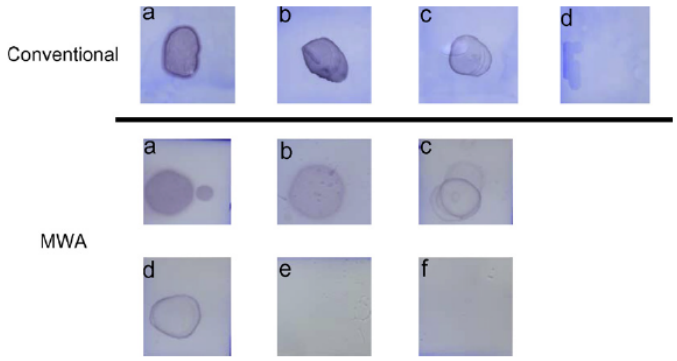

Fig. 1. Conventional and MWA dot blots in comparison. Samples from a conventional dot blot (top row) show whole cell lysate (a), peak fractions containing different amounts of FtsZ protein (b,c), and a late fraction (after peak elution) as a negative control (d). Samples from the MWA dot blot (middle and bottom rows) show whole cell lysate run at 37 °C (a) and 21 °C (b), peak fractions containing different amounts of the FtsZ protein (c,d), and two negative controls, that is, a late fraction (after peak elution) (e) and the S105 protein (f).

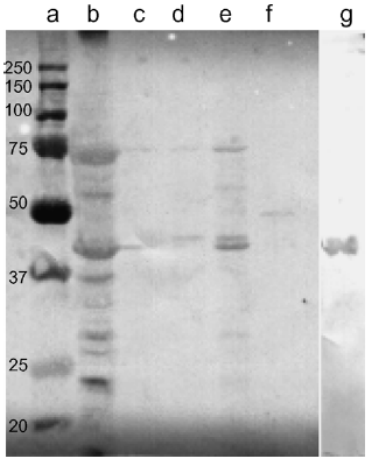

Fig. 2. MWA Western blot. Lanes a to g have been individually loaded as follows: (a) prestained protein standards (highlighted in kDa); (b) whole cell lysate; (c) late fraction (after peak elution); (d,e) peak fractions containing different amounts of FtsZ protein; (f) S105 protein as negative control (with a mass of 12.5 kDa); (g) conventional Western blot (positive control).

bags employed with the conventional protocols could not be used in the microwave. Experiments with only 5-ml volumes in miniblotting containers led to rampant background signal due to drying of the membrane during microwave steps (data not shown). To decrease the volume required for the MWA protocol, containers were rendered hydrophilic by glow discharging (in air) for 10 s at reduced atmospheric pressure immediately prior to use [26]. Glow discharging allowed a reduction in volume to 10 ml. However, glow-discharged MWA Western blots still required approximately three times the total reagent volume as compared with conventional protocols.

Table 1
Quantification of dot blots

	Mean density	Integrated density	% Signal
Dot blots, conventional			
Whole cell lysate	15.4	0.09	64
Peak fraction (1)	3.0	0.14	100
Peak fraction (2)	8.4	0.05	31
Late fraction	1.3	0.01	~ 0
Dot blots, MWA			
37 °C lysate	11.8	0.04	100
21 °C lysate	4.4	0.02	48
Peak fraction (1)	6.2	0.02	46
Peak fraction (2)	5.2	0.02	36
Late fraction	1.4	< 0.01	~ 0
S protein	0.9	< 0.01	~ 0

Table 2
Quantification of Western blots

	Mean density	Integrated density	% Signal
Western blots			
Whole cell lysate, MWA	34.6	0.32	71
Late fraction	10.9	0.10	6
Peak fraction (1)	36.0	0.33	75
Peak fraction (2)	15.7	0.14	19
S protein	9.1	0.08	1
Whole cell lysate, conventional	44.9	0.41	100

Conclusion

This article has described a new protocol for screening protein-expressing strains. It is comparable in total reagent use for dot blots and affords significant time savings over conventional protocols. MWA blots—both dot and Western—are capable of producing a signal that is comparable to or better than that of conventional protocols with regard to specificity, intensity, and level of background. We also

note that, in contrast to conventional Western blots, MWA protocols have the additional advantage of retaining protein standards, thereby obviating the need for manual post-transfer annotations.

In addition, we have provided further evidence in support of a microwave radiation effect versus a thermal effect. The fact that MWA and corresponding microwave-unassisted experiments were carried out under the same conditions with regard to blocking, buffer composition, incubation time, and temperature, but yielded a signal only in the presence of microwave radiation while keeping the temperature constant, suggests that antibody–antigen interactions are improved plainly by microwave radiation. When increasing the temperature, a further signal enhancement is observed owing to an additional thermal effect.

Acknowledgment

The authors thank Drs. Ry Young and Christos Savva for providing the S105 protein.

References

[1] H. Towbin, T. Staehelin, J. Gordon, Electrophoretic transfer of proteins from polyacrylamide gels to nitrocellulose sheets: Procedure and some applications, Proc. Natl. Acad. Sci. USA 76 (1979) 4350–4354.
[2] W.N. Burnette, Western blotting: Electrophoretic transfer of proteins from sodium dodecyl sulfate–polyacrylamide gels to unmodified nitrocellulose and radiographic detection with antibody and radioiodinated protein A, Anal. Biochem. 112 (1981) 195–203.
[3] R. Hawkes, E. Niday, J. Gordon, A dot-immunobinding assay for monoclonal and other antibodies, Anal. Biochem. 119 (1982) 142–147.
[4] M. Finney, Nonradioactive methods for visualization of protein blots, in: J.D. Pound (Ed.), Immunochemical Protocols, Humana Press, Totowa, NJ, 1998, pp. 207–216.
[5] C.P. Mayers, Histological fixation by microwave heating, J. Clin. Pathol. 23 (1970) 273–275.
[6] R.T. Giberson, R.S. Demaree Jr., Microwave fixation: Understanding the variables to achieve rapid reproducible results, Microsc. Res. Tech. 32 (1995) 246–254.
[7] R.T. Giberson, R.S. Demaree Jr., R.W. Nordhausen, Four-hour processing of clinical/diagnostic specimens for electron microscopy using microwave technique, J. Vet. Diagn. Invest. 9 (1997) 61–67.
[8] L.P. Kok, M.E. Boon, Microwave Cookbook for Microscopists: Art and Science of Visualization, Coulomb Press, Leiden, Netherlands, 1992.
[9] R.T. Giberson, R.L. Austin, J. Charlesworth, G. Adamson, G.A. Herrera, Microwave and digital imaging technology reduce turnaround times for diagnostic electron microscopy, Ultrastruct. Pathol. 27 (2003) 187–196.
[10] M.A. Sanders, Recent advances in microwave-assisted specimen processing: Keeping it cool, Microsc. Microanal. Proc. 8 (Suppl. 2) (2002) 158–159.
[11] J.R. Harris, G.A.J. Brown, M. Jorgensen, S. Kaushal, E.A. Ellis, M.B. Grant, E.W. Scott, Bone marrow-derived cells home to and regenerate retinal pigment epithelium after injury, Invest. Ophthalmol. Vis. Sci. 47 (2006) 2108–2113.
[12] V.J. Madden, M.M. Henson, Rapid decalcification of temporal bones with preservation of ultrastructure, Hear. Res. 111 (1997) 76–84.
[13] R.S. Demaree Jr., R.T. Giberson, R.L. Smith, Routine microwave polymerization of resins for transmission electron microscopy, Scanning 17 (Suppl. 5) (1995) 25–26.
[14] L. Chicoine, P. Webster, The effect of microwave irradiation on antibody labeling efficiency when applied to ultrathin cryosections through fixed biological material, Microsc. Res. Tech. 42 (1998) 24–32.
[15] R. Van Dorp, P.G. Kok, E. Marani, M.E. Boon, L.P. Kok, ELISA incubation time can be reduced by 2.45-GJz microwaves, J. Clin. Lab. Immunol. 34 (1991) 87–96.
[16] W. Li, Y. Murai, E. Okada, K. Matsui, S. Hayashi, M. Horie, Y. Takano, Modified and simplified Western blotting protocol: Use of intermittent microwave irradiation (IMWI) and 5% skim milk to improve binding specificity, Pathol. Intl. 52 (2002) 234–238.
[17] S. Toyokuni, W. Kawaguchi, S. Akatsuka, M. Makoto, H. Hiai, Intermittent microwave irradiation facilitates antigen–antibody reaction in Western blot analysis, Pathol. Intl. 53 (2003) 259–261.
[18] J.J. Galvez, R.T. Giberson, R.D. Cardiff, Microwave mechanisms: The energy/heat dichotomy, Microsc. Today 12 (2004) 18–23.
[19] U.K. Laemmli, Cleavage of structural proteins during the assembly of the head of bacteriophage T4, Nature 227 (1970) 680–685.
[20] M.D. Abramoff, P.J. Magelhaes, S.J. Ram, Image processing with ImageJ, Biophotonics Intl. 11 (2004) 36–42.
[21] S. Hovmöller, CRISP: Crystallographic image processing on a personal computer, Ultramicroscopy 41 (1992) 121–135.
[22] R.T. Giberson, R.S. Demaree, Microwave Techniques and Protocols, Humana Press, Totowa, NJ, 2001.
[23] K.W. Osteryoung, K.D. Stokes, S.M. Rutherford, A.L. Percival, W.Y. Lee, Chloroplast division in higher plants requires members of two functionally divergent gene families with homology to bacterial ftsZ, Plant Cell 10 (1998) 1991–2004.
[24] M.A. Sanders, T.E. Anderson, R.S. Giberson, Microwave methods: Evidence to support a microwave effect, Microsc. Microanal. Proc. 12 (Suppl. 2) (2006) 295–296.
[25] D.L. Smith, D.K. Struck, J.M. Scholtz, R. Young, Purification and biochemical characterization of the lambda holin, J. Bacteriol. 180 (1998) 2531–2540.
[26] J. Dubochet, M. Ducommun, M. Zollinger, E. Kellenberger, A new preparation method for dark field electron microscopy of biomacromolecules, J. Ultrastruct. Res. 35 (1971) 147–167.

APPENDIX F

Transformation	Line	Date
80 pSV339(FtsZ1-1-GFP)	SALK 073878 (FtsZ1-1) knockout	10-17-2008*#
81 pSV371(FtsZ2-1-GFP) cloneA	SALK 134970 (FtsZ2-1) knockdown	10-17-2008*#
82 pSV371(FtsZ2-1-GFP) cloneB	SALK 134970 (FtsZ2-1) knockdown	10-17-2008*#
83 pSV339(FtsZ1-1-GFP)	SALK 073878 (FtsZ1-1) knockout	10-22-2008*#
84 pSV371(FtsZ2-1-GFP) cloneB	SALK 134970 (FtsZ2-1) knockdown	10-22-2008*#
85 pSV371(FtsZ2-1-GFP) cloneA	SALK 134970 (FtsZ2-1) knockdown	10-22-2008*#
86 pSV339(FtsZ1-1-GFP) new Agro clone	*arc3* mutant (Ler background)	06-26-2009*
87 pSV371(FtsZ2-1-GFP) new Agro clone	*arc3* mutant (Ler background)	06-26-2009*
88 pSV339(FtsZ1-1-GFP)	*arc6* mutant (Ws background)	06-26-2009*
89 pSV371(FtsZ2-1-GFP)	*arc6* mutant (Ws background)	06-26-2009*
90 pSV339(FtsZ1-1-GFP)	SALK 073878 (FtsZ1-1) knockout	06-26-2009*
91 pSV371(FtsZ2-1-GFP)	SALK 073878 (FtsZ1-1) knockout	06-26-2009*
92 pSV339(FtsZ1-1-GFP)	SALK 134970 (FtsZ2-1) knockdown	06-26-2009*
93 pSV371(FtsZ2-1-GFP)	SALK 134970 (FtsZ2-1) knockdown	06-26-2009*
94 pSV339(FtsZ1-1-GFP)	SALK 073878 (FtsZ1-1) knockout	07-20-2009#
95 pSV371(FtsZ2-1-GFP)	SALK 073878 (FtsZ1-1) knockout	07-20-2009#
96 pSV339(FtsZ1-1-GFP)	*parc6* mutant	07-20-2009#
97 pSV339(FtsZ1-1-GFP)	*At* wt (Ler)	07-20-2009#
98 pSV339(FtsZ1-1-GFP)	*arc3* mutant (Ler background)	07-20-2009#
99 pSV339(FtsZ1-1-GFP)	*At* wt (Ws)	07-20-2009#
101pSV371(FtsZ2-1-GFP)	*arc6* mutant (Ws background)	08-27-2009#
100 pSV371(FtsZ2-1-GFP)	*parc6* mutant	07-22-2009#
102 pSV371(FtsZ2-1-GFP)	*At* wt (Ler)	07-22-2009#
103 pSV371(FtsZ2-1-GFP)	*At* wt (Ws)	07-22-2009#
104 pSV339 (FtsZ1-1-GFP)	*arc 6* mutant	10-18-2009#@
105 pSV371(FtsZ2-1-GFP)	SALK 134970	10-18-2009@#
106 pSV371 (FtsZ2-1-GFP)	*arc 3* mutant	10-18-2009#@
107 pCJ7 (FtsZ1-1mCFP)	SALK 073878	01-29-2010#
108 pCJ9 (FtsZ1-1-mYFP)	SALK 073878	01-29-2010#
109 pCJ8 (FtsZ2-1-mCFP)	SALK 134970	01-29-2010#
110 pCJ10 (FtsZ2-1-mYFP)	SALK 134970	01-29-2010#
111 pCJ7 + pCJ 14 (FtsZ1-1mCFP-bar+ FtsZ2-1-mYFP-hyg)	SALK 134970	01-29-2010#
112 pCJ9 + pCJ16 (FtsZ1-1-mYFP-bar + FtsZ2-1-mCFP-hyg)	SALK 073878	01-29-2010#
113 pCJ9 + pCJ16 (FtsZ1-1-mYFP-bar + FtsZ2-1-mCFP-hyg)	SALK 134970	01-29-2010#
114 pCJ7 + pCJ 14 (FtsZ1-1mCFP-bar+ FtsZ2-1-mYFP-hyg)	SALK 134970	01-29-2010#
115 pCJ7	*At* wt (Col)	03-25-2010#
116 pCJ8	*At* wt (Col)	03-25-2010#
117 pCJ9	*At* wt (Col)	03-25-2010#
118 pCJ10	*At* wt (Col)	03-25-2010#
119 pCJ7 + pCJ14	*At* wt (Col)	03-25-2010#
120 pCJ9 + pCJ16	*At* wt (Col)	03-25-2010#
121 pCJ10(FtsZ2-1-mYFP)	FtsZ2 double knockout	10-19-2010#
122 pCJ10(FtsZ2-1-mYFP)	FtsZ triple knockout	10-19-2010#
123 pCJ 8 (FtsZ2-1-mCFP)	FtsZ2 double knockout	10-20-2010!#

Transformed by: *=Stan != Ryan #=Carol @=Shanshan

APPENDIX G

Transgenic Seed Phenotypes		
Transformant	**Phenotype**	**Fluorescence**
90-12	Severe	high
90-8, 90-9, 90-12	Intermediate	low
90-1, 90-5	Severe	low
90-3, 90-6, 90-11	Severe	high
91A1, 91A4	severe	High
91A3	Severe	Low
91A9	Severe/intermediate	?
91A2, 91A5	Intermediate	None
91A14, 91A15	Intermediate	low
94E4, 94B8, 94E5, 94A1, 94E3	Severe	Med
94A6, 94A17	Severe	low
94B1	Intermediate/wild-type	None
94B4, 94D1	Severe	low
94E2, 94B5, 94E1, 94D2, 94D3	Severe	high
94B2, 94B14	Intermediate	low
94B1, 94C1, 94D4	Wild-type/intermediate	none
94A2, 94B16, 94A3, 94A4	Intermediate	none
94B6, 94A5, 94D5	Severe	none
95A2, 95C2, 95A7	Severe	med
95D1, 95A5, 95F3, 95F5,95B1	Severe	high
95A9	Intermediate	High
95B2	Intermediate/wild-type	low
95B4	Intermediate/wild-type	med
95B10	Intermediate/wild-type	high
95D2	Severe	none
95D3, 95E1, 95C1, 95F2	Severe	low
95E2	Intermediate	med
95A3, 95A1, 95A8, 95A12	Intermediate	low
95A6, 95D2	Intermediate	none
96A1, 96D2	severe	low
96B1	severe	med
96C3	severe	high
96C1	Wildtype	Low
96B2, 96C2, 96E1, 96E2	Severe	None

97A5, 97A1, 97A3, 97A2	Severe	none
97A4	Severe	low
98A1, 98A2, 98I1, 98I2, 98J2, 98L3	Severe	None
98I4, 98L2, 98J1	Severe	Low
98I3, 98K3	Severe	Med
98B1, 98I5, 98C1, 98G1	Severe	High
98E1	Severe/intermediate	None
99J5, 99B1, 99C1, 99D1, 99F2	Wild-type	none
99L2, 99E2, 99K1, 99N2	Severe	none
99M4, 99F3, 99B2, 99A1, 99L1, 99J2	Severe	High
99G4, 99J4, 99L4	Wild-type	Low
99M6	Severe	Low
99M2	Wild-type	med
99M1	Intermediate	Low
99M3, 99F1	Intermediate	none
100T1, 100T2, 100T3, 100A2, 100S1, 100F1	Severe	none
100R5, 100C2, 100P1, 100E1, 100C2	Severe	Med
100V2, 100R1, 100”O”1, 100I4, 100D3	Severe	High
100U1, 100R2, 100R3, 100R4, 100P2	Severe	Low
100R7, 100R6, 100Q1, 100Q2, 100I2	Severe	None
100V1	Intermediate	none
102H4,102G1, 102G2, 104H7	Severe	None
102A1, 102A4, 102A2, 102H6	Severe	Med
102E2, 102C1, 102A5, 102B2	Severe	high
102E3	Severe	low
103A3	Wild-type	None
103A1, 103B1, 103E6, 103B6, 103C2	Severe	High
103E3, 103X1, 103S5, 103I1,103N7, 103N3	Severe	Med
103F1, 104N4, 103G2, 103X4	Severe	Low

103A2, 103B4, 103W2, 103Q3, 103H3	Severe	None
103B2, 103G1, 103D1,103K3, 103K5, 103K7	Intermediate	None
103W1, 103B3, 103X2, 103H2, 103X3	Intermediate	low
103G3, 103P1, 103B5, 103V7	Intermediate	Med
103E5, 103E2	Intermediate	high

APPENDIX H

Sample	Cryoprotectant	Freeze Substitution				Embedding		Poststain	Reference
		Method	Solvent	Fixative	Temperature/ Time	Time	Resin		
A. thaliana – root tip	1-hexadecene	Styrofoam box with dry ice	Acetone	1-4% OsO_4	-80 ºC/48 h -20 ºC/12 h 4 ºC/4 h	2-3 d	Epon	N/A	(Kang, 2010)
A. thaliana – root tip	1-hexadecene	Styrofoam box with dry ice	Acetone	0.25%glutaraldehyde + 0.1% UA	-80 ºC/48 h -50 ºC	2-3 d	HM20	N/A	(Kang, 2010)
Pinus contorta seedlings	0.2M sucrose	Dry ice-acetone bath	Acetone	2% OsO_4 + 8% dimethoxypropane	-80 ºC/120 h -20 ºC/4 h 4 ºC/4 h	gradual	Spurr's	2% UA/Pb citrate	(Rensing, 2004)
Uromyces appendiculatus	None	FS apparatus	Acetone	2-4% OsO_4	-90 ºC/8 h -60 ºC/8 h -30 ºC/8 h 0 ºC	2-3 d	Epon/Araldite	3% UA/Pb citrate	(Welter, 1988)
A.thaliana-shoots. Roots. primordia	0.15M sucrose	FS apparatus	Acetone	4% OsO_4	-80 ºC/120 h -80 ºC to 25 ºC/2 d	4 h in 5 % 4 h in 10% 12 h in 25% 24 h in 50, 75, 100%	Epon	3% UA/Pb citrate	(Segui-Simarro, 2004)
N. sylvestris	1-hexadecene	Dry ice-acetone bath	Acetone Acetone	1% OsO_4 + 0.1%UA 1% OsO_4	-78.6 ºC/36 h -20 ºC/2 h 0 ºC/2 h 23 ºC/2 h	N/A	Spurr's	3% UA/Pb citrate	(Kiss et al., 1990)
A.thaliana *N. tobacum* *S. oleracea*	0.15M sucrose	FS apparatus	Acetone	2% OsO_4	-80 ºC/120 h Warm to - 20ºC Warm to RT over 24 h	Increasing concentrations	Epon	N/A	(Austin and Staehelin, 2011)
S. pombe *S. cerevisiae* MDCK cells	N/A	FS apparatus	Acetone	0.1%UA	-90 ºC/48 h -58h with 1-3% water -45 ºC(5ºC/ h)	10,25,50, 75% for 4 h each increasing to -25 ºC , 100% 3x 10 h each, UV polymerize 48h	HM20	Pb citrate	(Kukulski, 2011)
C. elegans *N. benthamiana*	*E.coli* paste Yeast filler	LN_2 cooled heat block submerged in dry ice in a Styrofoam box	Acetone	1% OsO_4 + 0.1%UA	-196 ºC to room temperature	25% (1 h), 50% (2 h), 75% (4 h), and pure resin (1 h, 15 h and1 h), and polymerized either for 2 days at 60◦C	Epon	2% UA + Pb citrate	(McDonald and Webb, 2011)

BHK cells *E.coli*	0.7% agarose in Growth media 2% agarose in growth media	LN_2 cooled heat block placed in a Styrofoam box	Acetone	1% OsO_4 + 0.5%UA + 5% water	-196 ºC to room temperature	50% (1 h), 100% (1 h, overnight) and polymerized for 2 days at 60◦C	Epon	2% UA/Pb citrate	(McDonald and Webb, 2011)
Ledebouria socialis-athers	1-Hexadecene	FS apparatus Self made device	See Table 1 in Hess 2003		-90 ºC/ 8-12h	5% , 10%, 30%, 70%, 100% for up to 3 d	See Table 1 in Hess	0.5%UA Or 1% $KMnO_4$ + 0.5%UA + Pb citrate Or 1% PTA	(Hess, 2003)

VITA

Name: Carol Beatrice Johnson

Address: P O Box 8252
The Woodlands, TX 77387

Email Address: cb12johnson@gmail.com

Education: B.S., Biology, Texas Southern University, 1997
M.A., Biology, Sam Houston State University, 2000

Awards:

National Science Foundation Information Technology and Science Research Fellow	2005-2007
American Society of Plant Biology Travel Award	2006, 2010
National Science Foundation GK-12 Fellow	2007-2009
Microscopy Society of America Student Poster Award- 1st Place Biological Science	2009
National Science Foundation ICAR Research Conference Travel Award	2007, 2009
National Science Foundation Award to the Microscopy and Microanalysis	2007